

Technische Universität München
Lehrstuhl für Technische Chemie II

**Kinetic and mechanistic studies on the liquid-phase
hydrogenation of nitriles and dinitriles over cobalt-based catalysts**

Peter Schärringer

Vollständiger Abdruck der von der Fakultät für Chemie der Technischen
Universität München zur Erlangung des akademischen Grades eines

Doktors der Naturwissenschaften (Dr. rer. nat.)

genehmigten Dissertation.

Vorsitzender: Univ.-Prof. Dr. Bernhard Rieger

Prüfer der Dissertation:

1. Univ.-Prof. Dr. Johannes A. Lercher
2. Univ.-Prof. Dr. Klaus Köhler

Die Dissertation wurde am 15.02.07 bei der Technischen Universität München eingereicht
und durch die Fakultät für Chemie am 13.03.07 angenommen.

Acknowledgements

A bit more than three years ago my gut feeling told me to start a PhD in Johannes' (Prof. Dr. J. A. Lercher) group. Now that this story comes to an end I can surely say that it was the right choice thanks to the help and support of many nice and interesting people.

First of all, I want to thank you Johannes for giving me the opportunity to work on a very interesting and versatile topic, for helpful discussions on scientific and private issues, for the chance to visit international and national conferences, workshops and research institutes, which I sincerely did not take for granted.

Special thanks go to PD Thomas Müller, who guided me through the thesis on a daily basis. Thank you Thomas for your time and patience for discussions even if being busy, for teaching me how to tackle complex data in a structured way and for the very nice working atmosphere.

I would like to express my gratitude to PD Andy Jentys who helped me with the calculation and interpretation of INS data and chose good slopes in Obertauern.

Thank you, Dr. Dirk Bühring, Andreas Gallas and Dr. Olaf Wachsen for fruitful discussions and a very cooperative and pleasant atmosphere in our meetings.

During the last 3 years life would not have been the same fun without the members of the TC II group. I very much appreciated getting to know nice people from all over the world, who created an exciting, exotic and always very cooperative working atmosphere, which made time running like hell. I would like to thank the technical team consisting of Xaver (the most demanded person in the institute), Andreas M. and Martin for their indispensable work and not to forget the TC II guys from the workshop. Thank you, Heike, Helen and Heidi Hermann for caring about administration. Thank you, Philipp, Hendrik, Virginia, Elvira, Benjamin, Wolfgang, Andreas, Felix, Manuel, Maria, Carsten, Christoph, Aon, Lay Hwa, Oriol, Manuela, Herui, Tobias, Christoph, Richard, Jürgen, Frederik, Stephan R., Deachao, Prado, Matteo, Florian, Sandra, Chintan, Krishna, Rhino, Olga, Roberta, Yongzhong, Ghosh, Praveen, Iker, Christian, Su, Alex, Florencia, Renate, Su, Stefan G., Wolfram, Xuebing, Adam, Ayumu, Ana and Augustiner. Thank you, Wolfgang, Franzi, Cen and Yuying for doing eminent experimental work during your diploma and semester theses.

Very special thanks go to my parents (Annemarie and Franz) and my sister (Patricia), without the help of which I would never have come to that point. And finally my biggest thanks go to Johanna simply for being there and for your optimistic way of interpreting things. When driving the long way home it was always good to know that you would soon make me smile.

Table of contents

Chapter 1	General Introduction	1
1.1.	IMPORTANCE AND INDUSTRIAL-SCALE PREPARATION OF ALIPHATIC AMINES	2
1.2.	CATALYSTS AND PROCESSES USED FOR THE HYDROGENATION OF NITRILES	3
1.3.	KINETIC AND MECHANISTIC ASPECTS OF THE HYDROGENATION OF NITRILES	4
1.4.	SCOPE AND OUTLINE OF THE THESIS	8
Chapter 2	Experimental	11
2.1.	STIRRED TANK REACTOR	12
2.2.	CONTINUOUS TRICKLE BED REACTOR	13
Chapter 3	Co-adsorption of CD₃CN and hydrogen on a Raney-Co catalyst studies by inelastic neutron scattering	15
3.1.	INTRODUCTION	16
3.2.	EXPERIMENTAL	17
3.2.1.	Materials	17
3.2.2.	Catalyst characterization	17
3.2.2.1.	H ₂ -Chemisorption and N ₂ -physisorption	17
3.2.2.2.	Thermogravimetry	17
3.2.3.	Hydrogenation experiment	18
3.2.4.	Inelastic Neutron Scattering experiments and sample preparation	18
3.2.5.	Computational methods	19
3.3.	RESULTS	20
3.3.1.	Adsorption of H ₂ and CD ₃ CN on Raney-Co	20
3.3.2.	H/D exchange and selectivity in the hydrogenation of CD ₃ CN	22
3.3.3.	Results of INS measurements	24
3.3.3.1.	Hydrogen adsorption on Raney-Co studied by INS	24
3.3.3.2.	Co-adsorption of CD ₃ CN and hydrogen on Raney-Co	26
3.4.	DISCUSSION	31
3.4.1.	Role of hydrogen sorption strength	31
3.4.2.	Intermediate species in the co-adsorption of CD ₃ CN and hydrogen on Raney-Co	32
3.5.	CONCLUSIONS	36

Chapter 4	<i>Investigations into the mechanism of the liquid-phase hydrogenation of nitriles over Raney-Co catalysts</i>	39
4.1.	INTRODUCTION	40
4.2.	EXPERIMENTAL	42
4.2.1.	Materials	42
4.2.2.	Catalysis	42
4.3.	RESULTS	44
4.3.1.	Hydrogenation of $C_1-C\equiv N$ and CD_3CN	44
4.3.2.	Hydrogenation of $C_3-C\equiv N$	49
4.3.3.	Co-hydrogenation of $C_1-C\equiv N$ and $C_3-C\equiv N$	50
4.3.4.	Hydrogenation of $C_1-C\equiv N$ in the presence of C_4-NH_2	53
4.3.5.	Hydrogenation of $C_3-C\equiv N$ in the presence of C_2-NH_2	55
4.4.	DISCUSSION	57
4.4.1.	H/D exchange and kinetic isotope effect in the hydrogenation of CD_3CN	57
4.4.2.	Role of the strength of adsorption	58
4.4.3.	Mechanistic aspects of the formation of dialkylimines	60
4.4.4.	Mechanistic aspects of dialkylimine hydrogenation	62
4.5.	CONCLUSIONS	64
Chapter 5	<i>Tailoring Raney-catalysts for the selective hydrogenation of butyronitrile to n-butylamine</i>	67
5.1.	INTRODUCTION	68
5.2.	EXPERIMENTAL	69
5.2.1.	Catalyst preparation and materials	69
5.2.2.	Catalysis	70
5.2.3.	Catalyst characterization	70
5.3.	RESULTS	72
5.3.1.	Catalytic activity in the reduction of butyronitrile and selectivity to <i>n</i> -butylamine	72
5.3.2.	Specific surface area and fraction of accessible metal atoms	74
5.3.3.	Residual water and hydrogen on the catalyst surface	76
5.3.4.	Temperature programmed desorption of ammonia	78
5.3.5.	Characterization by X-ray photoelectron spectroscopy	80
5.3.6.	Adsorption of butyronitrile and <i>n</i> -butylamine from the liquid phase	83

5.4. DISCUSSION	85
5.4.1. Reaction mechanism and role of surface intermediates in the formation of by-product	85
5.4.2. Accessible metal atoms, oxidation state of the surface atoms, and the presence of Lewis acid sites	87
5.4.3. The role of hydrogen in the reaction mechanism	88
5.4.4. Influence of the sorption mode on activity and selectivity.....	88
5.5. CONCLUSIONS	89
Chapter 6 <i>In situ measurement of dissolved hydrogen during the liquid-phase hydrogenation of dinitriles</i>	93
6.1. INTRODUCTION	94
6.2. EXPERIMENTAL SECTION.....	95
6.2.1. Materials	95
6.2.2. Catalytic experiments	95
6.2.3. Gas-liquid mass transfer coefficient $k_{L}a$	96
6.2.4. Measuring the concentration of dissolved hydrogen with the permeation probe	96
6.3. RESULTS AND DISCUSSION.....	97
6.3.1. Gas-liquid mass transfer	97
6.3.2. Case study: Hydrogenation of dinitriles	99
6.3.2.1. <i>Reaction without external mass transfer limitation</i>	99
6.3.2.2. <i>Reaction with external mass transfer limitation</i>	103
6.4. CONCLUSIONS	106
Chapter 7 <i>On the activity and selectivity in the hydrogenation of dinitriles with cobalt-based catalysts</i>	109
7.1. INTRODUCTION	110
7.2. EXPERIMENTAL SECTION.....	111
7.2.1. Materials	111
7.2.2. Experiments in the stirred tank reactor.....	111
7.2.3. Experiments in the trickle-bed reactor	112
7.2.4. Sample analysis with gas chromatography.....	113
7.2.5. Space time yield (SY) in batch wise and continuous operation	113
7.3. RESULTS	114
7.3.1. Kinetics of hydrogenation in a continuously stirred tank reactor.....	114

7.3.1.1.	<i>Reaction in presence and absence of ammonia</i>	114
7.3.1.2.	<i>Influence of the ammonia concentration on the selectivity</i>	116
7.3.1.3.	<i>Influence of the reaction temperature</i>	117
7.3.1.4.	<i>Influence of the hydrogen pressure</i>	118
7.3.1.5.	<i>Potential limitations by pore diffusion</i>	118
7.3.2.	Continuous hydrogenation in a trickle-bed reactor	119
7.3.2.1.	<i>Influence of ammonia content</i>	119
7.3.2.2.	<i>Dependence on reaction temperature</i>	120
7.3.2.3.	<i>Influence of hydrogen pressure</i>	121
7.3.2.4.	<i>Variation of hydrogen flow</i>	121
7.4.	DISCUSSION	122
7.4.1.	Influence of ammonia on selectivity	122
7.4.2.	Role of the liquid – vapor equilibrium of ammonia in the formation of by-products.....	122
7.4.3.	Influence of temperature on selectivity	124
7.4.4.	Influence of hydrogen pressure on selectivity.....	124
7.4.5.	Effect of hydrogen flow in the laboratory trickle-bed reactor.....	125
7.4.6.	Space time yield in batch wise and continuous operation.....	125
7.5.	CONCLUSIONS	125
Chapter 8	<i>Summary and conclusions</i>	128

Chapter 1

General introduction

Abstract

In this chapter a general introduction into the background of amine production is given. Special emphasis is placed on the hydrogenation of nitriles to primary amines. Catalyst strategies are discussed as well as industrial ways of nitrile hydrogenation.

1.1. Importance and industrial-scale preparation of aliphatic amines

Primary, secondary and tertiary aliphatic amines are important intermediates, which find a variety of applications in chemical industry. Lower aliphatic amines (C_1 - C_6), for example, are used as intermediates in the production of pharmaceuticals, agricultural chemicals, rubber chemicals, water treatment chemicals, and solvents.^[1] The world consumption of lower aliphatic amines is shown in Figure 1.1. The single commercially most important alkyl amine is ethylamine, which accounts for about 35% to 40% of the world's annual requirement for alkyl amines. Its main usage is in the production of triazine-type herbicides.^[2]

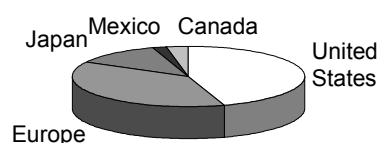


Figure 1.1: Relative contribution of selected countries to the world consumption of 610,000 tons per year of C_1 - C_6 alkylamines.^[3]

Aliphatic amines with longer alkyl chains (C_8 - C_{22}) are often derived from fatty acids or fatty esters and are, thereafter, referred to as fatty amines.^[2, 4] The worldwide production of fatty amines is estimated to be in excess 300,000 tons per year.^[2] Secondary fatty amines are usually derivatized to quaternary salts (e.g. dimethylalkyl ammonium salts with long-chain alkyl groups) for use, for instance, in personal hygiene and laundry products (fabric softeners, which is the largest single use of fatty amines).^[4, 5] Some other applications of fatty amines are as corrosion inhibitors (e.g. *N*-alkyl-1,3-propanediamines)^[2] and as deicing agents.^[6]

A particular class of amines are diamines, which polymerize with aliphatic diacids to give linear polyamides (nylon) and have conquered an important place in textile and mechanical industry.^[7] Hexamethylenediamine (HMDA), for example, is of supreme importance for the manufacture of nylon-6,6 and plays an increasing role as a component of foams and resins.^[8] In 1993, the world capacity for HMDA production was 1.20×10^6 tons per year.^[8]

Among the numerous processes of amine preparation on an industrial scale, the following are the main reactions:^[4]

- amination of alcohols with ammonia, which is the most common method for the manufacture of lower alkyl amines,
- reductive amination of carbonyl compounds, in which a carbonyl compound is reacted with NH_3 or a primary or secondary amine and the imine formed hydrogenated to amine,
- hydrogenation of nitriles.

1.2. Catalysts and processes used for the hydrogenation of nitriles

Among the industrially relevant preparation processes mentioned above the hydrogenation of nitriles, which was studied in this thesis, is an important method, in particular, when the process economics favors the use of a nitrile feed over the corresponding alcohol.^[2] In contrast to other hydrogenation reactions, a mixture of compounds is formed in the hydrogenation of nitriles, consisting mainly of primary, secondary and tertiary amines.^[9] However, the specifications for amines concerning purity are often very strict.^[10] For this reason, one of the most important issues in the hydrogenation of nitriles is the control of selectivity.^[11, 12] The catalyst employed is the most important factor determining the selectivity of nitrile hydrogenation.^[9] In this respect, metallic catalysts, which are often used in the hydrogenation of nitriles, can be ordered according to the increasing content of secondary and tertiary amines in the product mixture, as follows:^[13, 14] $\text{Co} < \text{Ni} < \text{Ru} < \text{Cu} < \text{Rh} < \text{Pd} < \text{Pt}$.

Due to their high selectivity, cobalt and nickel based catalysts are used, when primary amines are desired. Frequently, they are applied in a skeletal form, which is often referred to as Raney-type catalyst owing to their inventor's name.^[15] They are almost 100% pure metal and have a sponge-like structure stemming from the preparation process. Raney-Co catalysts show a higher selectivity to primary amines, whereas in most of the cases Raney-Ni is more active.^[11]

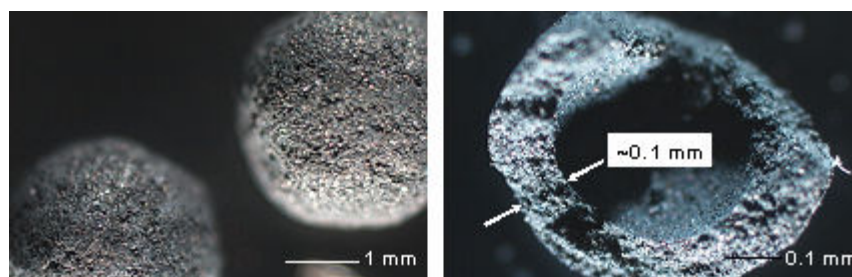


Figure 1.2: Hollow, porous spheres as an example for the concept of macroscopically shaped Raney-type catalysts.^[16]

Originally, Raney catalysts were manufactured in powder form. However, for fixed bed applications Raney-type catalysts with specific shapes (e.g. hollow spheres, Figure 1.2) consisting of up to 70% of the pure metal are now produced.^[16] An often considerable increase in selectivity to the primary amine can be achieved by doping the Raney-catalysts with alkali metals.^[17] Alternatively, supported catalysts (support: SiO_2 or Al_2O_3)^[18] are used, which are promoted with basic compounds (e.g. MgO) to reduce the acidity of the support. Acid sites are claimed to catalyze condensation reactions leading to undesired higher amines.^[19]

The hydrogenation of nitriles is usually carried out in the liquid phase.^[19] It can be performed in the continuous mode (e.g. in a trickle-bed reactor or a continuously stirred tank reactor) or discontinuously (in a stirred tank reactor). In Table 1.1 processes for the hydrogenation of nitriles are summarized including typical catalysts and process conditions. The data demonstrate that relatively high selectivities to primary amines can be achieved. However, as indicated in Table 1.1 and by almost all patents dealing with preparation of primary amines, ammonia is invariably added to the initial mixture when primary or secondary amines shall be prepared selectively.^[9, 20]

Table 1.1: Catalysts and processes used for the hydrogenation of nitriles to primary amines.^[4]

Catalyst	Process characteristics	Product	Selectivity [%]
Ni-Mg/support	Batch in the presence of NH ₃ , T = 413 K, P = 1.6 MPa	Dodecylamine	96
NiCr promoted Raney-Co	Continuous in the presence of NH ₃ , T = 398 K, P = 6.5 MPa	Hexamethylene- diamine	96
Ni/SiO	Batch in the presence of NH ₃ and NaOH, T = 423 K, P = 5.0 MPa	Fatty primary amines	87
Raney-Ni	Batch in the presence of NH ₃ T ~ 398 K – 413 K, P > 1.0 MPa	Primary amines	96

1.3. Kinetic and mechanistic aspects of the hydrogenation of nitriles

As the hydrogenation of nitriles is often carried out in the liquid phase,^[9] several mass transfer steps are included in the reaction. The three phases (gas, liquid, and solid) present in the reactor result in high complexity with respect to the interplay of mass transfer and heterogeneously catalyzed reaction. In Figure 1.3 mass transfer and surface reaction steps are shown together. During hydrogenation, molecular hydrogen has to diffuse from the gas into the liquid phase (gas-liquid mass transfer) and across the stagnant layer around the catalyst particle (liquid-solid mass transfer). If the catalyst is porous, hydrogen and the other reactants have to diffuse into the pores to the direct vicinity of the catalytically active sites (pore diffusion). After that, the reactants adsorb on the active sites, where the chemical reaction takes place. After desorption from the surface the products have to diffuse through the pore system towards the pore mouth and across the stagnant layer into the bulk phase.

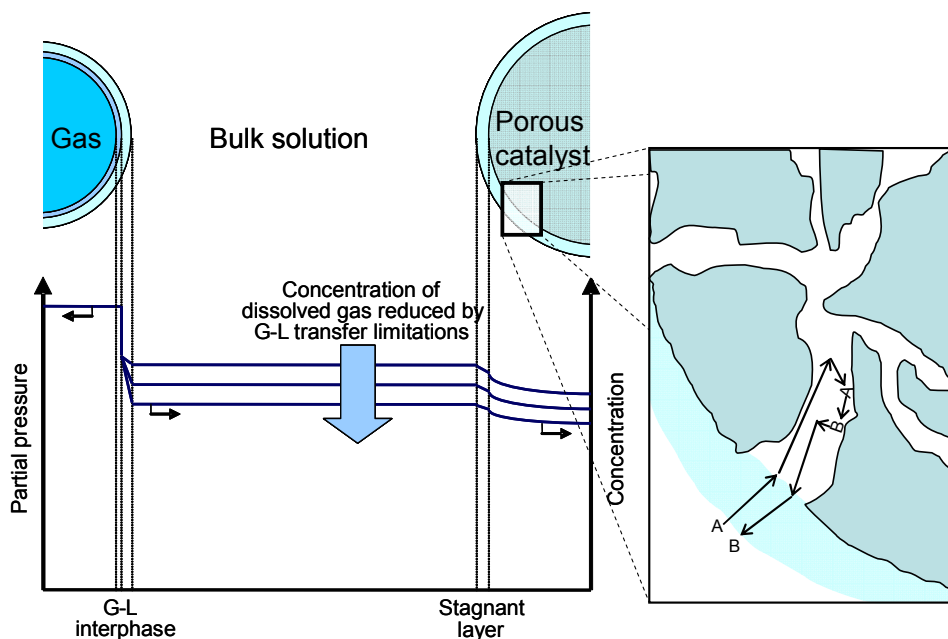


Figure 1.3: Concentration profile for gas/liquid/solid multiphase systems with mass transfer being present. The enlarged section shows the seven steps of heterogeneously catalyzed reactions.

Both, mass transfer and surface processes (adsorption, surface reaction, desorption) have to be discussed, when it comes to reaction rate and selectivity of the overall process. If the diffusion steps are slow compared to the surface processes the overall rate will be limited by mass transfer.^[21] Additionally, the selectivity can be influenced depending e.g. on the reaction order of main and side reactions.^[22] In the hydrogenation of nitriles the surface reaction is often considered to be the rate-determining step (provided mass transport limitations are absent).^[7, 23, 24] Hence, the sorption steps are in quasi-equilibrium. To undergo condensation reactions leading to secondary amines, it is assumed that primary amines have to re-adsorb on the catalyst surface.^[25] Thus, if nitriles and primary amines adsorb on the same sites their relative adsorption strength may affect the rate of hydrogenation and the selectivity.^[26] In this respect, it has been suggested that the beneficial effect of alkali promoters on selectivity is due to an enhanced adsorption of nitriles compared to amines.^[27, 28]

When it comes to the surface reaction itself, it is well established that due to the high reactivity of partially hydrogenated reaction intermediates a conventional nitrile hydrogenation always leads to a mixture of primary, secondary and tertiary amines.^[18] Thus, examination of the mechanism of the surface reaction requires a detailed investigation of the nature and geometry of the reactive adsorbed species on the catalyst.^[29] In 1905, Sabatier and Senderens^[30] proposed that the hydrogenation proceeds stepwise resulting in an aldimine intermediate. Based on his findings, von Braun^[31] was the first to suggest that the formation of by-products is due to the reaction of the reactive aldimine with amine. Later, Kindler and

Hesse^[32] proposed that formation of tertiary amines advances similarly by addition of a secondary amine to an aldimine intermediate. From the findings of the above mentioned authors, a formal reaction scheme for the formation of primary, secondary and tertiary amines can be drawn (Figure 1.4).

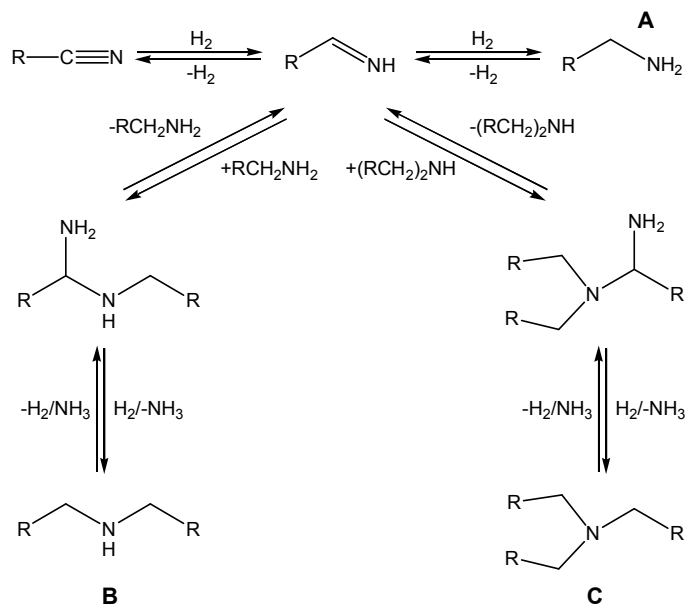


Figure 1.4: Formal reaction scheme for the hydrogenation of nitriles to primary (A), secondary (B) and tertiary amines (C).

The 1-amino-dialkylamine formed through reaction of aldimine with primary amine and the 1-amino-trialkylamine formed through reaction of aldimine with secondary amine can undergo either ammonia elimination with subsequent hydrogenation or direct hydrogenolysis, both resulting in secondary and tertiary amine, respectively.

As it has not been confirmed experimentally, it is not quite clear, if the partially hydrogenated intermediate is in deed an aldimine.^[26] Other authors suggested nitrene species (nitrogen-metal double bond),^[33-35] for which direct experimental observation has been reported,^[36] and carbene species (carbon-metal double bond),^[37] which have been shown to be possible stable intermediates by DFT calculations.^[34]

Another point frequently discussed is the site, where the reactions leading to by-products take place. In most literature, it has been suggested that hydrogenation and condensation take place on the catalyst surface.^[9, 17, 26] The fact that aldimine was not detected in the liquid phase was taken as a proof that it occurs only on the catalyst surface. Thus, condensation reactions can only take place on the surface.^[38] However, in the reaction of benzaldehyde with NH_3 in the absence of catalyst, benzylimine was not detected at any moment in the product composition, as it is highly reactive and readily forms hydrobenzamide. Therefore, it was

suggested that the fact that the primary imine is not identified in the liquid phase does not prove that condensation reactions proceed heterogeneously.^[12] It has been debated, if the formation of secondary amines occurs through a bifunctional mechanism^[38, 39] (Figure 1.5), in which aldimine migrates to the acidic function and subsequently reacts with amine, or exclusively on the metal sites.^[26] Contrary, Dallons et al.^[38] found that secondary amine formation was inhibited by acidic supports, presumably because the primary amine is more strongly adsorbed, remaining, in consequence, further away from the hydrogenation sites. Thus, they concluded that the reaction between amine and imine could take place solely on the metal surface, or on both metal and support surfaces in the case of supported metal catalysts.

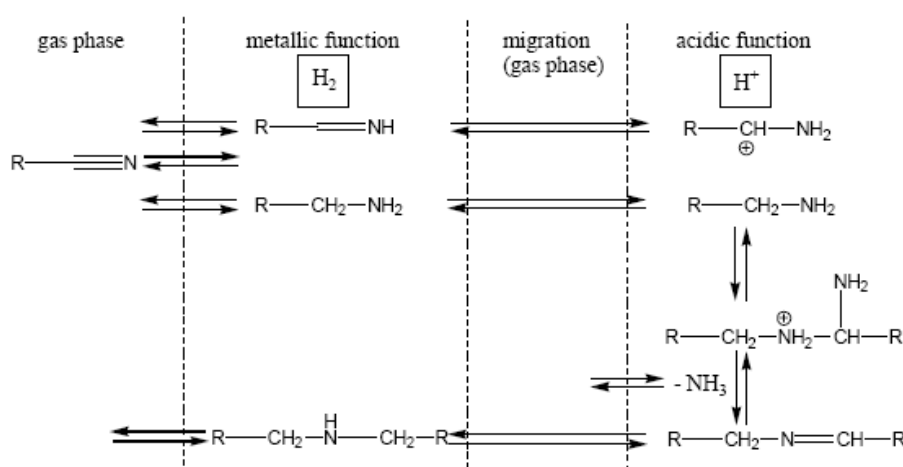


Figure 1.5: Bi-functional mechanism for the formation of by-products during the hydrogenation of nitriles.^[39]

As mentioned above, the hydrogenation of nitriles to primary amines is usually carried out in the liquid phase in the presence of ammonia, as it strongly ameliorates the selectivity. The way, ammonia influences the selectivity, has been discussed by numerous authors. Their explanations put forward were:^[40]

- As ammonia is released in the condensation reaction of the intermediate with an amine group under formation of a dialkylimine, the equilibrium is shifted to the primary amine and the alkylimine (Figure 1.4).^[41]
- Ammonia reacts directly with the alkylimine. Hydrogenolysis of the resulting 1-aminoamine leads to formation of ammonia and primary amine (Figure 1.6).^[42]
- Ammonia poisons the acid sites of the catalyst leading to inhibition of acid catalyzed side reactions.^[39]

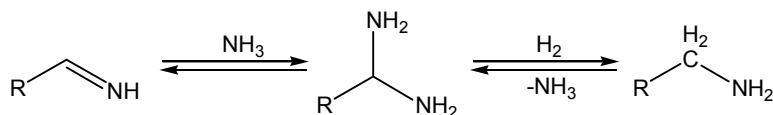


Figure 1.6: Reaction of ammonia with alkylideneimine and subsequent hydrogenolysis.

1.4. Scope and outline of the thesis

One aim of the investigations described in the present thesis was to understand the influence of the above-described single mass transfer and surface reaction steps on the rate and selectivity during liquid-phase nitrile hydrogenation. Another aim was to maximize rate and selectivity to primary amines by modification of Raney-Co catalysts and by optimization of the process parameters including the amount of ammonia.

Therefore, a stepwise approach was chosen. On the one hand, studies with model systems (acetonitrile and butyronitrile over Raney-Co) were performed to gain insight into the mechanistic aspects of nitrile hydrogenation. On the other hand, fatty nitriles were hydrogenated to understand the influence of mass transfer and process parameters under industrially relevant conditions.

First, the co-adsorption of acetonitrile- d_3 and hydrogen on Raney-Co was examined by inelastic neutron scattering (INS), as described in Chapter 3. The aim was to identify the nature of partially hydrogenated surface species, which is a crucial point for optimizing the selectivity to primary amines. As in INS spectra motions involving hydrogen dominate, the measurements were aimed at selectively probing the reaction centers in the intermediates by labeling with the appropriate isotopes. The objective of Chapter 4 was to gain further insight into the mechanism of by-product formation. Therefore, co-hydrogenation of acetonitrile and butyronitrile over Raney-Co was conducted in a stirred tank reactor. The role of the amine in the formation of by-products was examined by performing the hydrogenation of acetonitrile and butyronitrile in the presence of *n*-butylamine and ethylamine, respectively. The purpose of the research described in Chapter 5 was to elucidate the influence of LiOH promotion on Raney-Co catalysts for the selective hydrogenation of butyronitrile to *n*-butylamine. Based on a detailed characterization of the parent and the LiOH doped Raney-Co catalyst, structure-activity and structure-selectivity relationships were established. In Chapter 6, the role of external mass transfer (gas-liquid, liquid-solid) in the hydrogenation of dinitriles over a supported cobalt-based catalyst was examined. To measure the concentration of dissolved hydrogen and to identify external mass transfer limitations in a stirred tank reactor, a permeation probe was applied. A study on the activity and selectivity in the hydrogenation of dinitriles

over a supported cobalt-based catalyst is presented in Chapter 7. The reaction was carried out in both a stirred tank reactor and a laboratory scale trickle bed reactor to obtain insight into the kinetics and to study the influence of process parameters on reaction rate and selectivity. Chapter 8 provides a summary of the major results and conclusions of this thesis.

References

- [1] K. S. Hayes, *Appl. Catal. A* **2000**, *221*, 187.
- [2] S. A. Lawrence, *Amines*, Cambridge University Press, Cambridge, **2004**.
- [3] CEH Marketing Research Report 611.5030, *Alkylamines (C1-C6)*, **2005**.
- [4] J. Barrault, Y. Pouilloux, *Catal. Tod.* **1997**, *37*, 137.
- [5] F. E. Friedli, R. M. Gilbert, *J. Am. Oil. Chem. Soc.* **1990**, *67*, 48.
- [6] S. Dawtrey, H. C. King, US Patent No. 3,350,314, to Shell Oil Company, **1967**.
- [7] B. W. Hoffer, P. H. J. Schoenmakers, P. R. A. Mooijman, G. M. Hamminga, R. J. Berger, A. D. van Langeveld, J. A. Moulijn, *Chem. Eng. Sci.* **2004**, *59*, 259.
- [8] K. Weissermel, H. J. Arpe, *Industrial Organic Chemistry*, 3. ed., Wiley-VCH, Weinheim, **1997**.
- [9] J. Volf, J. Pasek, *Stud. Surf. Sci. Catal.* **1986**, *27*, 105.
- [10] B. Bigot, F. Delbecq, A. Milet, V. H. Peuch, *J. Catal.* **1996**, *159*, 383.
- [11] C. DeBellefon, P. Fouilloux, *Catal. Rev.-Sci. Eng.* **1994**, *36*, 459.
- [12] S. Gomez, J. A. Peters, T. Maschmeyer, *Adv. Synth. Catal.* **2002**, *344*, 365.
- [13] H. Greenfield, *Ind. Eng. Chem. Prod. Res. Dev.* 1967, *6*, 142.
- [14] J. Pasek, N. Kostova, B. Dvorak, *Collect. Czech. Chem. Commun.* **1981**, *46*, 1011.
- [15] M. Raney, US Patent No. 1,563,587, **1925**.
- [16] D. Ostgard, M. Berweiler, S. Roeder, European Patent No. 2002051791, to Degussa, **2002**.
- [17] A. Chojecki, Dissertation thesis, TU München **2004**.
- [18] M. J. F. M. Verhaak, Dissertation thesis, Universiteit Utrecht, **1992**.
- [19] F. Mares, J. E. Galle, S. E. Diamond, F. J. Regina, *J. Catal.* **1988**, *112*, 145.
- [20] L. K. Freidlin, T. A. Sladkova, *Russ. Chem. Rev.* **1964**, *33*, 319.
- [21] M. Baerns, H. Hofmann, A. Renken, *Chemische Reaktionstechnik*, 3 ed., Wiley-VCH, Weinheim, **2002**.
- [22] R. J. Berger, E. H. Stitt, G. B. Marin, F. Kapteijn, J. A. Moulijn, *Cattech* **2001**, *5*, 30.
- [23] M. Joucla, P. Marion, P. Grenouillet, J. Jenck, in *Catalysis of organic reactions III* (Eds.: J. R. Kosak, T. A. Johnson), Marcel Dekker, New York, **1994**, p. 127.
- [24] C. Joly-Vuillemin, D. Gavroy, G. Cordier, C. de Bellefon, H. Delmas, *Chem. Eng. Sci.* **1994**, *49*, 4839.
- [25] Y. Y. Huang, W. M. H. Sachtler, *J. Catal.* **2000**, *190*, 69.

- [26] Y. Y. Huang, W. M. H. Sachtler, *Appl. Catal. A-Gen.* **1999**, *182*, 365.
- [27] F. Hochardponcet, P. Delichere, B. Moraweck, H. Jobic, A. J. Renouprez, *J. Chem. Soc.-Faraday Trans.* **1995**, *91*, 2891.
- [28] S. N. Thomas-Pryor, T. A. Manz, Z. Liu, T. A. Koch, S. K. Sengupta, W. N. Delgass, in *Chemical Industries Series, Vol. 75* (Ed.: F. E. Herkes), Dekker, New York, **1998**, p. 195.
- [29] B. Bigot, F. Delbecq, V. H. Peuch, *Langmuir* **1995**, *11*, 3828.
- [30] P. Sabatier, J. B. Senderens, *Comptes Rendus* **1905**, *140*, 482.
- [31] J. von Braun, G. Blessing, F. Zobel, *Chem. Ber.* **1923**, *56*, 1988.
- [32] K. Kindler, F. Hesse, *Arch. Pharm.*, **1933**, *271*, 439.
- [33] A. Chojecki, H. Jobic, A. Jentys, T. E. Muller, J. A. Lercher, *Catal. Lett.* **2004**, *97*, 155.
- [34] B. Bigot, F. Delbecq, A. Milet, V. H. Peuch, *J. Catal.* **1996**, *159*, 383.
- [35] Y.-Y. Huang, W. M. H. Sachtler, *Stud. Surf. Sci. Catal.* **2000**, *130A*, 527.
- [36] H. Bock, O. Breuer, *Angew. Chem.-Int. Ed.* **1987**, *26*, 461.
- [37] B. Coq, D. Tichit, S. Ribet, *J. Catal.* **2000**, *189*, 117.
- [38] J.L. Dallons, A. Van Gysel, G. Jannes, in *Catalytic Organic Reactions, Vol. 47*, (Ed.: W. E. Pascoe), Dekker, New York, **1992**, p. 93-104.
- [39] M. Verhaak, A. J. Vandillen, J. W. Geus, *Catal. Lett.* **1994**, *26*, 37.
- [40] R. Novi, Dissertation thesis, ETH Zürich **2004**.
- [41] F. M. Cabello, D. Tichit, B. Coq, A. Vaccari, N. T. Dung, *J. Catal.*, **1997**, *167*, 142.
- [42] E. J. Schwoegler, H. Adkins, *J. Am. Chem. Soc.* **1939**, *61*, 3499.

Chapter 2

Experimental

Abstract

The experimental apparatuses used for kinetic and mechanistic studies are described in this chapter. The liquid-phase reactions were performed in either a batch wise or a continuously operated system.

2.1. Stirred tank reactor

Investigations concerning kinetics and the mechanism of nitrile hydrogenation were mainly conducted in the setup depicted in Figure 2.1. Here, a general description of the apparatus is given. A detailed explanation of the experimental techniques employed for the single studies will be given in the respective chapters.

The reaction vessel was a stirred tank reactor (R, 160 mL, Parr Instruments) with a magnetically coupled hollow shaft stirrer with gas entrainment (M). As all the catalysts used were sensitive to oxygen the reactor was transferred to the glove box before the reaction. Here, the catalyst was filled into the reactor either in pure form or suspended in the reactant mixture. The catalyst was either used in powder form or in the form of entire catalyst grains (with diameter of up to 6 mm). In the latter case a catalyst basket was used to immobilize the grains. While mounting the reactor to the setup it was flushed with nitrogen to avoid contact of the catalyst with air. Then, in the case of pure catalyst ammonia was admitted to the reactor and after that nitrile was pumped in. Before attaching the lines to the reactor they were flushed with hydrogen. By means of a heating/cooling jacket (H) the reaction mixture was heated to the desired temperature and subsequently equilibrated for at least 45 min. The desired pressure was then adjusted within 2 s at maximum by admitting hydrogen *via* the bypass. Then the stirrer was started, which was taken as starting point of the reaction. The pressure in the reactor was kept constant with a pressure/flow regulation *via* a mass flow controller (Bronckhorst) keeping the pressure constant. Temperature, hydrogen pressure and hydrogen consumption were recorded. For off-line analysis with gas chromatography samples were periodically withdrawn with a dip tube equipped with a filter for solids. Detailed information on the GC analyses methods can also be obtained from the single chapters.

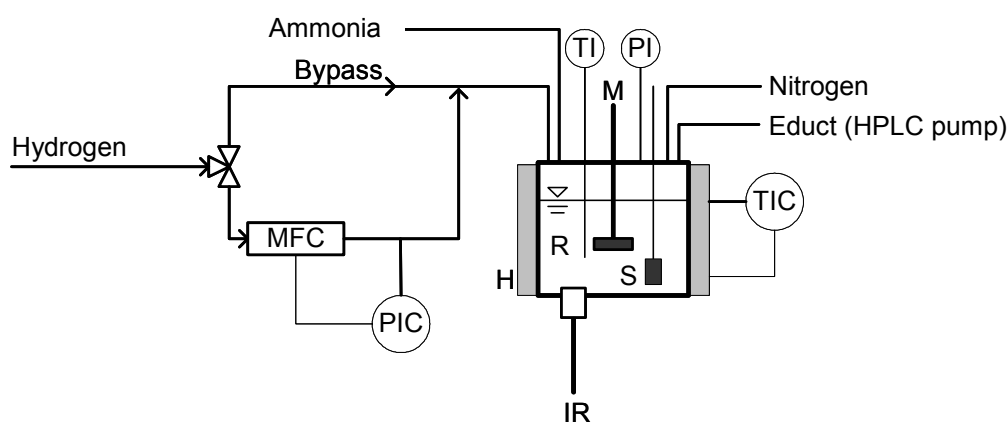


Figure 2.1: Scheme of the stirred tank reactor with *in situ* FTIR spectrometer.

For *in situ* analysis of the composition of the liquid phase the reactor was equipped with an Attenuated Total Internal Reflectance Infrared Spectrometer (ATR-IR). A ReactIR 1000 Reaction Analysis System (Mettler Toledo GmbH) equipped with a probe immersing into the reactor from the bottom was used. The probe consisted of a 0.625" DiComp assembly (diamond, gold seal) with an optical range 4400 – 2150 cm^{-1} and 1950 – 650 cm^{-1} . The probe was designed for operation at a temperature of 193 – 523 K and a pressure up to 100 bar.

2.2. Continuous trickle bed reactor

The setup used for the experiments in the continuous mode is shown schematically in Figure 2.2. The tubular stainless steel reactor (R) with an inner diameter of 0.9 cm and a length of 15 cm was filled with catalyst in the glove box. To avoid contact with oxygen it was equipped with a three-way valve to allow for flushing all lines before switching to the reactor. The flows of the nitrile (0.01 $\mu\text{L}/\text{min}$ – 25 mL/min) and the solvent ammonia (1 $\mu\text{L}/\text{min}$ – 170 mL/min) were controlled with two syringe pumps (Isco Co.) with a volume of 100 cm^3 and 500 cm^3 , respectively. Hydrogen was supplied with a mass flow controller (MFC, Bronckhorst). The reactants and solvent were mixed just before entering the reactor. In the reactor a zone with inert material (SiC, size F100, 0.106 mm – 0.150 mm) guaranteed good mixing and even distribution above the catalyst bed. The pressure in the reactor was controlled by a back pressure regulator (BPR, Tescom). A heating/cooling jacket was used to regulate the temperature in the reactor.

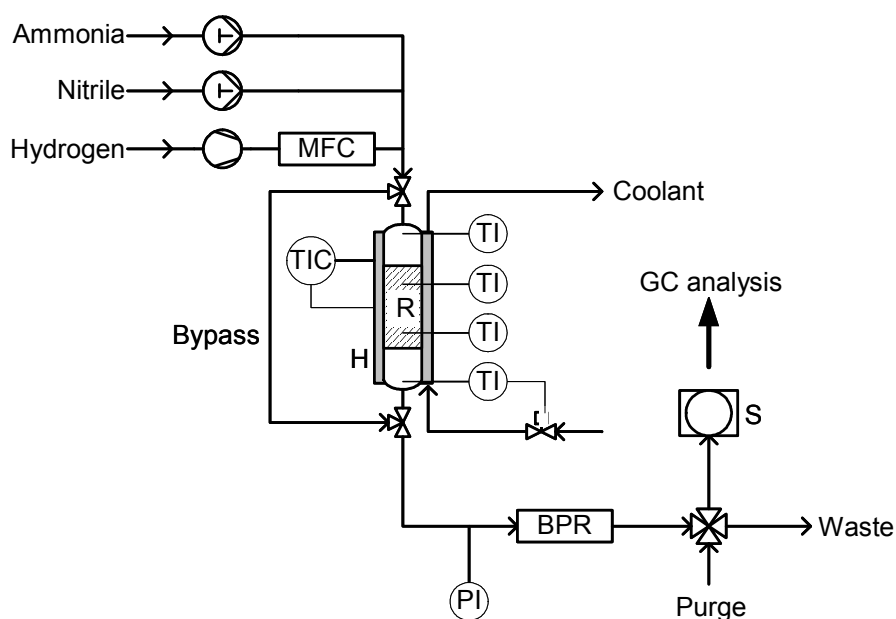


Figure 2.2: Schematic representation of the setup used for continuous nitrile hydrogenation in a trickle bed reactor.

Four thermocouples (TI) located inside the reactor gave information about the temperature gradient in the reaction zone. Pressure (PI), temperature and flows of the reactants and the solvent were recorded with a computer program (HPVee 5.0). To allow automatic sampling a 16-way valve was piloted with HPVee 5.0. The samples were analyzed with off line gas chromatography. The analyses methods will be explained in detail in the respective chapters. The setup was placed in a heated box ($T = 45\text{ }^{\circ}\text{C}$) to be able to process high boiling feeds (e.g. fatty nitriles) and products, which are solid under ambient conditions.

Chapter 3

Co-adsorption of CD₃CN and hydrogen on a Raney-Co catalyst studied by inelastic neutron scattering

Abstract

The co-adsorption of acetonitrile-d₃ (CD₃CN) and hydrogen on a Raney-Co catalyst was investigated by inelastic neutron scattering (INS). To elucidate the structure of partly hydrogenated surface species the hydrogen pressure was gradually increased (0.5, 1.5 and 2.0 equivalents with respect to CD₃CN). Comparison with reference spectra of H₂, CD₃CN and CD₃CH₂NH₂ adsorbed on Raney-Co as well as simulated INS spectra from *ab initio* calculations provided information on the interaction and the structure of the adsorbed molecules on Raney-Co. CD₃CN reacted preferentially with hydrogen bound on η^3 sites on the Co-001 plane. When contacted with hydrogen CD₃CN was found to be completely converted resulting in a mixture of adsorbed CD₃CH₂NH₂ and a nitrene-like surface species. Latter is proposed, as a strong CH₂ twisting vibrational mode was observed, which decreased in intensity relative to the other CH₂ vibrational modes upon increasing the amount of hydrogen.

3.1. Introduction

Primary amines are often used as feedstock in the production of, e.g., of fibres for textiles and surface active compounds. One important industrial process for their manufacture is the hydrogenation of the corresponding nitriles over transition metal catalysts,^[1] which is usually accompanied by the formation of secondary and tertiary amines as undesired by-products.^[2] However, in certain applications even very small quantities of the by-products result in poor quality of the final product.^[3, 4] Understanding the development of by-products from a mechanistic point of view is considered as an essential prerequisite for further optimization of catalysts and consequently higher selectivity. Already in 1923 it was suggested that the side reactions proceed via reactive aldimine intermediates^[2] and ever since numerous mechanistic discussions were based on von Braun's proposal.^[5-7] As direct observation of the aldimine had not been reported^[5] other possible surface intermediates, such as carbenes and nitrenes, were included in the discussion.^[8-10]

A widely used class of catalysts are skeletal Raney catalysts based on Co or Ni.^[11] Compared to other transition metals (e.g. Ni and Ru) Co is known to exhibit the highest selectivity to primary amines but generally provides relatively low activity.^[12] A present study in our group aims at establishing structure-selectivity correlations for Raney-Co^[13-15] with the aim to generate information on how to make catalysts with high activity more selective.

For the characterization of the adsorption characteristics in catalytic reactions Inelastic Neutron Scattering (INS) has proven to be a useful tool.^[16-18] A special feature of this technique is that the signal intensity depends on the momentum transfer, the amplitude of vibration and the incoherent scattering cross-section. As the cross-section of hydrogen is 10-100 times larger than that of all other elements, its amplitude of vibration in large motions involving hydrogen dominate the INS spectrum.^[19] Therefore, INS has also been used for investigations into the sorption of hydrogen and nitriles on Raney catalysts.^[13, 20-22]

In this work, special emphasis was placed on identifying the surface intermediates occurring during the hydrogenation of nitriles over a Raney-Co catalyst to unravel the elementary steps on the metal surface. The co-adsorption of acetonitrile- d_3 (CD_3CN) and hydrogen on Raney-Co was investigated as a model reaction. The choice of this model is based on the idea that, when reaction of hydrogen and the CN triple bond takes place, the vibrations of the resulting intermediate and the product in INS will be much more pronounced compared to the background including the CD_3 group. Thus, a better differentiation between the reactant and surface intermediates will be obtained.

3.2. Experimental

3.2.1. Materials

Raney-Co 2700 catalyst (Grace Davison division of W.R. Grace and Co.) was received as an aqueous suspension. The chemical composition was: 1.85 wt% Al; 97.51 wt% Co; 0.3 wt% Fe and 0.34 wt% Ni. It was washed with de-ionized water under nitrogen atmosphere until the pH of the washing water was ~ 7 . Due to its sensitivity to oxygen the catalyst was stored and handled under inert atmospheres throughout all further steps. The remaining water was removed by drying in partial vacuum ($p < 1$ kPa) for 30 h at 323 K. CD₃CN (Deutero GmbH), CH₃CN (Fluka) and acetaldehyde (Riedel-de Haën) with a purity of 99.5% each were used as received. D-labeled *n*-ethylamine (CD₃CH₂NH₂) was obtained by hydrogenation of CD₃CN over Raney-Co 2700.

3.2.2. Catalyst characterization

3.2.2.1. H₂-Chemisorption and N₂-physisorption

H₂-chemisorption and N₂-physisorption (BET) were measured on a Sorptomatic 1990 instrument (ThermoFinnigan). For both measurements the catalyst sample (~ 1 g) was outgassed for 6 h at 473 K ($p < 1$ mPa). The BET measurement was conducted at 77 K. H₂-chemisorption was carried out at 308 K with an equilibrating time of 2 – 180 min for each pressure step. Equilibration was continued until the pressure deviation was < 0.27 mbar within of a 2-min period. Isotherms were measured twice on the sample. Between the two measurements, the sample was evacuated to 10^{-3} mbar for 1h. The second isotherm (physisorbed H₂) was subtracted from the first isotherm (chemisorbed and physisorbed H₂). The amount of hydrogen adsorbed was determined by extrapolating the linear part of the difference isotherm ($p > 6.5$ kPa) to zero pressure. The number of accessible metal atoms was calculated assuming that one hydrogen atom was adsorbed per cobalt atom. By assuming a transversal section of 6.5 \AA^2 per cobalt atom the metal surface area was determined from the amount of chemisorbed hydrogen.

3.2.2.2. Thermogravimetry

The adsorption of gaseous CD₃CN on Raney-Co was investigated on a Setaram TG-DSC 111 thermoanalyzer. Before the measurement the catalyst sample (~ 24 mg) was outgassed for 6 h at 473 K ($p < 0.1$ mPa). Adsorption of CD₃CN was carried out at 308 K using pressure pulses of 0.02 – 2.5 mbar up to ~ 11 mbar. The weight increase and the corresponding heat flux were recorded for each pulse.

3.2.3. Hydrogenation experiment

The hydrogenation of CD_3CN was conducted in a stirred tank reactor (160 cm^3 ; Parr Instrument Comp.) at constant hydrogen pressure by re-supplying hydrogen consumed during the reaction. Raney-Co catalyst (1 g) was suspended in the reaction mixture composed of CD_3CN (40 cm^3) and hexane (40 cm^3) under inert atmosphere. Hexane was used both as solvent and as internal standard for GC chromatography. The suspension was filled into the autoclave under a flow of nitrogen. After closing the reactor was pressurized and depressurized five times with nitrogen to remove oxygen. The reaction mixture was heated to the reaction temperature (383 K). The reaction was started by rapidly pressurizing the reactor with hydrogen to 45 bar and subsequently starting the stirrer (1500 rpm). Samples for off-line NMR and GC analysis were periodically withdrawn through a dip-tube with a filter for solids. GC analysis was carried out on an HP Gas Chromatograph 5890 equipped with a cross linked 5% diphenyl-95% dimethylpolysiloxane column (Rtx-5 Amine, 30 m, Restek GmbH). ^1H NMR and ^2H NMR measurements were carried out on a Bruker DPX-400 (400 MHz) instrument with CD_3Cl as solvent containing 1 vol.-% trimethylsilane as standard. The selectivity was calculated as the ratio of the product yield to the amount of CD_3CN converted.

3.2.4. Inelastic Neutron Scattering experiments and sample preparation

Inelastic neutron scattering measurements (INS) were performed on the hot neutron 3-axis spectrometer IN1 at the Institut Laue-Langevin (Grenoble, France) using a Beryllium filter-analyser (BeF) and a Cu (220) monochromator, which allows INS spectra to be recorded in the energy transfer range 213 – 2500 cm^{-1} with variable resolution. IN1-BeF is optimized for the phonon density-of-states measurements, studies of molecular dynamics and atomic bonding in hydrogen-containing matter, materials and compounds. ^[23]

The samples of the pre-dried Raney-Co catalyst (each ~ 45 g) were transferred to cylindrical aluminum containers (height: 7.5 cm; diameter: 2.3 cm) under inert atmosphere. Subsequently, the samples were activated in vacuum ($p < 1$ mPa) at 473 K for 6 h. The respective adsorbate the amount of which corresponded to the maximum adsorption capacity of the Raney-Co catalyst was then added in liquid form. Two boundary conditions were taken into account. One is that it has to be assured that only CD_3CN or intermediates which are adsorbed on the catalyst contribute to the signal. Hence, it has to be avoided that excess CD_3CN is in the sample container. The other one is that sufficient signal intensity makes it necessary to find the maximum possible amount of CD_3CN to be filled into the INS cell. To estimate the maximum amount of CD_3CN , which can be adsorbed on the surface of the Raney-Co catalyst

adsorption of CD_3CN was followed by thermogravimetry and calorimetry. For adsorption of ethylamine- d_3 ($\text{CD}_3\text{CH}_2\text{NH}_2$) the same molar loading as for CD_3CN was assumed. The maximum uptake was ~ 0.30 molecules/ $\text{Co}_{\text{Surface}}$.

Four samples filled with CD_3CN were equilibrated with hydrogen to obtain a ratio of 0.5, 1.0, 1.5 and 2.0 $\text{mol}_{\text{H}_2}/\text{mol}_{\text{CD}_3\text{CN}}$. The amount of hydrogen added to the respective sample is summarized in Table 3.1. After sealing the filled aluminum containers were heated to 333 K for 10 h to ensure even distribution of the adsorbate and reaction of CD_3CN with hydrogen.

The sample containers were inserted in the cryostat, which was then cooled to 10 K. Spectra were recorded in the energy range 213 – 2070 cm^{-1} with a resolution of 16 cm^{-1} , 8 cm^{-1} and 32 cm^{-1} at energy transfers between 213 – 760 cm^{-1} , 760 – 1745 cm^{-1} and 1745 - 2070 cm^{-1} , respectively. In order to test the reproducibility of the sample preparation procedure and INS measurements, the same experiments were carried out in two different measurement cycles. The results from the two cycles showed good agreement.

Table 3.1: Amounts of catalyst, CD_3CN , $\text{CD}_3\text{CH}_2\text{NH}_2$ and hydrogen filled into the sample cells for INS measurement.

Sample	Amount of catalyst [g]	Amount of $\text{CD}_3\text{CN}/\text{CD}_3\text{CH}_2\text{NH}_2$ [mmol]	Amount of hydrogen [mmol]
Raney-Co	45.42	-	-
Raney-Co + H_2	38.94	-	10.36
Raney-Co + CD_3CN	44.98	8.80	-
Raney-Co + CD_3CN + 0.5 eq. H_2	45.23	8.85	4.43
Raney-Co + CD_3CN + 1.5 eq. H_2	45.27	8.86	13.29
Raney-Co + CD_3CN + 2.0 eq. H_2	44.70	8.75	17.50
Raney-Co + $\text{CD}_3\text{CH}_2\text{NH}_2$	45.80	8.96	-

3.2.5. Computational methods

For quantum mechanical examinations the structure of the different molecules investigated were optimized with respect to the total energy using density functional theory (DFT) as implemented in GAUSSIAN 98.^[24] The B3LYP hybrid functional and a 6-31G** basis set were applied. For the optimized geometry calculated vibrational modes were calculated. The

resulting displacement vectors for each vibrational mode were used to derive the INS-spectra with the program a-CLIMAX.^[25, 26] The vibrational modes were visualized and assigned with Molview 3.0.

3.3. Results

3.3.1. Adsorption of H_2 and CD_3CN on Raney-Co

Though Raney-Co is almost 100% pure cobalt under the conditions applied both reversibly (physisorbed) and irreversibly bound (chemisorbed) hydrogen were observed in H_2 chemisorption measurement is shown (Figure 3.1). Assuming a stoichiometry of 2 H atoms per Co atom for physisorption and 1 H atom per Co atom for chemisorption the overall number of surface metal atoms adsorbing H_2 was determined to be $0.46 \text{ mmol} \cdot \text{g}_{\text{Cat}}^{-1}$, the number of metal atoms physisorbing and chemisorbing H_2 was $0.10 \text{ mmol} \cdot \text{g}_{\text{Cat}}^{-1}$ and $0.36 \text{ mmol} \cdot \text{g}_{\text{Cat}}^{-1}$, respectively. Hence, physisorption took place on approximately 22% of the overall number of surface metal atoms. Assuming a transversal section of 6.5 \AA^2 for Co the metal surface area was calculated on the basis of the overall number of accessible metal atoms to be $18.7 \text{ m}^2 \cdot \text{g}_{\text{Cat}}^{-1}$. The BET area obtained by N_2 physisorption was $29.1 \text{ m}^2 \cdot \text{g}_{\text{Cat}}^{-1}$.

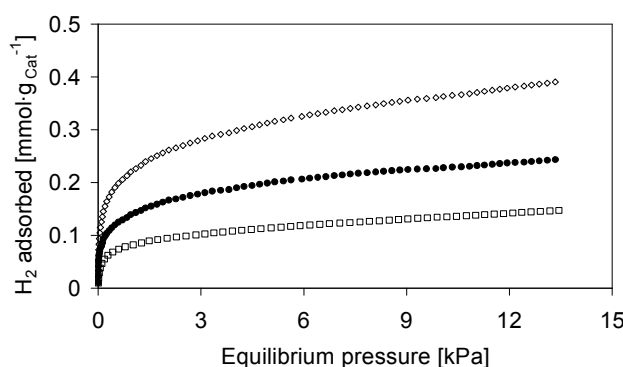


Figure 3.1: H_2 chemisorption data for Raney-Co ($T = 308 \text{ K}$). (\diamond) after outgassing for 6 h at $T = 473 \text{ K}$, (\square) after subsequent evacuation at $T = 308 \text{ K}$ ($p < 1 \text{ mPa}$ for 1 h), (\bullet) difference of (\diamond) and (\square). The amount adsorbed is obtained by extrapolating the linear part ($p = 6 \text{ kPa} - 13 \text{ kPa}$) of the respective curve to zero pressure.

Insight into the relative number and strength of different sorption sites was obtained by adsorption of CD_3CN . The sorption isotherm and the heat of adsorption as a function of the coverage (molecules of CD_3CN per surface atom of cobalt chemisorbing hydrogen [molecule/ $\text{Co}_{\text{Surface}}$]) are shown in Figure 3.2 and Figure 3.3, respectively. The coverage significantly increased at low pressures. Upon further increase of the pressure the sorption isotherm had showed a significant less steep increase, which suggests that it approaches a saturation value. The value was quantified by the fitting procedure described below. The differential

heat of adsorption was high ($200 - 215 \text{ kJ}\cdot\text{mol}^{-1}$) at low uptake ($< 0.08 \text{ molecules/Co}_{\text{Surface}}$) and showed a sharp decrease reaching an almost constant value of $57 - 65 \text{ kJ}\cdot\text{mol}^{-1}$ at higher coverage. The remarkably high heat of adsorption at low coverage can be attributed to the adsorption of CD_3CN on sites which strongly interact with the sorbate. Possibly, defect sites were present in small concentrations. At higher coverage sites, which exhibit weaker interaction with the sorbate resulted in lower heat of adsorption.

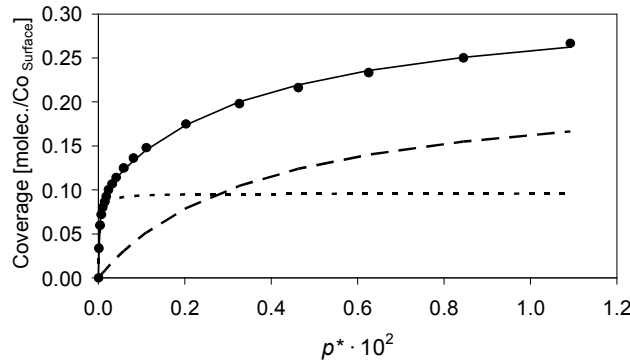


Figure 3.2: Sorption isotherm CD_3CN on Raney-Co at 308 K. (●) Experimental data and fitted curves with (-----) K_1 and q_1^{sat} , (- - -) K_2 and q_2^{sat} , (—) sum of both fitted curves. p^* is the partial pressure of CD_3CN normalized to standard conditions (i.e. $p^* = p/p^0$).

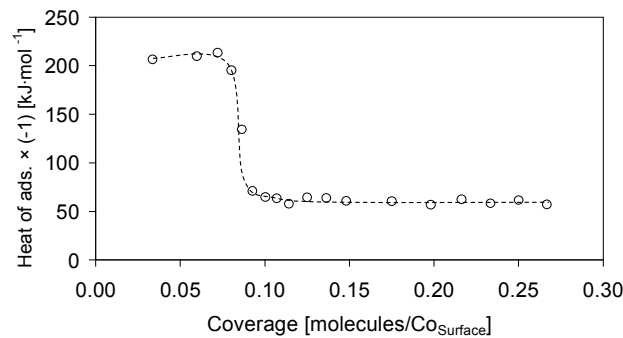


Figure 3.3: Differential heat of adsorption of CD_3CN on Raney-Co from calorimetry at 308 K.

The isotherm in Figure 3.2 was described by a dual-site Langmuir model in order to verify the assumption of two different adsorption sites. Therefore, the data was fitted with the following equation:^[27]

$$q = \sum_{j=1}^n q_j^{sat} \frac{K_j \cdot p^*}{1 + K_j \cdot p^*} \quad \text{Equ. 3.1}$$

in which K_j is the thermodynamic equilibrium constant for the sorption process on the site j , q_j^{sat} denotes the maximum sorption capacity on site j (molecules/metal atom) and p^* is the partial pressure of CD_3CN normalized to standard conditions ($p^* = p/p^0$). The contributions of

the individual sorption processes are included in Figure 3.2. A summary of the values obtained from the fitting procedure is given in Table 3.2. Here, q_1^{sat} nicely corresponds with the coverage, where the sudden change in the heat of adsorption was observed (see Figure 3.2). Thus, the dual-site model suggested based on two distinct heats of adsorption is underpinned by this result. Note that from Figure 3.2 and Table 3.2 it can be deduced that a fraction of $\sim 30\%$ of the overall number of sites is composed of strong sites (Sorption process 1). The sum of the saturation values of the two steps indicates that the overall saturation value approached ~ 0.3 molecules/ $\text{Co}_{\text{Surface}}$.

Table 3.2: Dual site Langmuir model for fitting the experimental sorption isotherm of CD_3CN on Raney-Co.

Sorption process	q_j^{sat} [molec./ $\text{Co}_{\text{Surface}}$]	K_j	$\Delta H_{ads} \times (-1)$ [kJ·mol $^{-1}$]
1	9.62×10^{-2}	3.94×10^4	200 – 215
2	22.23×10^{-2}	2.73×10^2	57 – 65

3.3.2. H/D exchange and selectivity in the hydrogenation of CD_3CN

In INS motions involving H atoms exhibit high signal intensity. This special characteristic was used to examine partially hydrogenated species on the catalyst surface. A low background was achieved by using a fully deuterated test molecule (CD_3CN).

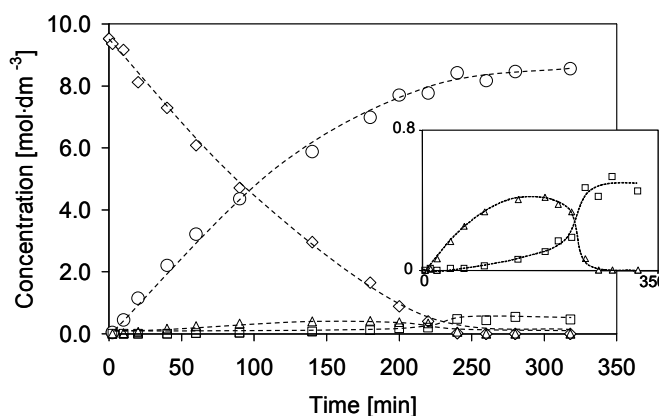


Figure 3.4: Concentration profile for the hydrogenation of CD_3CN over Raney-Co at 383 K, $p = 45$ bar and $c_0(\text{CD}_3\text{CN}) = 9.52 \text{ mol}\cdot\text{dm}^{-3}$. (\diamond) CD_3CN , (\circ) Ethylamine, (\triangle) N -ethylidene-ethylamine, (\square) Di-ethylamine.

However, this approach is appropriate only, if exchange between H atoms reacting with the nitrile group and D atoms from the methyl group can be excluded. Therefore, hydrogenation of CD_3CN over Raney-Co was carried out in the liquid phase and analyzed off-line

by ^1H and ^2H NMR spectroscopy to investigate the intramolecular distribution of H and D atoms. The focus here will be on examination of the H/D exchange with respect to the applicability in the INS experiments. A detailed discussion of the underlying mechanism will be presented in a parallel study.

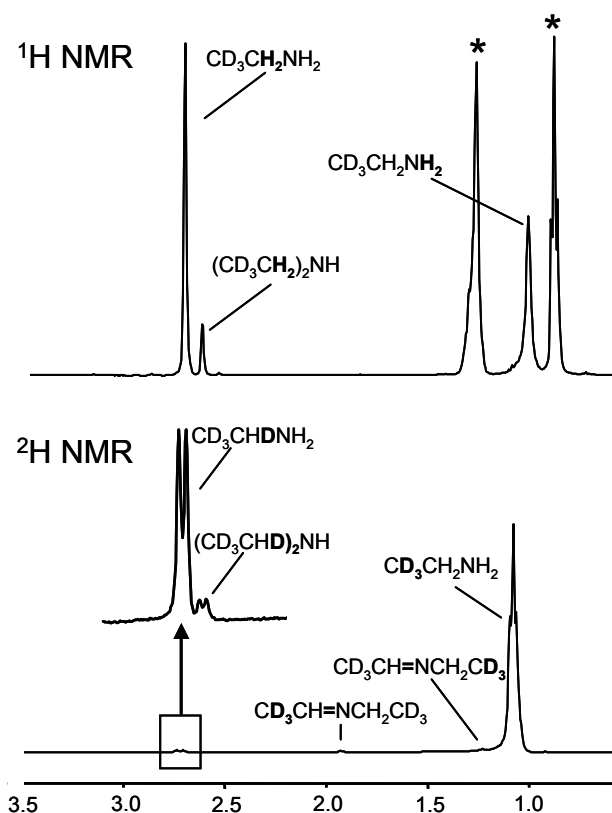


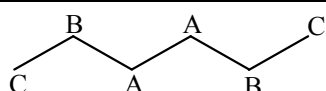
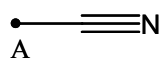
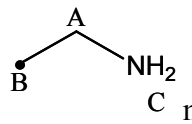
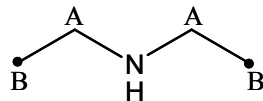
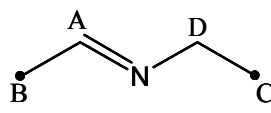
Figure 3.5: NMR spectra of the product mixture of the hydrogenation of CD_3CN . * = Hexane.

A concentration profile of the reaction derived from GC analysis is shown in Figure 3.4. The main product of the hydrogenation reaction was ethylamine- d_3 , which was formed with a selectivity of $\sim 90\%$. From the beginning of the reaction ethylamine and the intermediate *N*-ethylidene-ethylamine were found in the reaction mixture, which suggests that both are primary products. Only after most of CD_3CN ($\sim 90\%$) had been converted, the intermediate was further hydrogenated to the secondary product di-ethylamine. The selectivity obtained in the experiment was considered sufficient to prepare $\text{CD}_3\text{CH}_2\text{NH}_2$, which was used as a reference substance for INS measurements, by this procedure.

^1H NMR and ^2H NMR spectra of the final product mixture are shown in Figure 3.5. The assignment of the chemical shift to chemical groups is given in Table 3.3. The main product was $\text{CD}_3\text{CH}_2\text{NH}_2$ (peaks at 1.02 and 2.74 ppm in ^1H NMR and at 1.10 in ^2H NMR). Peaks with low intensity at 2.63 and at 2.74 ppm in ^2H NMR correspond to $(\text{CD}_3\text{CHD})_2\text{NH}$

and $\text{CD}_3\text{CHDNH}_2$, respectively. Thus, only little H/D exchange occurred (during the hydrogenation of CD_3CN of 0.83% the deuterons were found in products other than $\text{CD}_3\text{CH}_2\text{NH}_2$). With respect to the INS measurements it can, thus, be stated that the signals obtained can be attributed to hydrogen atoms, which reacted with the CN triple bond and not to hydrogen which exchanged with deuterons in the CD_3 group.

Table 3.3: Assignment of the chemical shift to chemical groups for the identification of the peaks obtained in the NMR-measurements of the final product resulting from the hydrogenation of CD_3CN .^[28, 29]

Molecule		Chemical shift [ppm]	Assignment
<i>n</i> -Hexane	A	1.27	
	B	1.27	
	C	0.88 t	
Acetonitrile	A	1.98	 consumed
Ethylamine	A	2.74	 main product
	B	1.10 t	
	C	(0.5 – 4.0)*	
Di-ethylamine	A	1.10	
	B	2.64	
<i>N</i> -ethylidene-ethylamine	A	3.35	
	B	1.80	
	C	1.20	
	D	not observed	

t = triplet, • = CD_3 , *position variable.

3.3.3. Results of INS measurements

3.3.3.1. Hydrogen adsorption on Raney-Co studied by INS

INS spectra of activated Raney-Co and hydrogen adsorbed on Raney-Co were taken to evaluate contributions from the background of hydrogen and Raney-Co in the measurements with CD_3CN . The results are presented in Figure 3.6. In a previous work a detailed DFT analysis of the INS spectrum of hydrogen adsorbed on Raney-Co had been performed.^[13] According to that data an assignment of the hydrogen vibrations observed in the present work

was conducted. In both cases, scattering contributions of hydrogen gave rise to a broad peak between 600 and 1100 cm^{-1} centred at around 850 to 900 cm^{-1} . For the sample with activated Raney-Co this suggests that some hydrogen could not be removed by the preparation procedure despite outgassing in high vacuum and at high temperature over several hours.

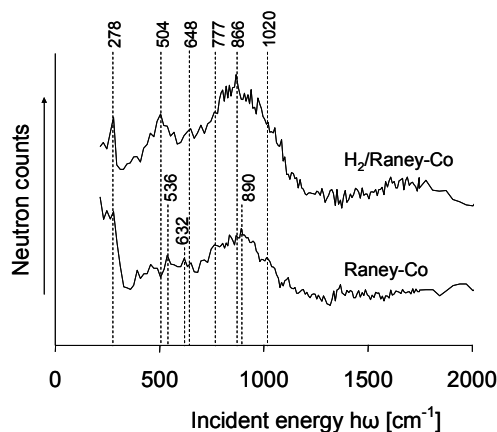


Figure 3.6: INS spectrum of activated Raney-Co and INS spectrum of hydrogen adsorbed on Raney-Co after subtraction of the spectrum of Raney-Co. The amount of hydrogen admitted was calculated based on a stoichiometry of one hydrogen atom per surface metal atom as determined by H_2 chemisorption.

This suggests that strongly bound hydrogen was present, which withstood the rather severe activation conditions. The contributions in this region with strongly bound hydrogen can be attributed to hydrogen on η^3 sites (Table 3.4).

Table 3.4: Vibrational frequencies and assignment of hydrogen adsorbed on Raney-Co.

ν_{INS}^a	ν_{INS}^b	ν_{INS}^c	Coord. mode	Plane	Symmetry	Vibration ^{c,d,e}
278	278	250	η^4	101	D_{4h}	$\text{Co}_4\text{-H}$ sym stretch
536	504	573	η^3	001	C_{3v}	$\text{Co}_3\text{-H}$ antisym stretch
632	648	637	η^3	101	C_{3v}	$\text{Co}_3\text{-H}$ antisym stretch
777	777	782	η^3	101	C_{3v}	$\text{Co}_2\text{-H}$ asym stretch
890	866	894	η^3	001	C_{3v}	$\text{Co}_2\text{-H}$ antisym stretch
1020	1020	1100	η^3	001	C_{3v}	$\text{Co}_3\text{-H}$ sym stretch
-	>1600	1660	f_σ	-	-	Co-H stretch

^aThis work (activated Raney-Co). ^bThis work (activated Raney-Co after addition of hydrogen). ^cRef^[13]. ^dRef^[22]. ^eRef^[20]. ^fProbably hydrogen on some 1-fold sites. However, the DFT calculations of single bound hydrogen on 101 and 001 planes yields a peak at 1800 – 1860 cm^{-1} .

After addition of hydrogen scattering contributions over the whole range increased in intensity. However, the main increase in scattering was observed in the range up to 1200 cm^{-1} . A distinct peak centred at 504 cm^{-1} appeared stemming most likely from hydrogen adsorbed on η^3 sites with C_{3v} symmetry in the 001 plane. Upon addition of hydrogen small scattering contributions above 1500 cm^{-1} occurred probably due to some hydrogen adsorbed on σ sites. However, the signal was relatively small compared to multiply bound hydrogen. The band positions of residual hydrogen on activated Raney-Co and on Raney-Co loaded with extra hydrogen should in principle be the same. The slight differences observed are, thus, a measure of the experimental error, which is very likely due to the resolution of incident energy in the respective regions.

3.3.3.2. Co-adsorption of CD_3CN and hydrogen on Raney-Co

To explore the structure and sorption properties of partially hydrogenated species during the reaction between acetonitrile and hydrogen, CD_3CN and different amounts of hydrogen were filled into the INS sample containers. The INS spectra of CD_3CN , CD_3CN with 0.5, 1.5 and 2.0 equivalents of hydrogen and $CD_3CH_2NH_2$ adsorbed on activated Raney-Co are presented in Figure 3.7.

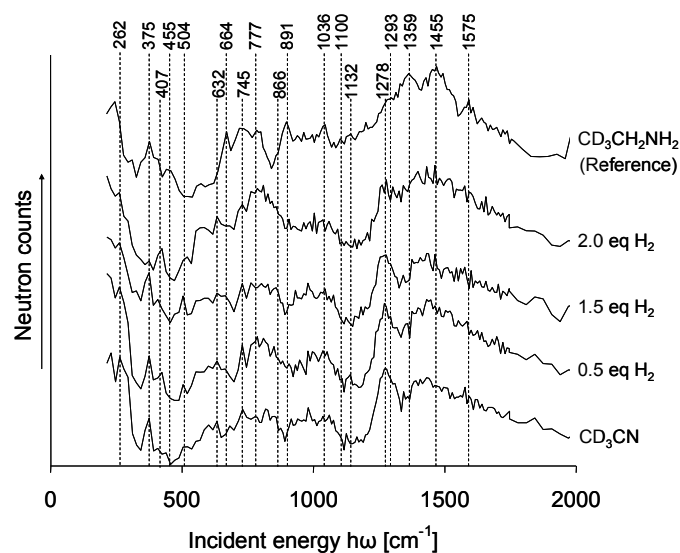


Figure 3.7: INS spectra of different amounts of hydrogen co-adsorbed with CD_3CN (loading 0.18 molecules per surface metal atom) on activated Raney-Co. The amount of hydrogen was calculated based on a ratio of H_2/CD_3CN of 0.5, 1.5 and 2.0, respectively. For comparison the spectra of CD_3CN and $CD_3CH_2NH_2$ adsorbed on activated Raney-Co are also given. The spectrum of activated Raney-Co has been subtracted from all the spectra shown.

For an assignment of the vibrational modes obtained experimentally, the results are compared to data available from literature and to calculated INS spectra. In Table 3.5 experi-

mental INS and IR frequencies for CH₃CN and CD₃CN from literature are compared to calculated vibrational modes from this work to verify the DFT data. From gas phase IR data and INS on solid CH₃CN it can be seen that slight deviations in the vibrational modes obtained with the two different techniques were obtained. INS data resulting from DFT calculations compared to gas phase IR data show a similar difference for CD₃CN. Thus, calculations are in good agreement with literature data reported by Friend et al.^[30] The respective spectrum with bands arising at 354, 842, 875, 1067, 1138, 2198 and 2268 cm⁻¹ is shown in Figure 3.9. The peaks with the highest intensity were assigned to the C-C-N bending mode at 354 cm⁻¹, the C-C stretching mode at 842 cm⁻¹ and the CH₃ symmetric bending mode at 1138 cm⁻¹.

Table 3.5: Vibrational frequencies of CH₃CN and CD₃CN. Experimental data from literature together with vibrational frequencies of CD₃CN calculated by DFT.

CH ₃ CN		CD ₃ CN		Assignment
IR gas ^a	INS ^b	IR ^{c,#}	DFT ^d	
	75			Lattice mode
	120			Lattice mode
	160			Methyl torsion
361	396	347	354	CCN bend
920	928	902	842	CC stretch
1041	1056	(833)	(875)	CH ₃ /(CD ₃) rock
1389	1390	(1093)	(1138)	CH ₃ /(CD ₃) sym bend
1454	1453		(1067)	CH ₃ /(CD ₃) antisym def
2268		2291	2198	CN stretch
2954		(2110)	(2268)	CH ₃ /(CD ₃) sym stretch

^aRef^[31]. ^bRef^[21]. ^cRef^[30]. [#]Calculated from CH₃CN data by using deuteration shift ratios given in the reference. ^dThis work.

For assignment of the vibrational modes in the experimental INS data, the spectra obtained for species adsorbed on Raney-Co were compared to literature data of CH₃CN and CD₃CN (summarized in Table 3.6) and of ethylamine (see Table 3.7) adsorbed on different metals. No data for adsorbed CD₃CH₂NH₂ were available. However, gas phase IR data of non-deuterated ethylamine^[32-34] was previously compared to ethylamine adsorbed on Ni(111).^[35] To conduct a similar comparison, DFT calculations were performed to obtain INS vibrational modes for pure CD₃CH₂NH₂. The experimental data together with DFT results are summarized in Table 3.7.

Table 3.6: Selected literature data on the vibrations of CD₃CN and CH₃CN adsorbed on different metals.

CH ₃ CN		CD ₃ CN		Assignment
Raney-Ni ^a	Ni(111) ^b Pt(111) ^c	Pt(111) ^c		
52				CH ₃ torsion
100				Hindered translations and motions
160				CH ₃ torsion
		280	265	Pt-MeCN stretch sym
		410	385	Pt-MeCN stretch asym
385, 392	360			CCN bend
520	520	605	580	CCN bend
	900 (sh)	950	930	CC stretch
1047, 1042	1020	1060	(850)	CH ₃ /(CD ₃) rock
1427, 1450	1400	1375	(1100)	CH ₃ /(CD ₃) sym bend
		1435		CH ₃ deg bend
	1680	1615	1625	CN stretch
	2910			CH ₃ sym stretch

^aRef^[21]. ^bRef^[30, 35]. ^cRef^[36].

The spectrum of CD₃CN on Raney-Co exhibited a distinct peak at 375 cm⁻¹, a broad scattering region with strongly overlapping features between 600 and 1100 cm⁻¹, a distinct peak at 1278 cm⁻¹ and a broad peak starting at 1300 cm⁻¹ with a long tailing to 1800 cm⁻¹. The experimental results are compared to the calculated INS spectrum of CD₃CN in Figure 3.9. It can be seen that there is little similarity of experiment and simulation. The fact that the rather distinct bands at 875 and 1067 cm⁻¹ were not observed in the experiment could be due to residual hydrogen masking the peaks. However, the intense bands at higher wavenumbers (1278 – 1800 cm⁻¹) cannot be attributed to this effect, as was shown by the measurements of hydrogen adsorbed on Raney-Co. It had been reported that the vibrational modes of CD₃CN and CH₃CN can be strongly influenced upon adsorption on Pt (111) and Ni(111), respectively.^[30, 35, 36] In both cases one signal was not observed, while a new one appeared (shifted by up to 650 cm⁻¹) after adsorption. However, in general the spectra of the gas phase and the adsorbed state were similar and did not change in such a distinct manner as observed here.

Experimental INS data reported for CH₃CN adsorbed on Raney-Ni,^[21] which is expected to behave similar as Raney-Co, only showed little difference between CH₃CN in the gas phase and adsorbed on Raney-Ni. The results described above lead to the assumption that

the observed INS spectrum was not due to CD_3CN coordinated to Raney-Co. It is rather likely that CD_3CN readily reacted with hydrogen not removed from the surface during the activation of Raney-Co resulting either in $\text{CD}_3\text{CH}_2\text{NH}_2$ or an intermediate.

In Figure 3.7 the main peaks of $\text{CD}_3\text{CH}_2\text{NH}_2$ adsorbed on Raney-Co are marked and the respective wavenumber values are depicted. As shown in Table 3.7 INS data simulated with DFT for $\text{CD}_3\text{CH}_2\text{NH}_2$ are similar to the IR gas phase data for $\text{CH}_3\text{CH}_2\text{NH}_2$ as measured by Hamada et al.^[32] Hence, it was decided to perform assignment of most of the bands exhibited by $\text{CD}_3\text{CH}_2\text{NH}_2$ adsorbed on Raney-Co based on the literature available for $\text{CH}_3\text{CH}_2\text{NH}_2$ adsorbed on Ni(111). Additionally, it was decided to simulate the *trans* form of $\text{CD}_3\text{CH}_2\text{NH}_2$ because it was suggested in literature that compared to the *gauche* form this is the form, which more likely occurs on the surface.^[35]

Smaller differences in the vibrational modes of CH_2 , NH_2 , CCN , CC and CN are most likely due to the shift between INS and IR bands as previously described for CD_3CN , whereas the remarkable difference (shift from 2880 to 2176 cm^{-1}) in the CH_3 symmetric stretch band is attributed to the exchange of H by D in the methyl group. As shown in Table 3.7 most of the experimental INS band positions were similar to gas phase, DFT and literature data for adsorbed ethylamine and could, thus, be assigned accordingly. The shoulder peak at 407 cm^{-1} was also observed in the DFT results (Figure 3.9), but could not be assigned. An additional peak at 455 cm^{-1} may be due to cobalt-nitrogen vibrations as the value is comparable to nickel-nitrogen vibrations observed at 500 cm^{-1} for ethylamine on Ni(111)^[35] and at 490 cm^{-1} for NH_3 on Ni(111).^[37] DFT simulation exhibited bands at 499 and 596 cm^{-1} (not assigned), which were either overlapped or of too low intensity to find them in the experimental INS results. A band at 1293 cm^{-1} (shoulder) experimentally observed may be attributed to a shifted CH_2 twist, found at 1226 cm^{-1} in the simulated vibrations. In general the relative peak intensity in the experiment is comparable to that from DFT calculations in the lower frequency region (up to $\sim 1200 \text{ cm}^{-1}$). At higher incident energy the intensity of the bands is relatively high compared to the simulation.

The INS results of the adsorption of CD_3CN on Raney-Co in presence of increasing amounts of hydrogen showed similar features as for $\text{CD}_3\text{CH}_2\text{NH}_2$ (see Figure 3.7). However, differences were observed, which require further attention. Again the data in Table 3.7 is consulted for band assignment. In order to distinguish co-adsorbed hydrogen from other surface species vibrations from Table 3.4 and Figure 3.6 were also taken into account and marked in Figure 3.7.

Table 3.7: Vibrational frequencies of CH₃CH₂NH₂ and CD₃CH₂NH₂ in the gas phase and adsorbed on different metals.

Gas phase			Ni(111) ^c	Raney-Co ^b		Assignment
gauche ^a	trans ^a	DFT ^b	HREELS	INS		
		297		245		NH ₂ rock
403		362		375		CCN bend
		664		664		CH ₂ rock
		755		745		CD ₃ /bend
773	790	850	760	891		NH ₂ wag
892	882	975	880	1036		CC stretch
1016		955				NH ₂ twist
1016	1119	(1086)	1140	(1100)		CH ₃ /(CD ₃) d rock
1086	1055	1122	1080	1132		CN stretch
1238	1350	1226		1293		CH ₂ twist
1378						CH ₃ sym def
1397		1387	>1360	1359		CH ₂ wag
1465			>1440			CH ₃ d def
1487		1508		1455		CH ₂ scission
1622		1673	1540	1575		NH ₂ scission
2880		(2176)	2960	-		CH ₃ /(CD ₃) sym stretch
		(2296)		-		CH ₃ /(CD ₃) asym stretch
2885		3040	2680	-		CH ₂ sym stretch

^aRef^[32-34], CH₃CH₂NH₂. ^bThis work, CD₃CH₂NH₂ in the *trans* form. ^cRef^[35].

Upon adding hydrogen stepwise to CD₃CN the scattering characteristics changed rendering spectra similar to the reference spectrum of CD₃CH₂NH₂. The spectra were similar to that for CD₃CN on Raney-Co, which again is an indication that CD₃CN was not the prevailing molecule in the sample. Additionally, it has to be considered that as shown in Figure 3.6 hydrogen exhibits bands mainly in the region below 1200 cm⁻¹. Hence, the significant scattering contributions above this value can be attributed to partially hydrogenated or product molecules.

For the three samples with hydrogen and for the sample with CD₃CN a band at 262 cm⁻¹ was assigned to co-adsorbed hydrogen on η⁴ sites with D_{4h} symmetry. The CCN bending mode was located at 375 cm⁻¹. Again, a band at 407 cm⁻¹ was observed, which could not be clearly identified. The weak band at 504 cm⁻¹ was assigned to Co₃-H antisymmetric stretch

on η^3 coordination modes. In the region between 600 cm^{-1} and 1200 cm^{-1} features of the partially hydrogenated or product molecules were overlapping with scattering contributions of co-adsorbed hydrogen making unambiguous peak assignment difficult. However, it can be stated that upon increasing the amount of hydrogen a broad band centred at 777 cm^{-1} , which was previously assigned to $\text{Co}_2\text{-H}$ asymmetric stretch η^3 sites, increased. The band at 745 cm^{-1} may be due to CD_3 bending modes. NH_2 wag and CC stretch modes found at 891 cm^{-1} and 1036 cm^{-1} for $\text{CD}_3\text{CH}_2\text{NH}_2$, respectively, were either relatively weak or overlapped by hydrogen vibration modes as no distinct peaks were found in that region. With exception of the hydrogen band at 777 cm^{-1} , no definitive trend in the intensity of the bands was obtained up to 1200 cm^{-1} . However, an interesting band was observed at 1278 cm^{-1} exhibiting relatively high intensity for CD_3CN only. Compared to the broad signal above 1300 cm^{-1} the relative intensity of this band decreased with increasing amount of hydrogen. In the case of $\text{CD}_3\text{CH}_2\text{NH}_2$ a shoulder at 1293 cm^{-1} was attributed to a CH_2 twisting mode. It will be considered in the discussion section, if this mode is also responsible for the relatively strong signal in the case of co-adsorption of CD_3CN and hydrogen

A broad band between 1300 and 1800 cm^{-1} was found for all samples with CD_3CN and CD_3CN plus hydrogen being similar to the pattern observed for $\text{CD}_3\text{CH}_2\text{NH}_2$. Compared to the band at 1278 cm^{-1} the relative intensity of the band increased with increasing amount of hydrogen. This is an indication that an intermediate species was converted upon adding hydrogen resulting in an increasing amount of $\text{CD}_3\text{CH}_2\text{NH}_2$. However, the single peaks as found for $\text{CD}_3\text{CH}_2\text{NH}_2$ at 1359 , 1455 and 1575 cm^{-1} were not as well resolved suggesting that other molecules were present which exhibited a different scattering behaviour. Thus, the broad band would be a result of overlapping signals from $\text{CD}_3\text{CH}_2\text{NH}_2$ and intermediate species.

3.4. Discussion

3.4.1. Role of hydrogen sorption strength

For Raney-Ni the presence of different sites strongly and weakly adsorbing hydrogen has been reported.^[22] H_2 chemisorption and INS experimental results for hydrogen adsorbed on Raney-Co also indicated the presence of strongly and weakly bound hydrogen. The two techniques cannot be directly compared but provide complementary results. INS measurements of activated Raney-Co showed that strongly bound hydrogen could not be removed from the surface by the activation procedure. The sample for H_2 chemisorption measurements underwent the same pre-treatment before adding hydrogen stepwise. Thus, hydrogen residing on the catalyst surface after pre-treatment could not be quantified. However, it was found that

hydrogen was partly chemisorbed and partly physisorbed suggesting that two different sorption sites are present on activated Raney-Co. Hence, taking into account hydrogen not removed during the activation procedure three different levels of adsorption prevail (strongly chemisorbed, chemisorbed and physisorbed hydrogen).

In the INS experiments the three levels could not be distinguished, but sorption sites for hydrogen were identified. Taking into account the experiments with varying amounts of hydrogen co-adsorbed with CD₃CN one may get insight into the reactivity of hydrogen adsorbed on those different sites. Especially in the sample with 2.0 equivalents of hydrogen (see Figure 3.7) it was observed that differences occur between Raney-Co (see Figure 3.6) and hydrogen co-adsorbed with CD₃CN assuming that reaction took place, but not all of the hydrogen added reacted. As it cannot be excluded that scattering contributions of intermediate species or CD₃CH₂NH₂ were overlapping with bands of non-reacted hydrogen the discussion will be restricted to bands, which can be attributed to hydrogen mainly. Upon increasing the amount of hydrogen scattering contributions assigned to hydrogen increased relatively strongly in the region around 632 and 777 cm⁻¹ (hydrogen on η³ sites with C_{3v} symmetry on the 101 plane). Whereas scattering contributions at 504, 866 and 1020 cm⁻¹ (all of them corresponding to various vibrational modes of hydrogen on η³ sites with C_{3v} symmetry on the 001 plane) increased less. Therefore, it is suggested that hydrogen adsorbed on the latter sites preferably reacted with CD₃CN. In agreement with literature^[22] it is concluded that hydrogen on latter sites is weakly chemisorbed hydrogen, as this kind of hydrogen is more reactive.

3.4.2. *Intermediate species in the co-adsorption of CD₃CN and hydrogen on Raney-Co*

Results of the INS experiment with CD₃CN as sole adsorbate did not show significant agreement with literature data of gas phase and adsorbed CD₃CN.^[36] Also the INS spectrum of CD₃CN calculated with (shown in Figure 3.9 for comparison) was quite different from experimental data especially at higher incident energy (above 1200 cm⁻¹). Thus, it was concluded that a species other than CD₃CN, which was formed by reaction with residual hydrogen prevailed on the surface. The assumption that a reaction took place is supported by TG/DSC results showing that on one type of sites strong adsorption of CD₃CN occurred, which leads to strong activation and hence high reactivity of CD₃CN.

Based on the assumption that a reaction took place, the question arises, which species are formed. The most obvious explanation would be that CD₃CN was completely converted to CD₃CH₂NH₂. As described above there are, in deed, some similarities with the spectrum of CD₃CH₂NH₂, but it has also been shown that remarkable differences appeared. Especially the

relatively strong band at 1278 cm^{-1} was much weaker (and slightly shifted to 1293 cm^{-1}) for $\text{CD}_3\text{CH}_2\text{NH}_2$ compared to the samples with CD_3CN co-adsorbed with hydrogen. Hence, it is suggested that a mixture of intermediate species, of which the most characteristic feature is the band at 1278 cm^{-1} and $\text{CD}_3\text{CH}_2\text{NH}_2$ co-exist on the surface. When increasing the hydrogen pressure, the peak area decreased relative to the band regions, which are more characteristic for $\text{CD}_3\text{CH}_2\text{NH}_2$ (above 1300 cm^{-1}). This observation suggests that by increasing the hydrogen pressure the equilibrium was shifted to fully hydrogenated product. Partially hydrogenated intermediate species co-exist, however, only on the surface if they are energetically comparable to adsorbed $\text{CD}_3\text{CH}_2\text{NH}_2$. In this respect, it has been shown in a molecular modelling study of amine dehydrogenation over Ni(111) that the partly dehydrogenated intermediate acimidoyl ($\text{CH}_3\text{-C}^*=\text{NH}$, where * symbolizes coordination to a metal atom) was energetically lower than adsorbed ethylamine.^[38]

Before discussing sorption structures of possible intermediates the adsorption mode of $\text{CD}_3\text{CH}_2\text{NH}_2$ will be examined. Based on observations in literature^[35, 37] it is suggested that it is adsorbed molecularly through its nitrogen lone pair electrons. The existence of a cobalt-nitrogen stretching mode supports this assumption. For the experimental spectrum of $\text{CD}_3\text{CH}_2\text{NH}_2$ the band at 1293 cm^{-1} was assigned to CH_2 twisting. For the same mode DFT calculations predict a band at 1226 cm^{-1} . Conversely, CH_2 wagging was shifted to a lower frequency upon adsorption on Raney-Co. In literature it was suggested that interaction of hydrogen with Ni(111) surface weakened the CH bond.^[35, 39] However, with the results obtained in this study this cannot be unambiguously stated.

Above it has been established that intermediate species are formed during co-adsorption of CD_3CN and hydrogen. The structure of this intermediate requires elucidation. In principle several surface structures are possible after reaction of CD_3CN with 2 atoms of hydrogen. In Figure 3.8 three such surface structures as proposed in literature are summarized. Here, it will be discussed, which of the intermediates is most likely according to the INS experiments.

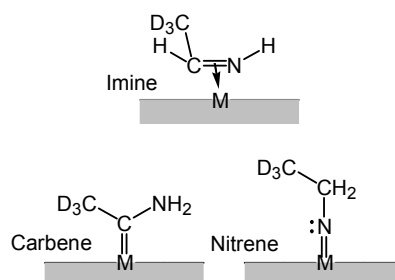


Figure 3.8: Surface structures after reaction of CD_3CN with 2 hydrogen atoms based on suggestions found in the literature.^[8, 40]

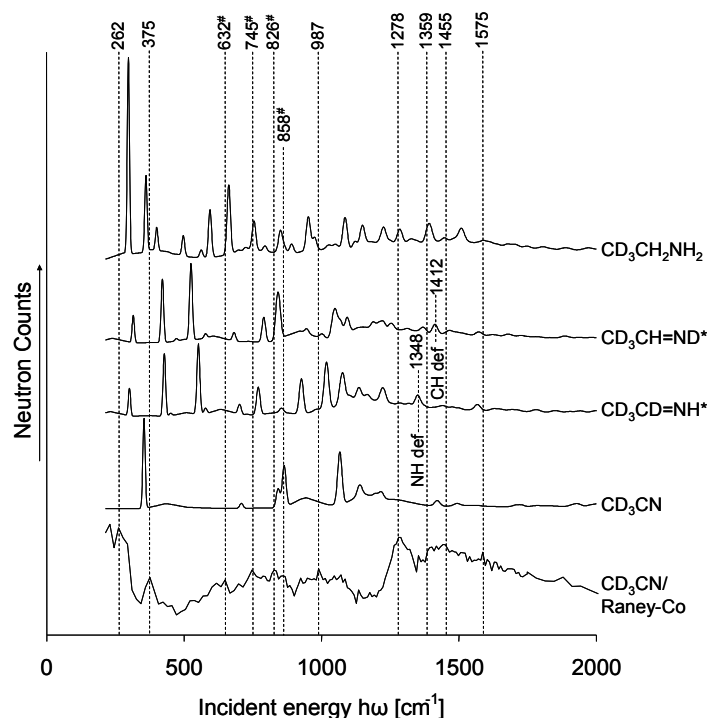


Figure 3.9: Experimental INS spectrum of CD_3CN adsorbed on activated Raney-Co compared to calculated gas phase INS spectra of reactant, possible intermediate and product species. #Region in which significant hydrogen contributions were observed for activated Raney-Co. *Calculated as a model for surface imine species. Exchanging H and D was performed to differentiate between CH and NH vibrational modes.

In order to investigate if imine-like species were formed INS data for pure imine were calculated by means of DFT and compared to experimental results (presented in Figure 3.9). As H atoms exhibit much higher intensity they were selectively exchanged by D atoms in the CN double bond to differentiate between contributions of CH and NH vibrational modes. The experimental spectrum for CD_3CN on Raney-Co is shown as comparison, as the band at 1278 cm^{-1} , which is assumed to be related with the intermediate species, is most intense. The high intensity suggests that H atoms must be involved in this vibrational mode. For comparison the simulated spectra of CD_3CN and $\text{CD}_3\text{CH}_2\text{NH}_2$ are shown. Distinct bands of the experimental spectrum are marked to evaluate the agreement with calculated spectra. However, it can be seen that the experimental data is somewhat noisy with not always clearly resolved peaks and may be overlapped by hydrogen in the region between 632 and 858 cm^{-1} . Additionally, the relative band intensity in the experimentally determined spectrum for $\text{CD}_3\text{CH}_2\text{NH}_2$ is quite different from the simulated spectrum, which might be an indication for very strong interaction with the surface. In none of the simulated spectra such a distinct peak at 1278 cm^{-1} is predicted. In the simulated imine spectra the vibrations involving hydrogen closest to this strong band are depicted. The NH deformation of $\text{CD}_3\text{CD}=\text{NH}$ exhibited a low intensity band at 1348 cm^{-1} . CH deformation of $\text{CD}_3\text{CH}=\text{ND}$ resulted in a band with even lower intensity at

1412 cm^{-1} . π -Coordination of the imine to the surface (see Figure 3.8) may result in a blue shift leading to the experimentally observed bands at 1278 cm^{-1} and 1387 cm^{-1} , respectively. However, due to the agreement of the strong band at 1278 cm^{-1} with the experimentally obtained band at 1293 cm^{-1} for CH_2 twisting modes of $\text{CD}_3\text{CH}_2\text{NH}_2$ it is assumed that it appears more likely that this mode is responsible for the strong band. Thus, no evidence for the existence of an imine-like intermediate was found.

Of the two species carbene and nitrene (shown in Figure 3.8), only nitrene can have CH_2 vibrational modes. Hence, only this compound may exhibit the band at 1278 cm^{-1} due to CH_2 twisting. In Figure 3.7 the NH_2 wagging mode resulted in a relatively well resolved band at 891 cm^{-1} for $\text{CD}_3\text{CH}_2\text{NH}_2$. No such distinct band was observed for the other spectra. It is assumed that hydrogen did not overlap the peak, which is appropriate, as the amount of hydrogen in the sample with CD_3CN and $\text{CD}_3\text{CH}_2\text{NH}_2$ only, was the same due to the same activation procedure. Hence, it is concluded that NH_2 groups were only of low concentration in the intermediate surface species suggesting that nitrene species were the most abundant intermediates. However, the question arises, why CH_2 twisting modes should be more intense relative to the CH_2 wagging and deformation modes with bands at 1359 cm^{-1} and 1455 cm^{-1} , respectively, in nitrene than in $\text{CD}_3\text{CH}_2\text{NH}_2$. This can tentatively be explained by assuming different adsorption modes of the respective molecules. As mentioned above $\text{CD}_3\text{CH}_2\text{NH}_2$ adsorbs most likely *via* its nitrogen lone electron pair resulting in an N-M σ -bond, whereas nitrene results in a N-M double bond. It is suggested that the CH_2 twisting mode leads to a torsional movement of the NM bond resulting in little change in the orbital overlap of nitrogen and the metal. Hence the difference between the two bonding modes might be smaller than with CH_2 wagging. This movement causes a stretch of the C-M bond, in which the change of the orbital overlap is assumed to be considerably higher. Consequently, the CH_2 wagging may have higher intensity with $\text{CD}_3\text{CH}_2\text{NH}_2$, as the overlap can take place more easily in a σ -bond.

Transition metal complexes can be used for comparison to help in the interpretation of the actual catalysis mechanism.^[8] Therefore, a search of the Cambridge Crystallographic Database was performed and several stable nitrene-like intermediates were found.^[41, 42] One of the complexes is exemplarily shown in Figure 3.10, supporting the assumption that similar nitrene species might also prevail in the hydrogenation over Raney-Co catalysts. In fact, they have also been reported in surface studies on a Ni/C catalyst^[43] and suggested to be the most stable intermediates in the hydrogenation of acetonitrile over Ni surfaces based on DFT results.^[3]

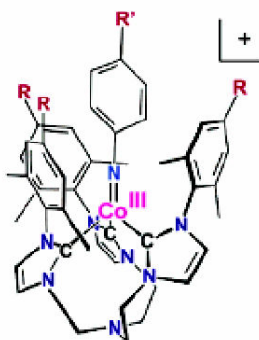


Figure 3.10: Organometallic complex with nitrene functionality.^[42]

3.5. Conclusions

Experimental and calculated INS spectra were combined with spectroscopic data from literature to examine partly hydrogenated surface species in the co-adsorption of CD₃CN and H₂ on Raney-Co. As INS is very sensitive to H atoms, CD₃CN was used as a probe molecule to keep scattering contributions stemming from the methyl group low. Preparatory experiments showed that very little H/D exchange occurred during hydrogenation of CD₃CN, which resulted in high selectivity (90%) to CD₃CH₂NH₂. In TG/DSC measurements two different types of sites for the adsorption of CD₃CN were found. One type shows a particularly strong interaction with CD₃CN. Combination with H₂ chemisorption results showed that at the maximum sorption capacity for CD₃CN ~ 30% of the cobalt surface atoms were occupied.

The combination of INS and H₂ chemisorption results confirmed that under the conditions applied three levels of hydrogen adsorption were present (strong chemisorption, chemisorption and physisorption). Additionally, it was suggested that hydrogen adsorbed on η^3 sites with C_{3v} symmetry was less strongly bound than hydrogen adsorbed on other sites and, thus, most reactive. Comparison of simulated and measured INS results confirmed that the sorbates strongly interacted with the adsorption sites. A band at 1278 cm⁻¹, which was relatively strong in the samples with co-adsorbed CD₃CN and H₂ and decreased in intensity with increasing amount of H₂, was tentatively assigned to the CH₂ twisting mode. The relative decrease of this band compared to CH₂ wagging led to the assumption that a nitrene-like compound was the most abundant intermediate species on the surface.

Acknowledgement

The authors thank the Institut Laue-Langevin for kindly granting measuring time at the IN1-BeF spectrometer to record the INS spectra. In particular, Dr. Alexander Ivanov and Pierre Palleau are thanked for their assistance during the INS experiments. W. R. Grace & Co is

thanked for the donation of the Raney-Co 2700 sample. Experimental support of Xaver Hecht and Manuel Stratmann is acknowledged. Klaus Ruhland and Ceta Krutsch from the Chair of Inorganic Chemistry are acknowledged for performing the NMR measurements.

References

- [1] K. Weissermel, H. J. Arpe, *Industrial Organic Chemistry*, 3. ed., Wiley-VCH, Weinheim, **1997**.
- [2] J. von Braun, G. Blessing, F. Zobel, *Chem. Ber.* **1923**, *56*, 1988.
- [3] B. Bigot, F. Delbecq, A. Milet, V. H. Peuch, *J. Catal.* **1996**, *159*, 383.
- [4] B. Bigot, F. Delbecq, V. H. Peuch, *Langmuir* **1995**, *11*, 3828.
- [5] Y. Y. Huang, W. M. H. Sachtler, *Appl. Catal. A-Gen.l* **1999**, *182*, 365.
- [6] Y. Y. Huang, W. M. H. Sachtler, *J. Catal.* **1999**, *188*, 215.
- [7] B. Coq, D. Tichit, S. Ribet, *J. Catal.* **2000**, *189*, 117.
- [8] C. DeBellefon, P. Fouilloux, *Catal. Rev.-Sci. Eng.* **1994**, *36*, 459.
- [9] Y. Y. Huang, W. M. H. Sachtler, *J. Catal.* **2000**, *190*, 69.
- [10] Y.-Y. Huang, W. M. H. Sachtler, *Stud. Surf. Sci. Catal.* **2000**, *130A*, 527.
- [11] M. S. Wainwright, in *Preparation of Solid Catalysts* (Eds.: G. Ertl, H. Knözinger, J. Weitkamp), Wiley-VCH, Weinheim, **1999**, p. 28-43.
- [12] J. Volf, J. Pasek, *Stud. Surf. Sci. Catal.* **1986**, *27*, 105.
- [13] A. Chojecki, H. Jobic, A. Jentys, T. E. Muller, J. A. Lercher, *Catal. Lett.* **2004**, *97*, 155.
- [14] A. Chojecki, Dissertation thesis, TU München **2004**.
- [15] P. Scharringer, T. E. Muller, W. Kaltner, J. A. Lercher, *Ind. Eng. Chem. Res.* **2005**, *44*, 9770.
- [16] R. Schenkel, A. Jentys, S. F. Parker, J. A. Lercher, *J. Phys. Chem. B* **2004**, *108*, 15013.
- [17] S. F. Parker, J. W. Taylor, P. Albers, M. Lopez, G. Sextl, D. Lennon, A. R. McInroy, I. W. Sutherland, *Vibr. Spectr.* **2004**, *35*, 179.
- [18] S. Vasudevan, J. M. Thomas, C. J. Wright, C. Sampson, *J. Chem. Soc.-Chem. Commun.* **1982**, 418.
- [19] R. Schenkel, A. Jentys, S. F. Parker, J. A. Lercher, *J. Phy. Chem. B* **2004**, *108*, 7902.
- [20] H. Jobic, A. Renouprez, *J. Chem. Soc.-Far. Trans. I* **1984**, *80*, 1991.
- [21] F. Hochard, H. Jobic, G. Clugnet, A. Renouprez, J. Tomkinson, *Catal. Lett.* **1993**, *21*, 381.
- [22] F. Hochard, H. Jobic, J. Massardier, A. J. Renouprez, *J. Mol. Catal. A-Chem.* **1995**, *95*, 165.
- [23] <http://www.ill.fr/YellowBook/INI> (accessed Dec 2006).

- [24] M. J. T. Frisch, G. W.; Schlegel, H. B.; Scuseria, G. E.; Robb, J. R. Z. M. A.; Cheeseman, V. G.; Montgomery, J. A., Jr., R. E. B. Stratmann, J. C.; Dapprich, S.; Millam, J. M.; Daniels, A., K. N. S. D.; Kudin, M. C.; Farkas, O.; Tomasi, J.; Barone, V.; Cossi, R. M. M.; Cammi, B.; Pomelli, C.; Adamo, C.; Clifford, S., J. P. Ochterski, G. A.; Ayala, P. Y.; Cui, Q.; Morokuma, K.; Malick, A. D. R. D. K.; Rabuck, K.; Foresman, J. B.; Cioslowski, J., J. V. B. Ortiz, A. G.; Stefanov, B. B.; Liu, G.; Liashenko, A.; Piskorz, I. G. P.; Komaromi, R.; Martin, R. L.; Fox, D. J.; Keith, T.; Al-Laham, M. A. P. Laham, C. Y.; Nanayakkara, A.; Challacombe, M.; Gill, P., B. C. M. W.; Johnson, W.; Wong, M. W.; Andres, J. L.; Gonzalez, C., M. R. Head-Gordon, E. S.; Pople, J. A., *GAUSSIAN 98*. Gaussian, Inc., Pittsburgh, PA, **1998**.
- [25] D. Champion, J. Tomkinson, G. Kearley, *Appl. Phys. A-Mater. Sci. Proc.* **2002**, *74*, S1302.
- [26] A. J. Ramirez-Cuesta, *Comput. Phys. Commun.* **2004**, *157*, 226.
- [27] A. Jentys, R. R. Mukti, H. Tanaka, J. A. Lercher, *Microp. Mesop. Mater.* **2006**, *90*, 284.
- [28] M. Hesse, H. Meier, B. Zeeh, *Spektroskopische Methoden in der organischen Chemie*, 3 ed., Georg Thieme Verlag, Stuttgart, **1987**.
- [29] E. Pretsch, T. Clerc, J. Seibl, S. Wilhelm, *Tabellen zur Strukturaufklärung organischer Verbindungen mit spektroskopischen Methoden, Vol. 15*, 3 ed., Springer-Verlag, Berlin, **1986**.
- [30] C. M. Friend, E. L. Muetterties, J. L. Gland, *J. Phys. Chem.* **1981**, *85*, 3256.
- [31] J. E. D. Davies, *J. Mol. Struct.* **1971**, *9*, 483.
- [32] Y. Hamada, K. Hashiguchi, A. Y. Hirakawa, M. Tsuboi, M. Nakata, M. Tasumi, S. Kato, K. Morokuma, *J. Mol. Spectrosc.* **1983**, *102*, 123.
- [33] H. Wolff, H. Ludwig, *J. Chem. Phys.* **1972**, *56*, 5278.
- [34] H. Wolff, H. Ludwig, *Ber. Bunsen-Ges. Phy. Chem.* **1967**, *71*, 911.
- [35] D. E. Gardin, G. A. Somorjai, *J. Phys. Chem.* **1992**, *96*, 9424.
- [36] B. A. Sexton, N. R. Avery, *Surf. Sci.* **1983**, *129*, 21.
- [37] J. L. Gland, G. B. Fisher, G. E. Mitchell, *Chem. Phys. Lett.* **1985**, *119*, 89.
- [38] P. D. Ditlevsen, D. E. Gardin, M. A. Vanhove, G. A. Somorjai, *Langmuir* **1993**, *9*, 1500.
- [39] R. Raval, M. A. Chesters, *Surf. Sci.* **1989**, *219*, L505.
- [40] A. Chojecki, M. Veprek-Heijman, T. E. Müller, P. Schäringer, S. Veprek, J. A. Lercher, *J. Catal.* **2007**, *245*, 237.
- [41] D. T. Shay, G. P. A. Yap, L. N. Zakharov, A. L. Rheingold, K. H. Theopold, *Angew. Chemie-Int. Ed.* **2005**, *44*, 1508.
- [42] X. Hu, K. Meyer, *J. Am. Chem. Soc.* **2004**, *126*, 16322.
- [43] H. Bock, O. Breuer, *Angew. Chem.-Int. Ed.* **1987**, *26*, 461.

Chapter 4

Investigations into the mechanism of the liquid-phase hydrogenation of nitriles over Raney-Co catalysts

Abstract

The co-hydrogenation of acetonitrile and butyronitrile over Raney-Co was investigated in order to get an insight into the mechanism underlying the formation of secondary amines. As reference experiments the hydrogenation of the pure nitriles, the hydrogenation of acetonitrile in the presence of *n*-butylamine as well as the hydrogenation of butyronitrile in the presence of ethylamine were studied. In the co-hydrogenation of the two nitriles acetonitrile was converted much faster due to a stronger adsorption on the catalyst surface. *n*-Butylamine was found to react much faster with partly hydrogenated intermediate species on the surface than ethylamine resulting in dialkylimines. This observation was attributed to the stronger inductive effect of the alkyl chain resulting in an increased nucleophilic attack at the C atom of the surface species. By following the C₂ and C₄ balance during the reaction of dialkylimines to dialkylamines it was found that hydrogenation cannot be the only way to form dialkylamines. Instead it was suggested that alkyl group transfer may occur by both the reaction of a monoalkylamine with a dialkylimine or the cross transfer between two dialkylimines.

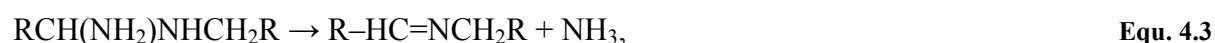
4.1. Introduction

The production of amines through the hydrogenation of nitriles is a common industrial process.^[1] Important examples include the hydrogenation of 1,4-dicyanobutane to 1,6-diaminohexane used for the production of nylon-6,6^[2, 3] and the conversion of fatty nitriles to fatty amines, which are used e.g. as feedstock for surface active substances like fabric softeners and detergents. In general, products formed during hydrogenation include primary, secondary and tertiary amines. The product distribution depends on the catalyst applied.^[4, 5] For the selective hydrogenation of nitriles to primary amines skeletal metal catalysts based on Co and Ni are often used as they provide the lowest cost per unit mass of catalyst^[6] combined with a high activity.^[4]

Frequently, the formation of secondary and tertiary amines is undesired. The mechanism of the condensation reaction leading to higher amines has therefore been analysed by numerous authors. The discussions have mostly been based on the mechanism by von Braun et al.^[7] and were summarized in several publications.^[8-10] However, for an understanding of the mechanistic aspects discussed in this study the main findings are given below. Von Braun proposed that an aldimine occurring as intermediate in the sequential nitrile hydrogenation^[11] reacts with amine to a 1-amino-dialkylamine,



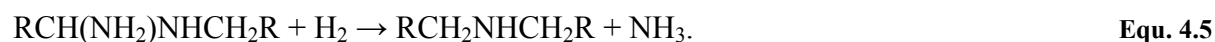
which can undergo ammonia elimination resulting in a dialkylimine,



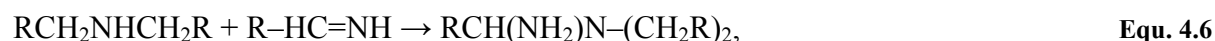
which is further hydrogenated to the secondary amine,



Alternatively, direct hydrogenolysis of the 1-amino-dialkylamine may occur,



For the formation of tertiary amines starting from addition of a secondary amine to an imine resulting in 1-amino-trialkylamine,^[12]



two different subsequent reaction steps were proposed. One is the direct hydrogenolysis of 1-amino-trialkylamine,



As an alternative reaction path, NH_3 elimination resulting in an enamine followed by hydrogenation to a tertiary amine was proposed,¹³



The aldimine intermediate has not been confirmed by direct observation, which is attributed to its high reactivity.^[8] High reactivity also holds for enamines, but they have been identified by GC-MS as reaction intermediates.^[8] Other studies based on indirect observations found the enamine mechanism be prevailing.^[4, 14] However, in the reductive amination of benzaldehyde a considerable amount of tribenzylamine was detected.^[9] As enamine formation requires a β -H atom, which is not available with benzaldehyde hydrogenolysis is considered as the mechanism responsible for the formation of a tertiary amine in this reaction.

Recently, Sivasankar and Prins^[10] found in their study on reactions of mixed di- and trialkylamines over Pd/ γ -Al₂O₃ that methyl groups can be transferred between alkylamines. This was taken as a proof that an aminotrialkylamine, which is formed by reaction of a dialkylamine with a dialkylimine, does not have to achieve alkylamine elimination through an enamine intermediate, but can also do so by direct hydrogenolysis. An imine radical was proposed as possible intermediate in the transfer of the methyl group.

In the deuteration of CH₃CN Huang and Sachtler^[15] observed a surprising discrepancy between the number of D atoms found in the products and that predicted by the straightforward stoichiometry for nitrile hydrogenation. Moreover, they found that D atoms were added to the C atom of the C \equiv N, group while H atoms added preferentially to the N atom. They explained the results by a concerted reaction mechanism as is exemplarily presented for Ru in Figure 4.1. It was further proposed that *cis* insertion of an alkyl group to the N=M bonded intermediate leads to a secondary amine and addition of another alkyl group to the lone pair of the N atom gives the tertiary amines.

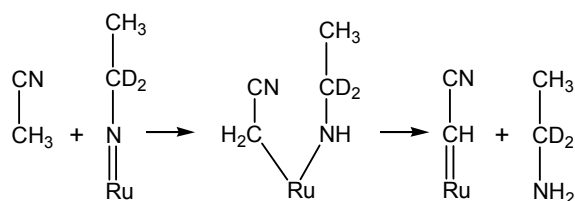


Figure 4.1: Concerted reaction mechanism for the deuteration of acetonitrile.^[15]

The aim of the present study was to obtain information on the reactions leading on the one hand to primary amines and on the other hand to the formation of secondary amines or tertiary amines. The liquid phase hydrogenation of acetonitrile and butyronitrile over a Raney-Co catalyst was explored as model reaction. To elucidate the role of alkyl group transfer, acetonitrile and butyronitrile were hydrogenated in the presence of *n*-butylamine and ethyl-

amine, respectively. Further, CD_3CN was hydrogenated to explore whether transfer of D atoms from the methyl group plays a role during the reaction of nitriles to amines and by-products.

4.2. Experimental

4.2.1. Materials

Raney-Co 2700 catalyst (Grace Davison division of W.R. Grace and Co.) was received as an aqueous suspension. The chemical composition was: 1.85 wt% Al; 97.51 wt% Co; 0.3 wt% Fe and 0.34 wt% Ni. It was washed with de-ionized water under nitrogen atmosphere until the pH of the washing water was ~ 7 . Due to its sensitivity to oxygen the catalyst was stored and handled under inert atmospheres throughout all the other preparation steps. The rest water was removed by drying in partial vacuum ($p < 1$ kPa) for 30 h at 323 K. After outgassing the catalyst at 473 K for 6 h its BET area was $22.4 \text{ m}^2 \cdot \text{g}_{\text{Cat}}^{-1}$ and the number of accessible metal atoms was $0.36 \text{ mmol} \cdot \text{g}_{\text{Cat}}^{-1}$.

The other chemicals applied for catalysis experiments and GC-calibration were used as received from the commercial suppliers (Acetonitrile- d_3 (CD_3CN), $\geq 99.5\%$, Deutero GmbH; acetonitrile, $\geq 99.5\%$ GC-assay, Fluka; ethylamine, $\geq 99.5\%$ GC-assay, Fluka; diethylamine, $\geq 99.5\%$ GC-assay, Fluka; butyronitrile, $\geq 99\%$ GC-assay, Fluka; mono- and di-*n*-butylamine, $> 99\%$ GC-assay, Aldrich; *N*-ethylbutylamine, $\geq 98.0\%$, Aldrich; 1-octanol, $\geq 99.5\%$ GC-assay, Fluka; *n*-hexane, $\geq 99.0\%$ GC-assay, Roth; H_2 , 99.999 vol%, Air Liquide).

4.2.2. Catalysis

The hydrogenation reactions were conducted in a batch reactor (160 cm^3 ; Parr Instrument Comp.) at constant hydrogen pressure by re-supplying hydrogen consumed during the reaction. Raney-Co catalyst was suspended under inert atmosphere in the reaction mixture the respective composition of which is specified in Table 4.2. Hexane was used both as solvent and as internal standard for GC chromatography. The reaction mixture was filled into the autoclave under a flow of nitrogen. After closing, the reactor was pressurized and depressurized with nitrogen several times to remove oxygen. The reaction mixture was heated to the reaction temperature (383 K). The reaction was then started by rapidly pressurizing the reactor with hydrogen to 45 bar and subsequently starting the stirrer (1500 rpm). Samples for off-line GC, gas chromatography-mass spectrometry (GC-MS) and NMR analysis were periodically withdrawn through a dip-tube with a filter for solids. GC analysis was carried out on an HP Gas Chromatograph 5890 equipped with a cross linked 5% diphenyl-95% dimethylpolysil-

loxane column (Rtx-5 Amine, 30 m, Restek GmbH). GC-MS analysis was performed on a Shimadzu GCMS-QP20105 equipped with a cross linked (5%-phenyl)-methylpolysiloxane column (HP-5, 32 m, Agilent). ^1H NMR and ^2H NMR measurements were conducted on a Bruker DPX-400 (400 MHz) instrument with CD_3Cl as solvent containing 1 vol.-% trimethylsilane as standard. The reaction rate was calculated from the decrease in acetonitrile and butyronitrile concentration in the linear range of the concentration curves (from 0 up to 80% conversion depending on the respective reaction). The selectivity was calculated by dividing the molar amount of the respective product by the amount of acetonitrile or butyronitrile converted. At full conversion the selectivity is thus obtained with the equation $S = (n_k \cdot |\nu_i|) / (n_{i,0} \cdot |\nu_k|)$. Prior to the experiments a test on mass transfer limitations at a stirring speed of 1500 rpm was performed by varying the amount of catalyst in the range of 0 – 2.0 g. It was observed that the reaction rate was doubled when double amount of catalyst was used showing that external mass transfer limitations were absent.

Table 4.1: Nomenclature of the compounds discussed in this work including abbreviations which are used in tables below.

Compound	Abbreviation	Nomenclature
Acetonitrile	AN	$\text{C}_1\text{-C}\equiv\text{N}$
Acetonitrile- d_3	AN- d_3	CD_3CN
Butyronitrile	BN	$\text{C}_3\text{-C}\equiv\text{N}$
Ethylamine	EA	$\text{C}_2\text{-NH}_2$
<i>n</i> -Butylamine	BA	$\text{C}_4\text{-NH}_2$
<i>N</i> -Ethylidene-ethylamine	EEI	$\text{C}_1\text{-HC=N-C}_2$
<i>N</i> -Butylidene-butylamine	BBI	$\text{C}_3\text{-HC=N-C}_4$
<i>N</i> -Ethylidene-butylamine	EBI	$\text{C}_1\text{-HC=N-C}_4$
<i>N</i> -Butylidene-ethylamine	BEI	$\text{C}_3\text{-HC=N-C}_2$
Di-ethylamine	DEA	$\text{C}_2\text{-NH-C}_2$
Di- <i>n</i> -butylamine	DBA	$\text{C}_4\text{-NH-C}_4$
<i>N</i> -Ethyl-butylamine	EBA	$\text{C}_2\text{-NH-C}_4$

Table 4.2: Concentration and amount of reactants and catalyst used in the different hydrogenation reactions performed.

Reactant	Concentration [mol·dm ⁻³]	Hexane [cm ³]	Amount of Catalyst [g]	AN [cm ³]	BN [cm ³]	BA [cm ³]	EA [cm ³]
AN	9.52	40.0	1.05	40.0	-	-	-
AN	4.08	50.0	0.95	13.6	-	-	-
AN-d ₃	9.52	40.0	1.06	40.0	-	-	-
BN	7.12	40.0	1.00	-	66.1	-	-
BN	4.08	40.0	1.01	-	22.14	-	-
AN+BN	4.08*	40.0	1.01	20.0	33.4	-	-
AN+BA	4.08*	36.0	1.00	20.0	-	37.5	-
BN+EA	4.08*	16.5	0.48	-	15.9	-	12.1

*For each of the two starting materials.

4.3. Results

4.3.1. Hydrogenation of C₁-C≡N and CD₃CN

Hydrogenation of C₁-C≡N was performed serving as a reference for the reaction of C₁-C≡N in presence of butylamine and C₃-C≡N. To investigate the influence of the starting concentration on the course of the reaction experiments with varying starting concentrations of C₁-C≡N were performed. Figure 4.2 shows the concentration profile for the hydrogenation of C₁-C≡N with a starting concentration $c_{0,AN} = 9.52 \text{ mol}\cdot\text{dm}^{-3}$. Part of the diagram was magnified to clarify the formation of the by-product C₂-NH-C₂. For comparison, the reaction rate and selectivity for the respective compounds obtained in the different reactions presented in this paper are summarized in Table 4.7 and Table 4.8, respectively. C₁-C≡N was converted at a rate of $4.50 \times 10^{-3} \text{ mol}\cdot\text{min}^{-1}\cdot\text{g}_{\text{Cat}}^{-1}$ showing an almost linear decrease in concentration with time. With a selectivity of 88.9% the main product of the hydrogenation reaction was C₂-NH₂. The only by-product found was C₂-NH-C₂ (11.1%). C₁-HC=N-C₂ was observed as a reaction intermediate, which, as C₂-NH₂, was formed immediately after the start of the reaction, indicating that both were primary products. The concentration of C₂-NH-C₂ increased with a time delay, suggesting that it is a secondary product. After 80-90% of C₁-C≡N had been converted the concentration of C₁-HC=N-C₂ decreased rapidly while C₂-NH-C₂ was formed in parallel. The reaction profile for a lower starting concentration ($c_{0,AN} = 4.08 \text{ mol}\cdot\text{dm}^{-3}$) is shown in Figure 4.3. The rate of C₁-C≡N conversion was slightly lower ($4.06 \times 10^{-3} \text{ mol}\cdot\text{min}^{-1}\cdot\text{g}_{\text{Cat}}^{-1}$), whereas a noteworthy enhancement of the selectivity to C₂-NH₂ (96.1%) was observed. Closer inspection of the formation of C₂-NH-C₂ (3.9%) reveals dif-

ferences compared to Figure 4.2. $C_1\text{-HC=N-C}_2$ was also formed and further converted to $C_2\text{-NH-C}_2$. However, $C_2\text{-NH-C}_2$ was not found before 90% of $C_1\text{-C}\equiv\text{N}$ had been hydrogenated. Then, a sudden decrease of $C_1\text{-HC=N-C}_2$ concentration occurred accompanied by the formation of $C_2\text{-NH-C}_2$.

For an insight into the role of the methyl hydrogen atoms of $C_1\text{-C}\equiv\text{N}$, hydrogenation of CD_3CN was carried out. The results are shown in Figure 4.4. The concentration profile was very similar to that during the hydrogenation of $C_1\text{-C}\equiv\text{N}$ at the same starting concentration ($c_{0,\text{AN}} = 9.52 \text{ mol}\cdot\text{dm}^{-3}$). The hydrogenation proceeded at a rate of $4.09 \times 10^{-3} \text{ mol}\cdot\text{min}^{-1}\cdot\text{g}_{\text{Cat}}^{-1}$. Hence, the rate was a factor of 1.10 lower than with non-deuterated $C_1\text{-C}\equiv\text{N}$. The selectivity to $C_2\text{-NH}_2$ was slightly higher (90.4%) and again $C_2\text{-NH-C}_2$ was the only by-product formed with a selectivity of 9.6%.

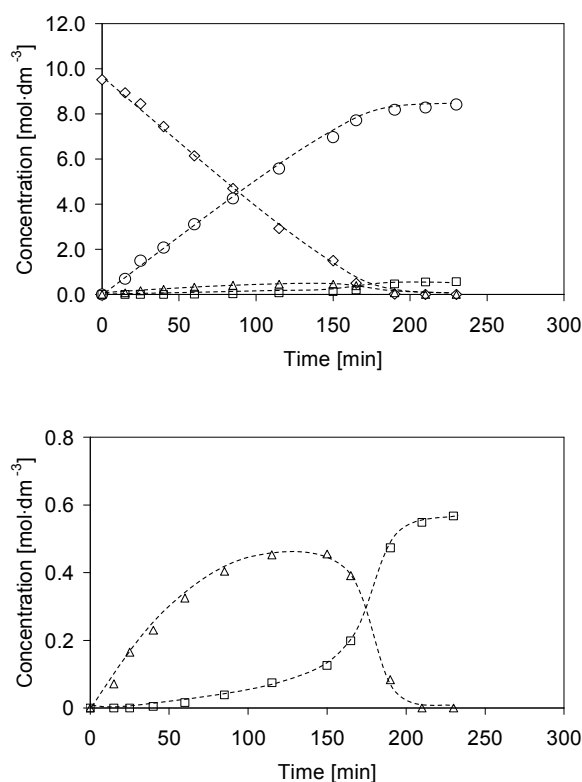


Figure 4.2: Concentration profile for the hydrogenation of $C_1\text{-C}\equiv\text{N}$ over Raney-Co at 383 K, $p = 45 \text{ bar}$, $c_{0,\text{AN}} = 9.52 \text{ mol}\cdot\text{dm}^{-3}$. (\diamond) $C_1\text{-C}\equiv\text{N}$, (\circ) $C_2\text{-NH}_2$, (\triangle) $C_1\text{-HC=N-C}_2$, (\square) $C_2\text{-NH-C}_2$.

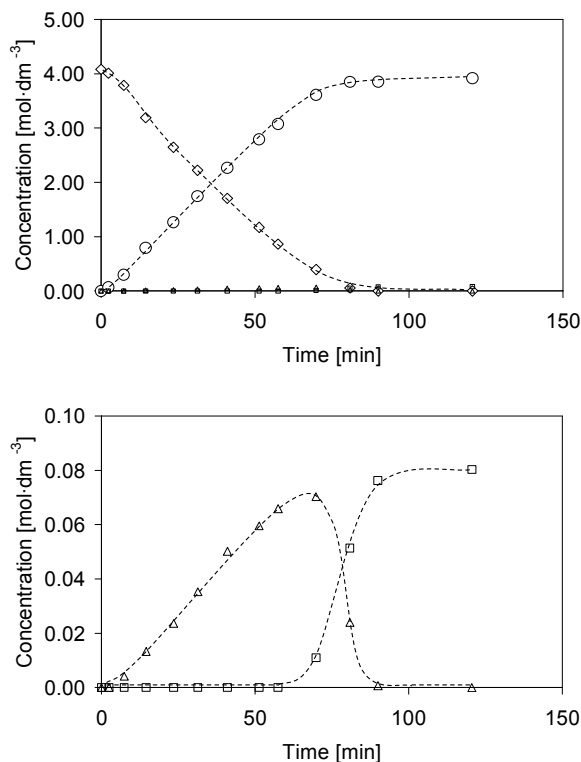


Figure 4.3: Concentration profile for the hydrogenation of $C_1-C\equiv N$ over Raney-Co at 383 K, $p = 45$ bar, $c_{0,AN} = 4.08 \text{ mol}\cdot\text{dm}^{-3}$. (\diamond) $C_1-C\equiv N$, (\circ) C_2-NH_2 , (\triangle) $C_1-HC=N-C_2$, (\square) C_2-NH-C_2 .

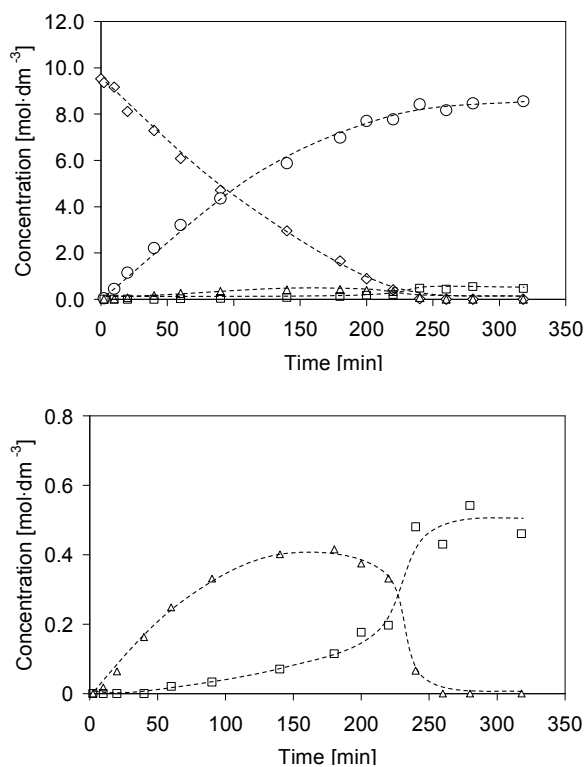


Figure 4.4: Concentration profile for the hydrogenation of CD_3CN over Raney-Co at 383 K, $p = 45$ bar, $c_{0,AN-d_3} = 9.52 \text{ mol}\cdot\text{dm}^{-3}$. (\diamond) CD_3CN , (\circ) C_2-NH_2 , (\triangle) $C_1-HC=N-C_2$, (\square) C_2-NH-C_2 .

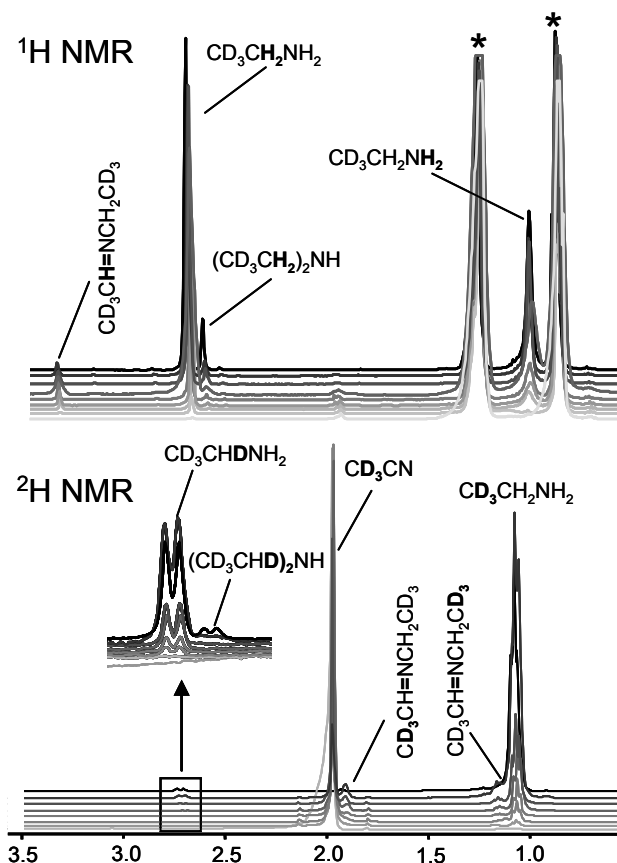


Figure 4.5: Time resolved ^1H NMR and ^2H NMR results obtained during the hydrogenation of CD_3CN . Spectra were taken after 2.3, 10, 20, 40, 60, 90, 120, 200 and 318 min.

The results of the ^2H NMR measurements are shown in Figure 4.7. The conversion of CD_3CN and the corresponding formation of $\text{C}_2\text{-NH}_2$ were in accordance with the GC results. It can be seen that little H/D exchange occurred during the reaction. Deuterium was found in 0.83% of the $\text{C}_2\text{-NH}_2$ molecules formed ($\text{CD}_3\text{CHDNH}_2$). Additionally, a very low amount (0.15%) of secondary amine $(\text{CD}_3\text{CHD})_2\text{NH}$ was observed. The two peaks at 1.20 ppm and 1.80 ppm, which first increased and then decreased, were assigned to the CD_3 group in $\text{CD}_3\text{CH}=\text{NCH}_2\text{CD}_3$ in right and left position of the CN double bond, respectively. In ^1H NMR the H atom left of the double bond exhibited a signal at 3.35 ppm. In the ^2H NMR spectra no peak at 3.35 ppm was found, which suggests that $\text{CD}_3\text{CD}=\text{NCH}_2\text{CD}_3$ was either not formed or its concentration below the detection limit. Information about the H/D exchange behaviour during the reaction was gained by following the reaction with ^1H and ^2H NMR spectroscopy. To clarify the peak assignment the results of the NMR measurements are depicted in Figure 4.5. Table 3.3 shows the respective compounds, which were assigned to the peak positions found. To obtain a clearer picture of the course of the reaction the areas of the peaks (normalised to the area of TMS or CDCl_3) were plotted versus time (Figure 4.6 and Figure 4.7).

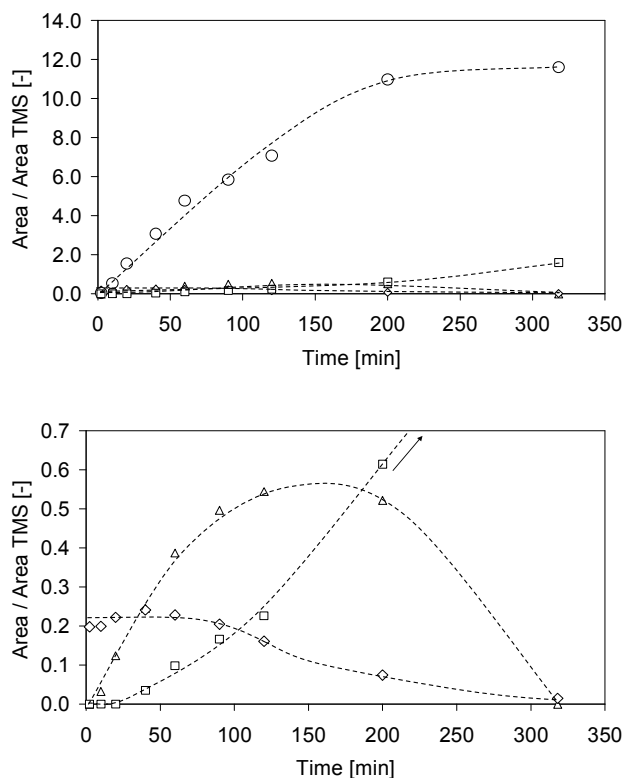


Figure 4.6: Profile for the hydrogenation of CD_3CN over Raney-Co at 383 K, $p = 45$ bar generated from ^1H NMR measurements. (\diamond) CH_3CN , (\circ) $\text{CD}_3\text{CH}_2\text{NH}_2$, (\triangle) $\text{CD}_3\text{CH}=\text{NCH}_2\text{CD}_3$, (\square) $(\text{CD}_3\text{CH}_2)_2\text{NH}$.

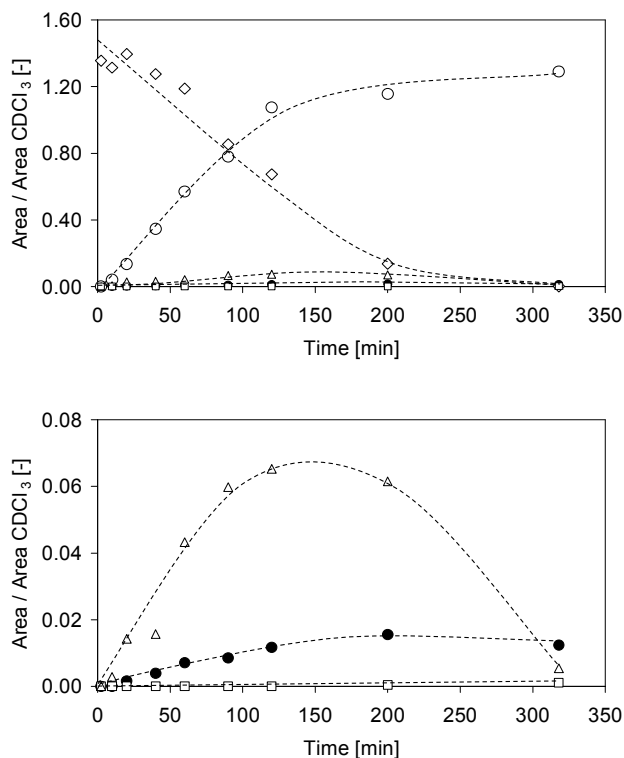

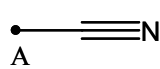
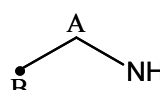
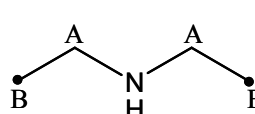
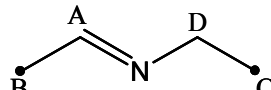


Figure 4.7: Profile for the hydrogenation of CD_3CN over Raney-Co at 383 K, $p = 45$ bar generated from ^2H NMR measurements. (\diamond) CD_3CN , (\circ) $\text{CD}_3\text{CH}_2\text{NH}_2$, (\bullet) $\text{CD}_3\text{CHDNH}_2$, (\square) $(\text{CD}_3\text{CHD})_2\text{NH}$, (\triangle) $\text{CD}_3\text{CH}=\text{NCH}_2\text{CD}_3$, mean values of the areas at 1.20 ppm and 1.80 ppm.

Table 4.3: Assignment of the chemical shift to chemical groups for the identification of the peaks obtained in the NMR-measurements of the final product resulting from the hydrogenation of CD_3CN .^[16, 17]

Molecule		Chemical shift [ppm]	Assignment
<i>n</i> -Hexane	A	1.27	
	B	1.27	
	C	0.88 t	
Acetonitrile	A	1.98	 consumed
Ethylamine	A	2.74	 main product
	B	1.10 t	
	C	(0.5 – 4.0)*	
Di-ethylamine	A	1.10	
	B	2.64	
<i>N</i> -ethylidene-ethylamine	A	3.35	
	B	1.80	
	C	1.20	
	D	not observed	

t = triplett, • = CD_3 , *position variable.

The decrease of CD_3CN and the increase of $\text{C}_2\text{-NH}_2$ concentration nicely corresponded with the reaction profiles obtained from GC data. In Figure 4.6 the formation of the dialkylimine and its hydrogenation to $\text{C}_2\text{-NH-C}_2$ are shown. $\text{C}_1\text{-C}\equiv\text{N}$, which is found as impurity in CD_3CN is hydrogenated after an induction period of ~ 60 min. The corresponding peak at 1.10 ppm in ^1H NMR stemming from the methyl group in $\text{CH}_3\text{CH}_2\text{NH}_2$ is probably overlapped by the peak assigned to the NH_2 group.

4.3.2. Hydrogenation of $\text{C}_3\text{-C}\equiv\text{N}$

To study the influence of the length of the alkyl chain on the rate of reaction $\text{C}_3\text{-C}\equiv\text{N}$ was hydrogenated. A typical concentration profile for the hydrogenation of $\text{C}_3\text{-C}\equiv\text{N}$ at 383 K and $c_{0,\text{BN}} = 4.08 \text{ mol}\cdot\text{dm}^{-3}$ is shown in Figure 4.8. The course of the reaction looks very similar to that for the hydrogenation of $\text{C}_1\text{-C}\equiv\text{N}$. After a short induction period (< 2 min) the reaction started at a rate of $3.44 \times 10^{-3} \text{ mol}\cdot\text{min}^{-1}\cdot\text{g}_{\text{Cat}}^{-1}$. At full conversion of $\text{C}_3\text{-C}\equiv\text{N}$ a selectivity

to C_4-NH_2 of 96.1% and to C_4-NH-C_4 of 3.9% was obtained. As described in a previous paper^[18] C_4-NH_2 and $C_3-HC=N-C_4$ were observed right after the start of the reaction suggesting that both were primary products. After ~ 30 min the rate of $C_3-HC=N-C_4$ formation increased compared to the rate in the beginning of the reaction. Only after more than 90% of $C_3-C\equiv N$ had been converted the formation of C_4-NH-C_4 was observed. Its increase in concentration correlated with the rapid decrease in $C_3-HC=N-C_4$ concentration. It is, thus, assumed that C_4-NH-C_4 is a sequential product of the hydrogenation of $C_3-HC=N-C_4$. As with $C_1-C\equiv N$, the hydrogenation was also carried out at a higher starting concentration ($c_{0,BN} = 7.12 \text{ mol}\cdot\text{dm}^{-3}$) to evaluate its influence on rate and selectivity. As the reaction profile strongly resembled that at lower concentration also with respect to the formation of the only by-product C_4-NH-C_4 the graph is not shown here. However, as can be seen in Table 4.8 the rate increased only slightly to $3.48 \times 10^{-3} \text{ mol}\cdot\text{min}^{-1}\cdot\text{g}_{\text{Cat}}^{-1}$. On the other hand the selectivity to C_4-NH_2 decreased (88.0%) significantly.

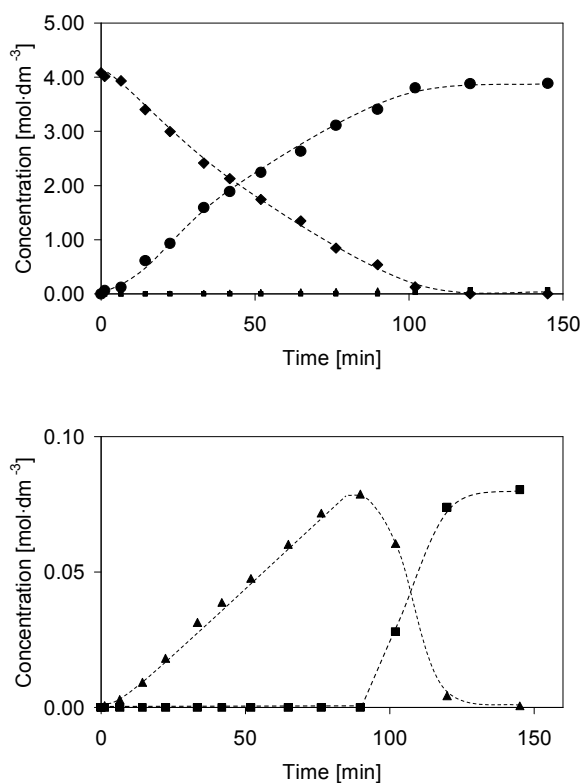


Figure 4.8: Concentration profile for the hydrogenation of $C_3-C\equiv N$ over Raney-Co at 383 K, $p = 45$ bar, $c_{0,BN} = 4.08 \text{ mol}\cdot\text{dm}^{-3}$. (\blacklozenge) $C_3-C\equiv N$, (\bullet) C_4-NH_2 , (\blacktriangle) $C_3-HC=N-C_4$, (\blacksquare) C_4-NH-C_4 .

4.3.3. Co-hydrogenation of $C_1-C\equiv N$ and $C_3-C\equiv N$

In Figure 4.9 the results of the co-hydrogenation of $C_1-C\equiv N$ and $C_3-C\equiv N$ are shown. The reaction conditions were equal to those in the hydrogenation of the single compounds

(383 K, $c_{0,AN}$ and $c_{0,BN} = 4.08 \text{ mol}\cdot\text{dm}^{-3}$). Both compounds were hydrogenated immediately after the start of the reaction. The profile of $C_1-C\equiv N$ depletion and C_2-NH_2 formation is similar to that with hydrogenation of pure $C_1-C\equiv N$, whereas the rate of $C_3-C\equiv N$ hydrogenation is significantly affected by the presence of $C_1-C\equiv N$. $C_1-C\equiv N$ and $C_3-C\equiv N$ were converted at a rate of $3.67 \times 10^3 \text{ mol}\cdot\text{min}^{-1}\cdot\text{g}_{\text{Cat}}^{-1}$ and $1.87 \times 10^3 \text{ mol}\cdot\text{min}^{-1}\cdot\text{g}_{\text{Cat}}^{-1}$, respectively. The sum of the concentration of the two compounds gives an overall nitrile concentration of $8.16 \text{ mol}\cdot\text{dm}^{-3}$. Thus, the selectivity is qualitatively compared to the hydrogenation of the single nitriles at higher starting concentration. The selectivity to C_2-NH_2 was reduced to 83.6% and for C_4-NH_2 it was slightly increased to 89.4%. As by-products, the symmetric secondary amines C_2-NH-C_2 and C_4-NH-C_4 were formed with a selectivity of 8.7% and 2.9%, respectively. The selectivity to the asymmetric secondary amine C_2-NH-C_4 was 7.7%. Table 4.4 gives an overview of the reaction network. Four different imines were formed as primary products. The asymmetric imines $C_3-HC=N-C_2$ and $C_1-HC=N-C_4$ were identified by GC-MS analysis. As summarized in Table 4.7, $C_1-HC=N-C_4$ exhibited the highest rate of formation of all the intermediates followed by $C_1-HC=N-C_2$. The dialkylimines $C_3-HC=N-C_2$ and $C_3-HC=N-C_4$ were formed with the same albeit lower rate. The secondary amines started forming with a time delay of 50 min in the case of C_2-NH-C_2 and C_2-NH-C_4 and 130 min in the case of C_4-NH-C_4 .

With respect to the development of by-products, the reaction can roughly be divided into two sections. Formation of the imine intermediates occurred during the first section, while the further reaction of these intermediates giving rise to secondary amines constitutes the second part. The primary nature of all the imine intermediates suggests that at least in the beginning they were formed by the same elementary reactions. Formally the formation of dialkylimine intermediates can be explained by the reactions,



and also by the disproportionation of the respective amines as e.g.,



As will be shown later, the latter reaction (Equ. 4.14) is relatively slow in the presence of hydrogen as a dehydrogenation step is involved. The primary nature of the dialkylimines suggests that surface species were involved, which did not desorb from the surface before the condensation reaction occurred.

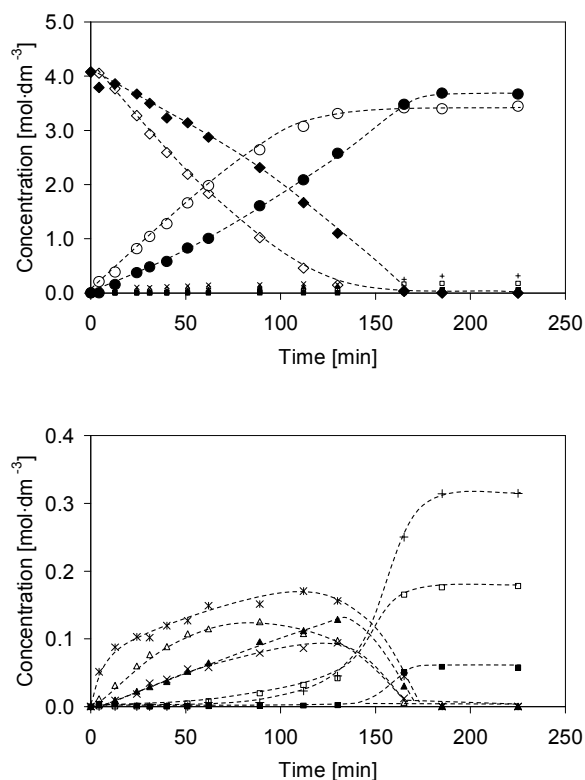
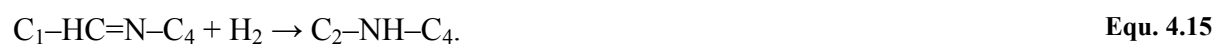


Figure 4.9: Concentration profile for the co-hydrogenation of $C_1-C\equiv N$ and $C_3-C\equiv N$ over Raney-Co at 383 K, $p = 45$ bar, $c_{0,AN}$ and $c_{0,BN} = 4.08$ mol·dm $^{-3}$. (\diamond) $C_1-C\equiv N$, (\circ) C_2-NH_2 , (\triangle) $C_1-HC=N-C_2$, (\square) C_2-NH-C_2 , (\blacklozenge) $C_3-C\equiv N$, (\bullet) C_4-NH_2 , (\blacktriangle) $C_3-HC=N-C_4$, (\blacksquare) C_4-NH-C_4 , (\times) $C_3-HC=N-C_2$, ($*$) $C_1-HC=N-C_4$, ($+$) C_2-NH-C_4 .

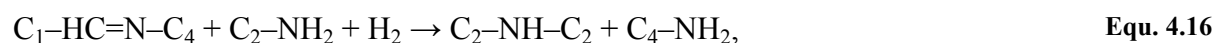
Table 4.4: General reaction network for the co-hydrogenation of $C_1-C\equiv N$ in the presence of $C_3-C\equiv N$.

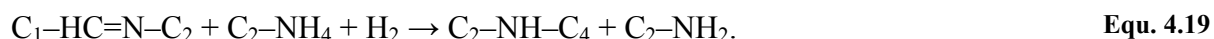
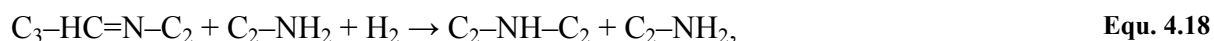
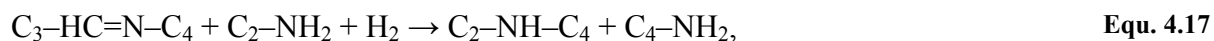
Reactant	Primary products	Secondary products
$C_1-C\equiv N$	C_2-NH_2	C_2-NH-C_2
$C_3-C\equiv N$	C_4-NH_2	C_2-NH-C_4
	$C_1-HC=N-C_4$	C_4-NH-C_4
	$C_1-HC=N-C_2$	
	$C_3-HC=N-C_4$	
	$C_3-HC=N-C_1$	

In the second section of the reaction the dialkylimines were transformed to dialkylamines, which is possible by hydrogenation of the dialkylimines as e.g.,

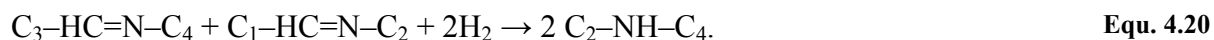


An alternative reaction is the reaction of an amine with a dialkylimine to 1-alkylamino-dialkylamine followed either by formation of an imine and subsequent hydrogenation or by direct hydrogenolysis resulting in another amine and dialkylamine as e.g.,





Cross-disproportionation of two dialkylimines followed by hydrogenation resulting in two dialkylamines may also occur,



Note that, when comparing the mass balance of the dialkylimine intermediates with that of the final products (dialkylamines) only a slight deviation of $\sim 5\%$ was observed. Taking into account experimental error this suggests that all dialkylimine intermediates further reacted to dialkylamines. Thus, the hydrogenolysis of dialkylimines leading to a primary amine and an alkane as e.g.,



or the elimination reaction resulting in primary amine and an alkene,



as recently described for reactions over $\text{Pd}/\gamma\text{-Al}_2\text{O}_3$,^[10] did not occur to a significant extent.

To differentiate between the reactions given in Equ. 4.15, Equ. 4.16 - Equ. 4.19 and Equ. 4.20 mass balances for C_2 groups and C_4 groups were calculated at selected times. If alkyl group transfer occurred, the mass balances for the respective groups were likely to be changed though the overall mass balance was constant. The first point chosen was that shortly before the rapid consumption of the dialkylimines started ($t = 130$ min). For comparison, the balance mass was calculated at the end point of the reaction ($t = 225$ min). It was observed that the number of C_2 groups approximately increased by the same amount ($0.12 \text{ mol}\cdot\text{dm}^{-3}$) as the number of C_4 groups decreased. This suggests that C_4 groups were replaced by C_2 groups originating most likely from $\text{C}_2\text{-NH}_2$ (Equ. 4.16 - Equ. 4.18). Hydrogenation of the dialkylimine very likely occurred in parallel. Cross-disproportionation cannot be excluded but seems to play a minor role.

4.3.4. Hydrogenation of $\text{C}_1\text{-C}\equiv\text{N}$ in the presence of $\text{C}_4\text{-NH}_2$

The hydrogenation of $\text{C}_1\text{-C}\equiv\text{N}$ in the presence of an equimolar amount of $\text{C}_4\text{-NH}_2$ was carried out at 383 K and $c_{0,\text{AN}} = 4.08 \text{ mol}\cdot\text{dm}^{-3}$. Figure 4.10 shows the concentration profiles of the reaction. Compared to the hydrogenation of $\text{C}_1\text{-C}\equiv\text{N}$ the rate of reaction surprisingly increased by 10% ($4.46 \times 10^3 \text{ mol}\cdot\text{min}^{-1}\cdot\text{g}_{\text{Cat}}^{-1}$). The selectivity to $\text{C}_2\text{-NH}_2$ was 91.7% and thus 4.4% lower than in absence of $\text{C}_4\text{-NH}_2$. As by-products $\text{C}_2\text{-NH-C}_2$ and $\text{C}_2\text{-NH-C}_4$ were formed with a selectivity of 5.6% and 2.7%, respectively. With respect to the starting concen-

tration of C_4-NH_2 , the selectivity to C_4-NH-C_4 was 1.5%. In Table 4.5, the compounds formed during the reaction are separated according to the nature of their appearance. In a sample drawn before the addition of hydrogen ($t = 0$ min) already a considerable amount of $C_3-HC=N-C_4$ was found. In the further course of the reaction this intermediate was formed with the second lowest rate (Table 4.7). Right after the addition of hydrogen $C_1-HC=N-C_4$ was formed with the highest rate. $C_1-HC=N-C_2$ started developing after an induction period of 10 min with the second highest rate. After a further delay $C_3-HC=N-C_2$ was formed. After most of the acetonitrile ($\sim 80\%$) had been hydrogenated, the fast formation of the secondary amines coincided with a rapid depletion of the imine intermediates. Between 66 min and 80 min the final product C_2-NH-C_4 developed shortly before C_2-NH-C_2 ; both were then formed in parallel, while the concentration of the imine intermediates decreased. In the final part of the reaction the concentration of both amines increased at approximately the same rate. A significant amount of C_4-NH-C_4 was only formed after the maximum concentration of $C_3-HC=N-C_4$ had been reached.

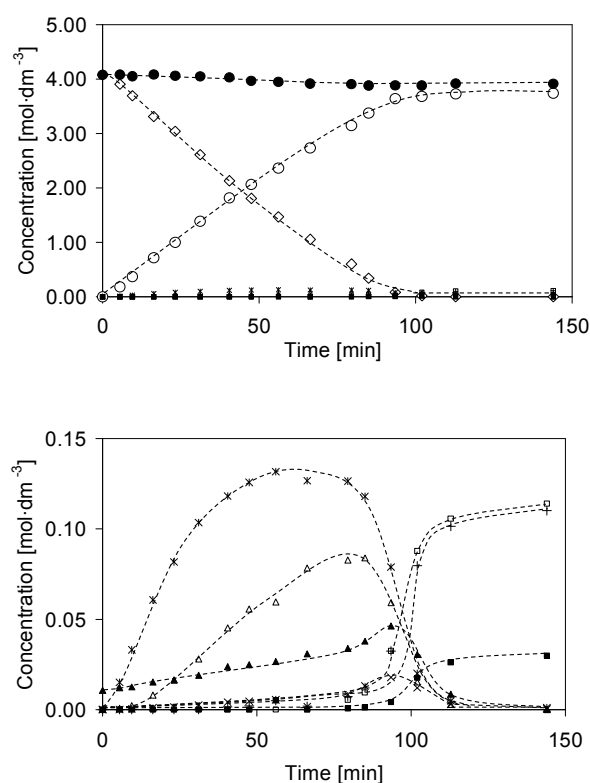


Figure 4.10: Concentration profile for the hydrogenation of $C_1-C\equiv N$ in the presence of C_4-NH_2 over Raney-Co at 383 K, $p = 45$ bar, $c_{0,AN} = 4.08$ mol·dm⁻³. (\diamond) $C_1-C\equiv N$, (\circ) C_2-NH_2 , (\bullet) C_4-NH_2 , (\triangle) $C_1-HC=N-C_2$, (\square) C_2-NH-C_2 , (\blacktriangle) $C_3-HC=N-C_4$, (\blacksquare) C_4-NH-C_4 , (\times) $C_3-HC=N-C_2$, ($*$) $C_1-HC=N-C_4$, ($+$) C_2-NH-C_4 .

Again, in the formation of by-products two distinct sections could be observed. The first is the formation of dialkylimine intermediates, which is formally due to the reactions as

shown in Equ. 4.10 - Equ. 4.13. The mass balance³ shows that in the second part of the reaction, the hydrogenation of dialkylimines (Equ. 4.15) was accompanied by reaction of a dialkylimine with a primary amine (Equ. 4.16 - Equ. 4.19) and/or cross-disproportionation of two dialkylimines (Equ. 4.20).

Table 4.5: General reaction network for the hydrogenation of $C_1-C\equiv N$ in the presence of C_4-NH_2 .

Reactant	Primary products	Secondary products	Final products
$C_1-C\equiv N$	C_2-NH_2	$C_1-HC=N-C_2$	C_2-NH-C_4
C_4-NH_2	$C_1-HC=N-C_4$ ($C_3-HC=N-C_4$)*	$C_3-HC=N-C_4$	C_2-NH-C_2 C_4-NH-C_4

*Primary product due to adsorption and reaction of C_4-NH_2 on the surface prior to the addition of hydrogen.

The occurrence of $C_3-HC=N-C_4$ before the start of the reaction can be explained by a disproportionation reaction analogous to Equ. 4.14,



To see, whether the length of the alkyl groups influences the reaction of the dialkylimine intermediates to the dialkylamines and whether the cross-disproportionation of two dialkylimines (Equ. 4.20) plays a significant role, the C_2 and C_4 mass balances for the dialkylimines and dialkylamines were again calculated. The balances were calculated at a time, where the amount of dialkylimines was approximately at maximum ($t = 80$ min) and when the reaction was finished ($t = 145$ min). Between the two times the number of C_2 groups increased by the same amount ($0.033 \text{ mol}\cdot\text{dm}^{-3}$) as the number of C_4 groups decreased. This strongly suggests that C_4 got separated from the C_4 containing dialkylimines and replaced by C_2 stemming from C_2-NH_2 . The concentration of *n*-butylamine decreased steadily during the reaction. Only in the time interval, in which dialkylimines were rapidly converted (between 85 and 112 min) a slight increase of the concentration was observed. It was approximately of the same value ($0.036 \text{ mol}\cdot\text{dm}^{-3}$) as the decrease of the C_4 groups in dialkylamine ($0.033 \text{ mol}\cdot\text{dm}^{-3}$). Cross-disproportionation (Equ. 4.20) cannot be the only way of alkyl group transfer, as in this case the C_2 and C_4 mass balances should not change.

4.3.5. Hydrogenation of $C_3-C\equiv N$ in the presence of C_2-NH_2

$C_3-C\equiv N$ was hydrogenated in the presence of an equimolar amount of C_2-NH_2 at 383 K and $c_{0,BN} = 4.08 \text{ mol}\cdot\text{dm}^{-3}$. The concentration profile of the reaction is depicted in Figure 4.11. In comparison to the reaction without C_2-NH_2 the rate of reaction increased by 15% ($3.94 \times 10^3 \text{ mol}\cdot\text{min}^{-1}\cdot\text{g}_{\text{Cat}}^{-1}$). With 94.9%, the selectivity to C_4-NH_2 was 1.2% lower than in

the absence of C_2-NH_2 . C_4-NH-C_4 and C_2-NH-C_4 were observed as by-products with a selectivity of 2.1% and 3.0%, respectively. Additionally, with respect to the starting concentration of C_2-NH_2 , 3.4% of C_2-NH-C_2 were found. To clarify the course of the reaction, Table 4.6 summarizes the nature of the reaction products. $C_1-HC=N-C_2$ occurred as a primary product before the addition of hydrogen and was then formed at a relatively low rate. Another primary product was the imine $C_3-HC=N-C_2$, which developed at approximately the same rate as $C_3-HC=N-C_4$ (after a time delay of 10 min). Only after 80% of $C_3-C\equiv N$ had been hydrogenated considerable increase in the concentration of secondary amines was observed coinciding with rapid conversion of the imine intermediates.

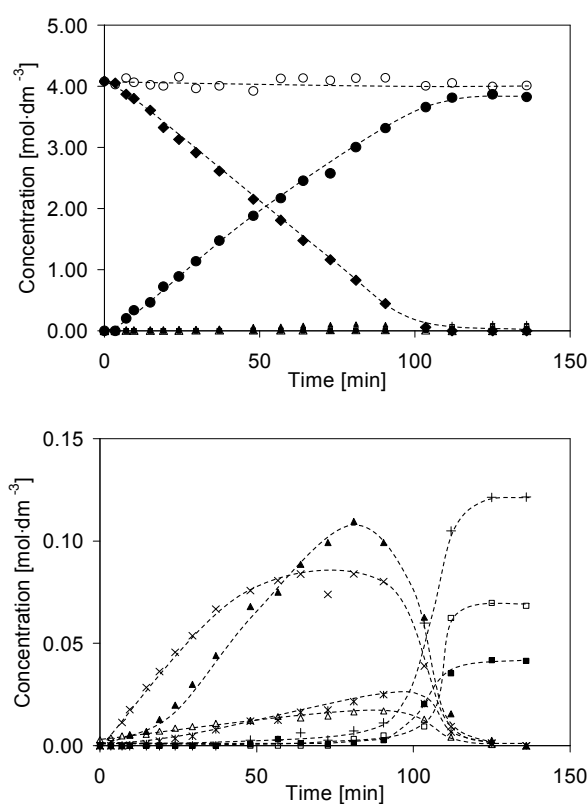


Figure 4.11: Concentration profile for the hydrogenation of $C_3-C\equiv N$ in the presence of C_2-NH_2 over Raney-Co at 383 K, $p = 45$ bar, $c_{0,BN} = 4.08$ mol·dm⁻³. (○) C_2-NH_2 , (△) $C_1-HC=N-C_2$, (□) C_2-NH-C_2 , (◆) $C_3-C\equiv N$, (●) C_4-NH_2 , (▲) $C_3-HC=N-C_4$, (■) C_4-NH-C_4 , (×) $C_3-HC=N-C_2$, (*) $C_1-HC=N-C_4$, (+) C_2-NH-C_4 .

Table 4.6: General reaction network for the hydrogenation of $C_3-C\equiv N$ in the presence of C_2-NH_2 .

Reactant	Primary products	Secondary products	Final products
$C_3-C\equiv N$	C_4-NH_2	$C_3-HC=N-C_4$	C_2-NH-C_4
C_2-NH_2	$C_3-HC=N-C_2$ ($C_1-HC=N-C_2$)*	$C_1-HC=N-C_4$	C_2-NH-C_2 C_4-NH-C_4

*Primary product due to adsorption and reaction of C_4-NH_2 on the surface prior to the addition of hydrogen.

As for the hydrogenation of $C_1-C\equiv N$ in the presence of C_4-NH_2 , the side reactions can roughly be subdivided in two regions. Dialkylimine intermediates are formed due to the formal reactions as shown in Equ. 4.10 - Equ. 4.13. These undergo further reaction to dialkylamines (Equ. 4.15 - Equ. 4.20). The occurrence of $C_1-HC=N-C_2$ before the start of the reaction can be explained by a disproportionation of two C_2-NH_2 (Equ. 4.14).

Note, that as above the mass balances of the dialkylimine intermediates and dialkylamines are almost equal (maximum deviation of 5%) suggesting that all dialkylimine intermediates further reacted to dialkylamines. Hence, hydrogenolysis of dialkylimines leading to a primary amine and an alkane (Equ. 4.21) or the elimination reaction resulting in a primary amine and an alkene (Equ. 4.22) appear unlikely.

The C_2 and C_4 mass balances were calculated at two distinct points. The number of C_2 groups increased by $0.09 \text{ mol}\cdot\text{dm}^{-3}$ between $t = 90 \text{ min}$ (point with maximum concentration in dialkylimine) and $t = 140 \text{ min}$ (final concentration of dialkylamines). In the same time interval the number of C_4 groups decreased by the same amount. Hence, a considerable amount of C_4 groups was exchanged by C_2 groups. The source is concluded to be C_2-NH_2 .

4.4. Discussion

4.4.1. H/D exchange and kinetic isotope effect in the hydrogenation of CD_3CN

For a better overview in the following discussion the rates and selectivities in the different reactions conducted are summarized in Table 4.7 and Table 4.8, respectively. As mentioned before in the deuteration of CH_3CN over Ru catalysts the H/D exchange behaviour indicated participation of the nitrile methyl group in the formation of ethylamine (see Figure 4.1).^[15] The very small degree of H/D exchange observed in this study for the hydrogenation of CD_3CN over Raney-Co suggests that deuterons from the methyl group hardly interacted with other molecules adsorbed on the catalyst surface. Thus, a mechanism, in which transfer of D from the CD_3 group to either C or N of the CN triple bond occurs, can be excluded. However, a kinetic isotope effect of $k_H/k_D = 1.10$ was found suggesting that nitrile participates in the rate determining step of the reaction. The ratio of the reaction rates of CH_3CN and CD_3CN (1.10) was close to the inverse ratio of the molar masses ($CD_3CN/CH_3CN = 1.07$) indicating that lower diffusivity of CD_3CN due to its higher mass plays a key role in the isotope effect. The rate of formation of dialkylimine is higher with CH_3CN than with CD_3CN (factor 1.4) resulting in a lower selectivity to ethylamine. This is an indication that deuterated compounds also participate in the rate determining step of the bimolecular reaction leading to by-products.

Table 4.7: Summary of the rates of conversion of the respective nitrile and the rates of formation of the imine intermediates (dialkylimines)

Reaction	Concentration [mol·dm ⁻³]	Rate of conversion × 10 ³ [mol·min ⁻¹ ·g _{Cat} ⁻¹]		Rate of formation × 10 ³ [mol·min ⁻¹ ·g _{Cat} ⁻¹]			
		AN	BN	EEI	BBI	EBI	BEI
AN	9.52	4.50	-	0.42	-	-	-
AN	4.08	4.06	-	0.09	-	-	-
AN-d ₃	9.52	4.09	-	0.30	-	-	-
BN	7.12	-	3.48	-	0.19	-	-
BN	4.08	-	3.44	-	0.05	-	-
AN+BN	4.08	3.67	1.87	0.20	0.10	0.46	0.09
AN+BA	4.08	4.46	-	0.13	0.03	0.32	0.01
BN+EA	4.08	-	3.94	0.04	0.17	0.03	0.18

Table 4.8: Summary of the selectivities in the different hydrogenation reactions.

Reaction	Concentration [mol·dm ⁻³]	Selectivity [%]				
		EA	BA	DEA	DBA	EBA
AN	9.52	88.9	-	11.1	-	-
AN	4.08	96.1	-	3.9	-	-
AN-d ₃	9.52	90.4	-	9.6	-	-
BN	7.12	-	88.0	-	12.0	-
BN	4.08	-	96.1	-	3.9	-
AN+BN	4.08	83.6	89.4	8.7	2.9*	7.7
AN+BA	4.08	91.7	-	5.6	1.5*	2.7
BN+EA	4.08	-	94.9	3.4	2.1	3.0

*Calculated based on the amount of amine present in the reaction mixture prior to the start of the reaction. Therefore, overall selectivity > 100% in the two specific cases. All other selectivities were determined with respect to the nitriles applied.

4.4.2. Role of the strength of adsorption

In both, hydrogenation of the single nitriles and co-hydrogenation of C₁-C≡N and C₃-C≡N, the rate for C₁-C≡N consumption was higher than for C₃-C≡N. The difference may be caused by a stronger adsorption of C₁-C≡N and/or by a faster intrinsic reaction rate.^[10] In the co-hydrogenation of the two compounds, the rate of C₃-C≡N consumption was lower than that of C₁-C≡N when compared to the reactions with only one nitrile as reactant. With de-

creasing amount of $C_1-C\equiv N$ the reaction rate of $C_3-C\equiv N$ hydrogenation increased. Both observations indicate that $C_1-C\equiv N$ adsorbs more strongly on the surface.

In most of the recent studies it had been stated that condensation takes place on the catalyst surface.^[8, 19, 20] In this study, the primary nature of the dialkylimines confirms that their formation occurred on the surface. With both nitriles investigated the selectivity to primary amines was lowered upon an increase of the starting concentration of the reactants. Thus, it is concluded that the concentration of precursors necessary for the formation of secondary amines is influenced by the concentration of nitrile. For example in the hydrogenation of $C_1-C\equiv N$ the rate of hydrogenation increased by a factor of 1.13, whereas the rate of formation of $C_1-HC=N-C_2$ was a factor of 4.7 higher when raising the starting concentration from $4.08 \text{ mol}\cdot\text{dm}^{-3}$ to $9.52 \text{ mol}\cdot\text{dm}^{-3}$. Thus, the formation of primary amines is almost independent of the starting concentration indicating an order close to zero due to full coverage of the sites participating in the hydrogenation, whereas for the formation of dialkylimines a positive order was observed. The strong influence on the rate of by-product formation indicates that the two processes – hydrogenation and condensation – take place on different sites. While the sites for hydrogenation were almost saturated at lower pressure those for condensation still had sorption capacity. In literature it was reported that adding amines to the reaction mixture has no effect^[19, 21] or a retarding effect on the rate of hydrogenation.^[22] This suggests that amines are adsorbed on other sites than those used for hydrogenation and that amines are more strongly adsorbed on the metal sites than the nitriles, respectively. In this study, in the presence of an equimolar amount of amine the rate of hydrogenation was slightly increased for both nitriles, which is another indication for the dual site mechanism proposed. In fact, the rate of nitrile conversion in presence of amine was approximately the sum of the rate without amine being present and the rate of formation of the asymmetric dialkylimines. Hence, faster reaction of the nitrile is due to enhanced by-product formation, in which part of the nitrile is involved. Again, this observation strongly suggests that the by-product formation takes place on other sites than the hydrogenation. Note that a hydrogenation step is involved in the formation of the precursor of the condensation product. Either, a partly hydrogenated intermediate migrates to the condensation sites as proposed by Verhaak et al.^[20] or, which is considered less likely, hydrogenation also takes place on the condensation sites resulting in a surface intermediate more susceptible to condensation than to further hydrogenation.

4.4.3. Mechanistic aspects of the formation of dialkylimines

The formation of secondary amines occurred in two distinct steps. In parallel to the formation of primary amines dialkylimines were formed first, which at least partly left the catalyst surface. After most of the nitrile had been depleted the dialkylimines re-adsorbed on the surface to react further to dialkylamines. At first sight, the first step governs the selectivity to secondary amines. As mentioned above, the formation of secondary dialkylimines can formally be explained by von Braun's mechanism (Equ. 4.1 - Equ. 4.5).^[7] However, aldimines have not been directly observed^[8] and other pathways are therefore taken into account in this discussion. Two main paths other than the aldimine path were suggested (shown together with the aldimine path in Figure 4.12).^[5, 18, 23] The first two hydrogen atoms can be transferred either to the nitrile nitrogen or carbon atom resulting in a carbene or nitrene, respectively. In the following discussion the different reactivity of the surface structures will be considered.

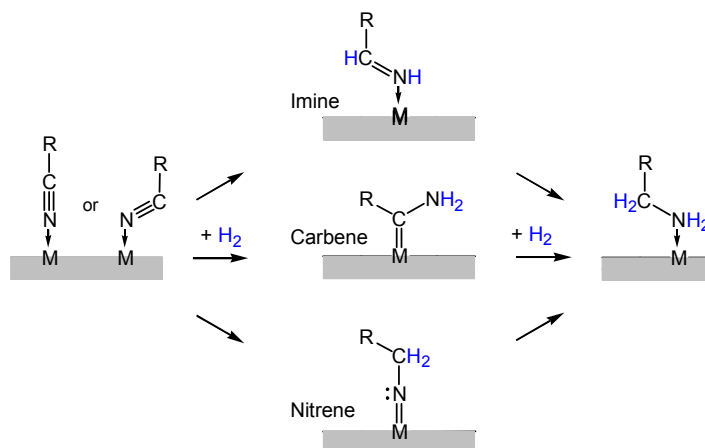


Figure 4.12: Surface reactions suggested for the hydrogenation of nitriles.

First, the relative rates of the formation of dialkylimines will be discussed. In the co-hydrogenation of $C_1-C\equiv N$ and $C_3-C\equiv N$ all possible dialkylimines appeared as primary products. Interestingly, $C_1-HC=N-C_4$ the formal condensation product of C_4-NH_2 and $C_1-HC=NH$ showed the highest rate of formation though C_2-NH_2 was formed at a much higher rate than C_4-NH_2 and very little C_4-NH_2 was detected in the liquid phase. The second highest rate was observed for $C_1-HC=N-C_2$, which would have been expected highest considering the relative concentrations of C_2-NH_2 and C_4-NH_2 . Similar results were obtained for the reactions of the respective nitriles in the presence of amine. In both cases, the highest rate is observed for the asymmetric dialkylimine, which is the result of the formal condensation of $C_1-HC=NH$ with C_4-NH_2 and of $C_3-HC=NH$ with C_2-NH_2 . However, the rate in the case of the

reaction with C_4-NH_2 is almost twice as high as with C_2-NH_2 . Thus, the nature of the amine seems to play an important role.

Assuming that both reactants have to adsorb on the surface, a stronger adsorption of C_4-NH_2 compared to C_2-NH_2 might explain the preferred reaction of C_4-NH_2 . Note, that according to our experimental results $C_1-C\equiv N$ adsorbs more strongly than $C_3-C\equiv N$ whereas on the other hand it is the other way round with the amines. Analysis of the proton affinity showed that butyronitrile and butylamine are more basic than acetonitrile and ethylamine.^[24] Weaker adsorption of butyronitrile on cobalt compared to acetonitrile can be explained by the higher steric demand of the propyl group. Volf and Pasek^[4] compared the selectivities of nitriles with varying chain length with the Tafts constant σ^* , which is a measure for the inductive effect of the alkyl chain on the nitrogen atom. They found that with increasing chain length the selectivity to the primary amine decreased. In consequence of the increasing inductive effect, C_4-NH_2 ($\sigma^* = -0.130$) would more likely attack the electrophilic C atom in $C_1-HC=NH$ than C_2-NH_2 ($\sigma^* = -0.100$). Similar argumentation holds for the carbene route.

Contrary to the co-hydrogenation of $C_1-C\equiv N$ and $C_3-C\equiv N$, only the disproportionation product of the amine ($C_3-HC=N-C_4$ and $C_1-HC=N-C_2$, respectively) and the respective asymmetric dialkylimine ($C_1-HC=N-C_4$ and $C_3-HC=N-C_2$) were observed as primary by-products in hydrogenation of the single nitriles in presence of an amine (C_4-NH_2 and C_2-NH_2). It is speculated that the amine added from the beginning to the reaction mixture blocks sites, on which the reaction leading to dialkylimines occurs, which again suggests that in our case the formation of the by-product took place on the catalyst surface.

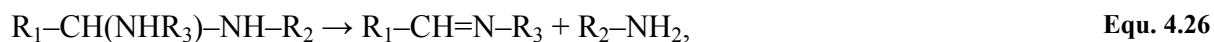
From the results described the different models shown in Figure 4.12 cannot be clearly discriminated. However, nucleophilic attack of the nitrogen electron lone pair seems to be an important factor. In principle, it can only occur at the carbon atom of the carbene or the imine, which - after proton transfer - provides an 1-amino-dialkylamine. Elimination of ammonia yields the dialkylimine. Direct hydrogenolysis of the 1-amino-dialkylamine (Equ. 4.5) can be excluded due to the appearance of dialkylimines. With the nitrene route, an attack of the electron lone pair of the nitrene nitrogen atom at the C atom of an amine adsorbed in vicinity is possible. Subsequent proton transfer from the dialkylamide to the surface NH_2 group provides the dialkylimine.

The higher rate for the reaction of C_4-NH_2 compared to C_2-NH_2 is consistent with a higher reactivity during the nucleophilic attack (carbene and imine route). Considering the nitrene route, stronger adsorption of C_4-NH_2 than C_2-NH_2 might lead to positive polarisation

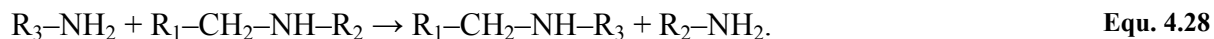
of the α -carbon atom facilitating the attack of the nitrene. However, this route to dialkylimine appears less likely.

4.4.4. Mechanistic aspects of dialkylimine hydrogenation

In the second step of the formation of secondary amines the dialkylimines are hydrogenated to dialkylamines. This rather straightforward reaction is, surprisingly, accompanied by considerable exchange of alkyl groups as shown by the C_2 and C_4 balances calculated for different reaction times. It was mentioned that in all reactions, in which alkyl group exchange was observed, the number of C_2 groups increased and the number of C_4 groups decreased in the dialkylamines relative to the dialkylimines. The results strongly suggest that C_2-NH_2 is the source of the C_2 groups. Sivasankar and Prins^[10] proposed that the reaction of a monoalkylamine and a dialkylamine can take place in the following steps:



The overall exchange reaction starting from a monoalkylamine and a dialkylamine provides another alkylamine and dialkylamine,



Starting with a dialkylimine, Equ. 4.25 - Equ. 4.27 can explain the reaction sequence observed in this study (compare e.g. Equ. 4.16). The 1-alkyl-aminodialkylamine (product in Equ. 4.25) may also undergo direct hydrogenolysis to give a dialkylamine and an alkylamine. As mentioned above it is quite certain that both hydrogenation (or hydrogenolysis) and alkyl group transfer take place on the catalyst surface, making re-adsorption of dialkylimine necessary. Hence, the exchange of the alkyl groups can only occur in the final phase of the reaction (see above).

Calculation of C_2 and C_4 mass balances at two distinct points of the reaction showed that the probability of C_2-NH_2 replacing C_4-NH_2 in the dialkylimines is considerably higher than the other way round. It was found that, among the dialkylimines, $C_3-CH=N-C_4$ was converted to the respective dialkylamine to the lowest extent. It is suggested that the alkyl group transfer takes place on the catalyst surface via the formation of 1-alkyl-aminodialkylamine (Figure 4.13). To demonstrate the reaction network the reactions of the dialkylimines with C_2-NH_2 and C_4-NH_2 are shown in Figure 4.13. The reaction of dialkylimine and monoalkylamine may either occur with both reactants adsorbed on the surface or

through nucleophilic attack of an amine on the adsorbed imine. The resulting 1-alkylaminodialkylamine can either split off C_2-NH_2 or C_4-NH_2 by direct hydrogenolysis or form another dialkylimine, which is further hydrogenated to dialkylamine. It is proposed that the product distribution depends on the relative thermodynamic stability of the dialkylimines formed. As the stabilities follow the order $C_1-CH=N-C_2 > C_1-CH=N-C_4 \approx C_3-CH=N-C_2 > C_3-CH=N-C_4$, the amount of $C_n-CH=N-C_2$ is expected to increase relative to the amount of $C_n-CH=N-C_4$ ($n = 1, 3$).

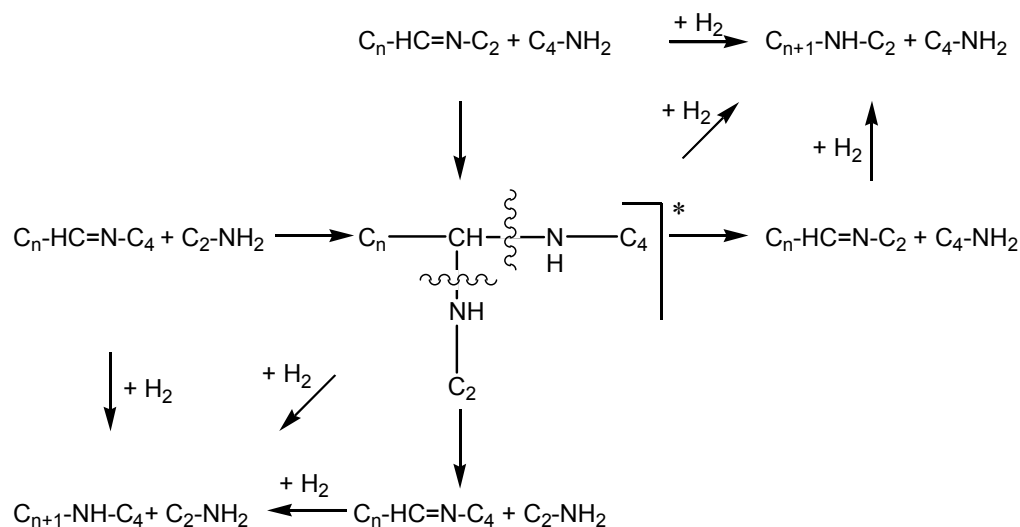


Figure 4.13: Alkyl group transfer between a dialkylimine and a monoalkylamine ($n = 1, 3$). *Adsorbed on surface.

However, the reaction shown cannot be the only way of alkyl group transfer. In the reaction of $C_3-C\equiv N$ in presence of C_2-NH_2 , e.g., the intermediates $C_1-CH=N-C_2$ and $C_1-CH=N-C_4$ only account for 70% of C_2-NH-C_2 and C_2-NH-C_4 formed. Thus, it is concluded that other reactions occur, which are accountable for the alkyl group transfer. Recently, Sivankar and Prins^[10] have proposed that dialkylamines can decompose to surface-chemisorbed amino and alkyl groups. As mentioned above, this reaction can be excluded in our case, as the mass balance in the liquid phase was closed. Instead, cross transfer of alkyl groups between two dialkylimines is considered to be a possible explanation for the change of the distribution of C_2 and C_4 during the reaction of dialkylimines to dialkylamines (Figure 4.14). Note that this reaction can only occur on the catalyst surface, as 2+2 cycloadditions are orbital forbidden under thermal conditions.

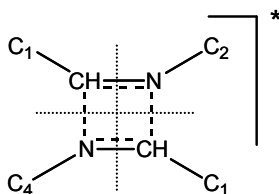


Figure 4.14: Cross transfer of alkyl groups between two dialkylimine molecules.*Adsorbed on surface.

4.5. Conclusions

To gain information on the mechanism underlying the formation of secondary amines during the hydrogenation of nitriles, acetonitrile and butyronitrile were co-hydrogenated and hydrogenated in the presence of *n*-butylamine and ethylamine, respectively. In the co-hydrogenation of the two nitriles, acetonitrile was hydrogenated at a significantly higher rate, which in comparison with the hydrogenation of the single nitriles indicates that acetonitrile is more strongly adsorbed on the active sites. The experiments with mixed reactants suggested that the rate of formation of dialkylimines strongly depended on the type of amine (*n*-butylamine, ethylamine) participating in the condensation reaction. The reaction of the partly hydrogenated surface intermediate with *n*-butylamine occurred at a higher rate, which was mainly attributed to the inductive effect of the alkyl group on the N atom and/or to stronger adsorption of *n*-butylamine compared to ethylamine.

The rate of hydrogenation remained approximately constant in the presence of amines in the starting reaction mixture and only a slight decrease in selectivity to the primary amine was observed. This led to the conclusion that the condensation to dialkylimine occurred on other sites than the hydrogenation to the corresponding primary amine. After most of the nitrile had been hydrogenated, the dialkylimine was converted further to dialkylamine. During the reaction of the dialkylimines to the dialkylamines an increase of the number of C₂ groups was observed, whereas the number of C₄ groups decreased. This strongly suggests that alkyl group transfer between monoalkylamines and dialkylimines occurred. The exchange might occur through formation of a surface bound 1-alkyl-aminodialkylamine with subsequent cleavage of the CN bond. A change of the distribution of C₂ and C₄ between different dialkylimines was tentatively attributed to a surface bound intermediate formed by 2+2 cycloaddition of two dialkylimines.

In summary, this study provided insight into the reaction pathways, which lead to the formation of condensation products during the hydrogenation of nitriles. More detailed understanding of the reactions, which occur on the surface of the metal catalyst, will provide the basis for tuning the catalysts with respect to activity and selectivity to primary amines.

Acknowledgements

Xaver Hecht and Andreas Marx are thanked for experimental support. Experimental assistance of Cen Liu and Yuying Liang is acknowledged. Klaus Ruhland and G. Krutsch from the Chair of Inorganic Chemistry are acknowledged for performing the NMR measurements.

References

- [1] M. G. Turcotte, T. A. Johnson, in *Kirk-Othmer Encyclopedia of Chemical Technology*, Vol. 2 (Ed.: J. I. Koschwitz), 4 ed., Wiley, New York, **1992**, pp.396-389.
- [2] B. Bigot, F. Delbecq, A. Milet, V. H. Peuch, *J. Catal.* **1996**, *159*, 383.
- [3] B. Bigot, F. Delbecq, V. H. Peuch, *Langmuir* **1995**, *11*, 3828.
- [4] J. Volf, J. Pasek, *Stud. Surf. Sci. Catal.* **1986**, *27*, 105.
- [5] C. DeBellefon, P. Fouilloux, *Catal. Rev.-Sci. Eng.* **1994**, *36*, 459.
- [6] M. S. Wainwright, in *Preparation of Solid Catalysts* (Eds.: G. Ertl, H. Knözinger, J. Weitkamp), Wiley-VCH, Weinheim, **1999**, p. 28-43.
- [7] J. von Braun, G. Blessing, F. Zobel, *Chem. Ber.* **1923**, *56*, 1988.
- [8] Y. Y. Huang, W. M. H. Sachtler, *Appl. Catal. A-Gen.* **1999**, *182*, 365.
- [9] S. Gomez, J. A. Peters, T. Maschmeyer, *Adv. Synth. Catal.* **2002**, *344*,365.
- [10] N. Sivasankar, R. Prins, *J. Catal.* **2006**, *241*, 342.
- [11] P. Sabatier, J. B. Senderens, *Comptes Rendus* **1905**, *140*, 482.
- [12] K. Kindler, F. Hesse, *Arch. Pharm.*, **1933**, *271*, 439.
- [13] H. Greenfield, *Ind. Eng. Chem. Prod. Res. Dev.* **1967**, *6*, 142.
- [14] P.N. Rylander, L. Hasbrouck, *Engelhard Ind. Tech. Bull.* **1970**. *11*. p. 19.
- [15] Y. Y. Huang, W. M. H. Sachtler, *J. Catal.* **2000**, *190*, 69.
- [16] M. Hesse, H. Meier, B. Zeeh, *Spektroskopische Methoden in der organischen Chemie*, 3 ed., Georg Thieme Verlag, Stuttgart, **1987**.
- [17] E. Pretsch, T. Clerc, J. Seibl, S. Wilhelm, *Tabellen zur Strukturaufklärung organischer Verbindungen mit spektroskopischen Methoden*, Vol. 15, 3 ed., Springer-Verlag, Berlin, **1986**.
- [18] A. Chojecki, M. Veprek-Heijman, T. E. Müller, P. Schäringer, S. Veprek, J. A. Lercher, *J. Catal.* **2007**, *245*, 237.
- [19] J.L. Dallons, A. Van Gysel, G. Jannes, in *Catalytic Organic Reactions*, Vol. 47, (Ed.: W. E. Pascoe), Dekker, New York, **1992**, p. 93-104.
- [20] M. Verhaak, A. J. Vandillen, J. W. Geus, *Catal. Lett.* **1994**, *26*, 37.
- [21] F. Hochard, H. Jobic, J. Massardier, A. J. Renouprez, *J. Mol. Catal. A-Chem.* **1995**, *95*, 165.
- [22] Y. Y. Huang, W. M. H. Sachtler, *J. Catal.* **1999**, *188*, 215.

- [23] B. Coq, D. Tichit, S. Ribet, *J. Catal.* **2000**, 189, 117.
- [24] *Proton affinity in kJ/mol: Acetonitrile: 798.4; Butyronitrile: 779.2; Ethylamine: 921.5; 912.0.* [NIST database] (accessed 28.12.2006).

Chapter 5

Tailoring Raney-catalysts for the selective hydrogenation of butyronitrile to *n*-butylamine*

Abstract

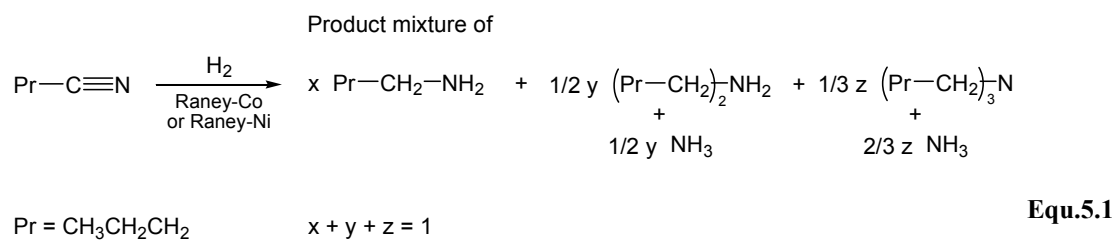
LiOH promotion of Co-based Raney-catalysts for the selective hydrogenation of butyronitrile to *n*-butylamine was explored. Doping with LiOH led to an increase in the fraction of metallic surface area and reduced concentration of Lewis acid sites resulting from alumina particles decorating the metal surface. Two factors were found to be crucial for achieving high selectivity to primary amines. These factors include a low adsorption constant of *n*-butylamine relative to butyronitrile (as adsorbed butylamine is necessary for by-product formation) and a low concentration of Lewis acid sites catalyzing condensation reactions.

* The measurements presented in this chapter were performed by Adam Chojecki. The results were analyzed and interpreted by the author of this thesis.

5.1. Introduction

The reduction of nitriles to primary amines is a large-scale commercial process route.^[1] One of the most important applications is the conversion of 1,4-dicyanobutane to 1,6-diaminohexane, which is used in the production of nylon-6,6.^[2, 3] It is known that the hydrogenation of $C\equiv N$ groups proceeds stepwise through reactive intermediates.^[4, 5] Consequently, condensation reactions may occur and mixtures of ammonia and primary, secondary and tertiary amines are generally obtained. The factors that influence the product distribution are manifold and originate from catalyst composition (e.g., choice of metal and support, presence of promoters) and reaction conditions.^[6] High selectivities to primary amines were reported for Co, Ni and Ru catalysts.^[7] In contrast, nitriles can be reduced to secondary and tertiary amines using Rh, Pd and Pt catalysts.^[8] In the industrial process, a high selectivity to primary amines is achieved by working at high hydrogen pressures (up to 600 bar) and with ammonia as solvent.^[9] Skeletal metal catalysts based on Ni and Co, provide the lowest cost per unit mass of active catalyst and are widely used.^[10] Their selectivity can be enhanced by modification with small amounts of alkali metal hydroxides.^[11-13] The reduction of nitriles with Raney-Ni has been studied repeatedly,^[14-16] while less reports have been published on Raney-Co.^[17-20] For Raney-Ni, also the effect of bases on the selectivity was investigated.^[21, 22]

The rational development of next generation catalysts with high selectivity to primary amines requires deeper insights into the processes, which govern the selectivity. This study was, therefore, aimed at establishing for the first time correlations between the surface properties of unmodified and LiOH doped Raney-Co catalyst, the sorption characteristics not only for hydrogen but also for nitrile and amine, and the catalytic activity in the reduction of nitriles. The hydrogenation of butyronitrile to *n*-butylamine was explored as a model reaction for the reduction of nitriles over Raney-catalysts (Equ.5.1). Several techniques for the characterization of Raney-catalysts were utilized focusing on surface properties. Special emphasis was placed on understanding the beneficial effect of LiOH modification on the intrinsic activity and selectivity of Raney-Co. As reference materials, commercial catalysts with low selectivity but relatively high activity (Raney-Ni), high selectivity and low rate (Raney-Co), and both high selectivity and high reactivity (Ni-Cr promoted Raney-Co) were chosen. For those materials, the characterization was aimed at establishing boundary conditions for designing catalysts for the selective hydrogenation of nitriles to primary amines.



5.2. Experimental

5.2.1. Catalyst preparation and materials

The catalysts Raney-Ni (#2800, lot #7716, mean grain diameter 45.6 μm), Raney-Co (#2700, lot #7865, mean grain diameter 30.1 μm) and Ni-Cr promoted Raney-Co (#2724, lot #7733, mean grain diameter 28.5 μm) were obtained as aqueous suspension from W.R. Grace & Co, GRACE Davison Chemical Division (chemical composition see Table 5.1).

Table 5.1: Chemical composition of the catalysts used in this study (data of catalyst manufacturer).

Catalyst	Element	Co	Ni	Cr	Al
	[wt%]	[wt%]	[wt%]	[wt%]	[wt%]
Raney-Ni	< 0.5	92.8	—	6.77	
Raney-Co	97.5	< 0.5	< 0.5	1.85	
Ni-Cr promoted Raney-Co	91.3	2.8	2.2	3.50	

Catalysts used for characterization and hydrogenation experiments underwent the following pre-treatment. The catalysts were washed with de-ionized water until pH 7 was measured taking thorough care that the catalyst was sufficiently covered with liquid in order to avoid contact with atmospheric oxygen. After drying in a flow of Argon (4 h at 328 K, and 1 h at 378 K) the catalysts were handled and stored under inert atmospheres throughout all other preparation and characterisation steps. For doping with LiOH, a thoroughly washed sample of Raney-Co (143 g) was suspended in an aqueous solution of LiOH (3.25 g in 100 cm³ de-ionized water). The water was removed in partial vacuum (< 4 mbar) and the sample dried (10 h at 323 K). The concentration of Li⁺ was 0.5 wt% Li as determined with AAS (UNICAM 939 AA-Spectrometer). All other chemicals used in this study were obtained from commercial suppliers and used as received (butyronitrile, ≥ 99 % GC-assay, Fluka; mono-, di- and tri-*n*-butylamine, > 99 % GC-assay, Aldrich; *n*-octane and *n*-undecane, ≥ 99 GC-assay, Aldrich;

and H₂, Ar, NH₃, 99.999, 99.999 and 99.98 vol. %, respectively). All solvents and reactants were degassed in partial vacuum.

5.2.2. Catalysis

The hydrogenation of butyronitrile was carried out in a high-pressure 160 cm³ semi-batch reactor at constant hydrogen pressure. Oxygen was removed from the autoclave by several cycles of pressurizing and depressurizing with argon. The autoclave was then charged under a flow of argon with 50 cm³ reaction mixture, composed of butyronitrile (2.18 cm³, 0.025 mol, corresponding to 0.5 mol·dm⁻³), octane (47.6 cm³) and catalyst (0.2 g). *n*-Undecane (0.2 g) was added as internal standard for GC chromatography. The mixture was stirred at 1500 rpm and equilibrated at the reaction temperature (353, 373 or 383 K) for 45 - 60 min. The reaction was started by rapidly pressurizing the autoclave with hydrogen to 15, 30 or 45 bar. During the experiment samples of the liquid phase were taken for off-line GC-analysis and analyzed with an HP Gas Chromatograph 5890 equipped with a cross linked 5% diphenyl-95% dimethylpolysiloxane column (Rtx-5 Amine, 30 m, Restek GmbH). The reaction rate was calculated from the decrease in butyronitrile concentration in the linear range between 20 and 80 % conversion. A test on mass transfer limitations showed that the reaction rate did not depend on the stirring speed in the range 1000 – 1850 rpm.

5.2.3. Catalyst characterization

N₂-physisorption and H₂-chemisorption measurements were carried out on a Sorptomatic 1990 instrument (ThermoFinnigan). For N₂-physisorption, the catalyst samples (0.4 – 1.0 g) were outgassed for 1 h in high vacuum at the temperature stated in the text (298 – 633 K). The measurements were carried out at 77 K using N₂ as probe molecule. BET area and pore volume were calculated from the isotherm. The micropore volume was calculated from a Horvath Kawazoe Plot in the pressure range p/p° 0 to 0.2. For hydrogen chemisorption, the catalysts were outgassed for 1 h at 383 K. Isotherms were recorded at 298 K, equilibrating between 2 and 180 min for each pressure step. Equilibration was continued until the pressure deviation was less than 0.27 mbar within of a period of 2 min. Isotherms were measured twice on the same sample. Between the two measurements, the sample was evacuated to 10⁻³ mbar for 1 h. The second isotherm (physisorbed H₂) was subtracted from the first isotherm (chemisorbed and physisorbed H₂). For determination of the amount of chemisorbed hydrogen, the linear part of the isotherm at $p > 3$ Pa was extrapolated to zero. The fraction of accessible

metal atoms was calculated assuming that one hydrogen atom was adsorbed per nickel or cobalt atom.

Temperature programmed desorption (TPD) measurements were carried out in a custom-built vacuum setup. The catalyst (50 mg) was outgassed for 8 h at 378 K. The temperature was then raised at $10 \text{ K}\cdot\text{min}^{-1}$ to 973 K and the desorbing molecules analyzed with mass spectrometry. The masses $m/z^+ = 2$ and 18 were used for monitoring desorption of hydrogen and water, respectively. To determine the desorption maxima, the MS traces were fitted with Gaussian curves using Grams/AI (Thermo Galactic, Version 7.02). For temperature programmed desorption of ammonia, the samples (100 mg) were heated in high vacuum at $5 \text{ K}\cdot\text{min}^{-1}$ to 473 K, outgassed for 5 min and cooled to 423 K. Subsequently, the sample was equilibrated for 1 h with ammonia ($p_{\text{NH}_3} = 1 \pm 0.3 \text{ mbar}$) and outgassed for 3 h. Finally, the sample was heated at $10 \text{ K}\cdot\text{min}^{-1}$ and the desorption of ammonia was followed with mass spectrometry using $m/z^+ = 15$.

For X-ray photoelectron spectroscopy (XPS) measurements, also thorough care was taken to avoid contact of the catalyst samples with atmospheric oxygen. In a glove box, the dried catalyst was placed on adhesive conducting tape. The sample was transferred under Argon to a Leybold LH 10 surface analysis system and analyzed without further pre-treatment. For each sample, a survey spectrum was collected. The detailed spectra were excited with Al-K_α (1486.6 eV, 0.83 nm) and recorded in $\Delta E = \text{constant}$ mode. Selected spectral regions were repetitively scanned and the signals averaged to improve the signal-to-noise ratio. To compensate for charge effects, the C 1s signal at 285 eV was used as reference^[23] and the binding energy scale corrected. Data were fitted (solid lines in Figure 5.7) to account for the different species on the catalyst surface. Spectral resolution and error in the peak position was approximately 0.5 eV.

The adsorption constants were calculated from breakthrough curves, which were obtained in a custom built setup. A chromatographic column was packed under Argon with the dried catalyst (2.5 g). The void space below and above the catalyst was filled with glass beads. Using a by-pass, all lines were flushed with Argon prior to the experiments. The column was equilibrated at room temperature with thoroughly degassed *n*-pentane. A solution of the adsorbate (*n*-butylamine or butyronitrile) and internal standard (octane) in *n*-pentane (both $12.5 \text{ mmol}\cdot\text{dm}^{-3}$) was passed over the catalyst at constant rate ($2.2 - 2.3 \text{ cm}^3\cdot\text{min}^{-1}$). The effluent was sampled every 0.2 min until steady state was obtained at the exit of the column. The composition of the eluent was evaluated by gas chromatography. The concentration of the

adsorbate in the feed was then increased step-wise to 12.5, 25, 50, 75 and 100 mmol·dm⁻³. For competitive sorption, an equimolar solution of *n*-butylamine and butyronitrile (50 mmol·dm⁻³) was passed over the catalyst.

5.3. Results

5.3.1. Catalytic activity in the reduction of butyronitrile and selectivity to *n*-butylamine

Activity and selectivity of four different Raney catalysts (Raney-Ni, Raney-Co, Ni-Cr promoted Raney-Co, and LiOH modified Raney-Co) were tested for the hydrogenation of butyronitrile. A typical concentration profile for Raney-Ni is shown in Figure 5.1a. After a short induction time (2 min), the hydrogenation of butyronitrile proceeded at a rate of $0.97 \cdot 10^{-4} \text{ mol}_{\text{butyronitrile}} \cdot (\text{g}_{\text{cat}} \cdot \text{s})^{-1}$. The butyronitrile concentration decreased almost linearly with time. In parallel, the integral hydrogen consumption increased linearly (Figure 5.1b). Only at high conversions (> 80 %), the reaction slowed down. The main product was *n*-butylamine, which was formed with 66% selectivity. Di-*n*-butylamine and traces of tri-*n*-butylamine were formed as by-products; *N*-butylidene-butylamine was observed as a reaction intermediate (maximum concentration $20 \cdot 10^{-3} \text{ mol} \cdot \text{dm}^{-3}$). Its concentration started decreasing, as soon as more than ~ 70 % of butyronitrile had been converted. At the end of the experiment, no *N*-butylidene-butylamine was found. The concentration of *n*-butylamine and *N*-butylidene-butylamine started increasing right after the start of the reaction indicating that both are primary reaction products. In contrast, di-*n*-butylamine and tri-*n*-butylamine were formed with a time delay, which suggests that they are secondary reaction products.

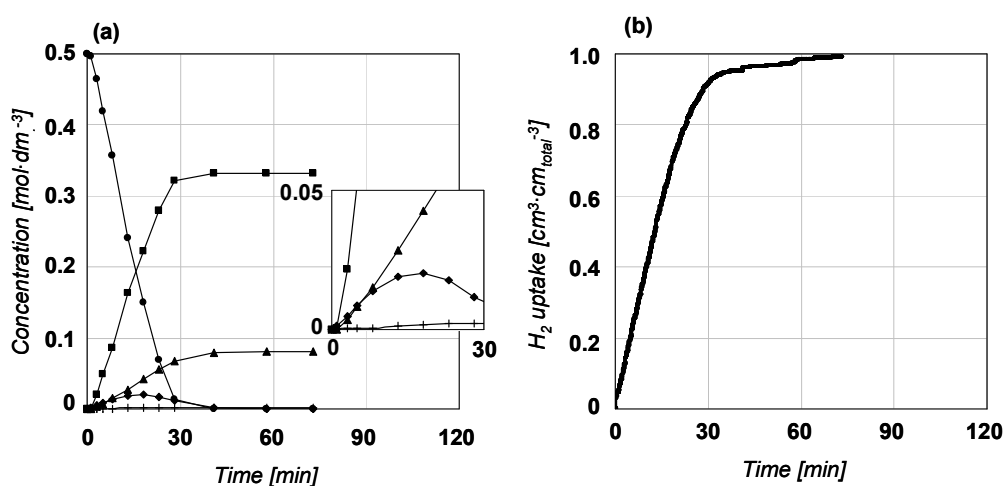


Figure 5.1: (a) Concentration profile for the hydrogenation of butyronitrile over Raney-Ni at 373 K, $p = 30$ bar, $c_0(\text{butyronitrile}) = 0.50 \text{ mol} \cdot \text{dm}^{-3}$ (● butyronitrile, ■ *n*-butylamine, ▲ di-*n*-butylamine, ◆ *N*-butylidene-butylamine, + tri-*n*-butylamine). (b) Integral hydrogen uptake.

A typical concentration profile for the hydrogenation of butyronitrile over Raney-Co is related to the integral hydrogen consumption in Figure 5.2. After a short induction period (< 3 min), the hydrogenation commenced at a rate of $3.25 \cdot 10^{-5} \text{ mol}_{\text{butyronitrile}} \cdot (\text{g}_{\text{cat}} \cdot \text{s})^{-1}$ and was finished after 90 min. The selectivity to *n*-butylamine was high (98.0 %). *n*-Butylamine and *N*-butylidene-butylamine were detected right after the start of the reaction, and appeared to be primary reaction products.

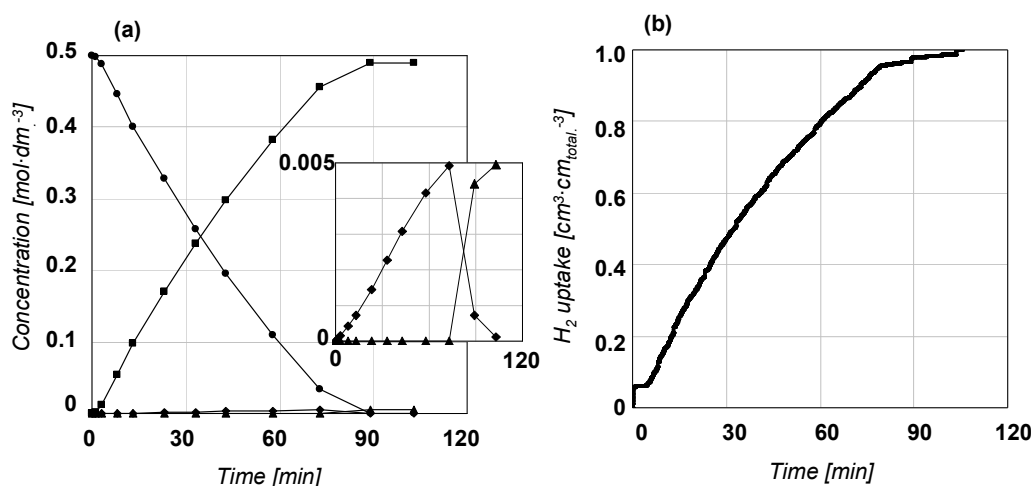


Figure 5.2: (a) Concentration profile during the hydrogenation of butyronitrile over Raney-Co at 373 K, $p = 30$ bar, $c_0(\text{butyronitrile}) = 0.50 \text{ mol} \cdot \text{dm}^{-3}$ (● butyronitrile, ■ *n*-butylamine, ▲ di-*n*-butylamine, ◆ *N*-butylidene-butylamine). (b) Hydrogen uptake normalized to the total H_2 -uptake.

The formation of di-*n*-butylamine was only observed, once more than 90 % of butyronitrile had been hydrogenated. It is particularly noteworthy that the final concentration of di-*n*-butylamine was equal to the maximum concentration of *N*-butylidene-butylamine. This strongly suggests that di-*n*-butylamine is a sequential product of the hydrogenation of *N*-butylidene-butylamine. Tri-*n*-butylamine was not observed.

Over Ni-Cr promoted Raney-Co and LiOH modified Raney-Co, the reaction proceeded in a similar way as with Raney-Co, but with improved activity ($2.47 \cdot 10^{-4}$ and $0.39 \cdot 10^{-4} \text{ mol}_{\text{butyronitrile}} \cdot (\text{g}_{\text{cat}} \cdot \text{s})^{-1}$, respectively) and selectivity to *n*-butylamine (99.0 and 99.5 %, respectively). Also, the maximum concentration of *N*-butylidene-butylamine ($2.0 \cdot 10^{-3}$ and $1.0 \cdot 10^{-3} \text{ mol} \cdot \text{dm}^{-3}$, respectively) was lower than with the parent Raney-Co ($4.9 \cdot 10^{-3} \text{ mol} \cdot \text{dm}^{-3}$). As with Raney-Co, the final concentration of di-*n*-butylamine was equal to the maximum transient concentration of *N*-butylidene-butylamine. Note that *N*-butylidene-butylamine was hydrogenated to di-*n*-butylamine only at high conversions of butyronitrile.

Table 5.2: Activity and selectivity of Raney catalysts in the hydrogenation of butyronitrile.

Catalyst	Rate normalized to catalyst weight [mol _{butyronitrile} ·(g _{cat.} ·s) ⁻¹]	Rate normalized to accessible metal atoms [mol _{butyronitrile} ·(mol _{surface atoms} ·s) ⁻¹]	Selectivity [%]
Raney-Ni	0.97·10 ⁻⁴	0.14	66.0
Raney-Co	0.33·10 ⁻⁴	0.08	98.0
Ni-Cr promoted Raney-Co	2.47·10 ⁻⁴	0.31	99.0
LiOH modified Raney-Co	0.39·10 ⁻⁴	0.22	99.5

The intrinsic activity (normalized to the number of accessible metal atoms) is compared with the weight normalized catalytic activity in Table 5.2. The sequence in the activity of the four catalysts depends on the definition of the activity. This indicates that the differences in activity are not a mere consequence of the number of metal surface atoms, but rather intrinsic differences of the catalytically active sites. Thus, detailed characterization of the catalysts seemed to be necessary.

5.3.2. Specific surface area and fraction of accessible metal atoms

The BET surface area of Raney-Ni and Raney-Co varied with the temperature applied for outgassing the samples prior to the measurement (Table 5.3). For Raney-Ni, the largest BET area was measured after activation at 383 K (58 m²·g_{cat.}⁻¹), whereas the maximum for Raney-Co was observed after outgassing at 483 K (25 m²·g_{cat.}⁻¹). Lower activation temperatures were probably insufficient to remove the adsorbates completely from the pores of the catalyst, whereas higher temperatures led to particle sintering. The higher activation temperature required for Raney-Co indicates that adsorbates, such as water and hydrogen, were bound more strongly than on Raney-Ni. However, the differences caused by changing the activation temperature were small in comparison to the variations between the four catalysts. The BET surface area was higher for Raney-Ni (58 m²·g_{cat.}⁻¹) than Raney-Co (19 m²·g_{cat.}⁻¹). The presence of promoters, as in Ni-Cr promoted Raney-Co, stabilized a high BET surface area (67 m²·g_{cat.}⁻¹). In contrast, the LiOH modified Raney-Co had a lower surface area (15 m²·g_{cat.}⁻¹). Note that after LiOH modification of Raney-Co the pore volume (0.094 cm³·g_{cat.}⁻¹) did not change within the experimental error. However, the volume of the pores with diameter

≤ 1.0 nm decreased from 0.008 to $0.006 \text{ cm}^3 \cdot \text{g}_{\text{cat.}}^{-1}$. This suggests that LiOH resided mostly in the small pores, which contribute little to the void volume, but significantly to the surface area.

Table 5.3: BET surface area measured after outgassing the catalyst samples for 1 h at the temperature stated.

$T_{\text{activation}}$	Raney-Ni	Raney-Co	Ni-Cr promoted Raney-Co	LiOH modified Raney-Co
[K]	$[\text{m}^2 \cdot \text{g}_{\text{cat.}}^{-1}]$	$[\text{m}^2 \cdot \text{g}_{\text{cat.}}^{-1}]$	$[\text{m}^2 \cdot \text{g}_{\text{cat.}}^{-1}]$	$[\text{m}^2 \cdot \text{g}_{\text{cat.}}^{-1}]$
298	55.4	19.2	67.5	14.8
383	57.7	19.3	66.8	14.8
483	52.2	24.6	61.7	—
533	—	24.1	—	—
583	47.9	23.7	—	—
633	45.7	19.5	—	—

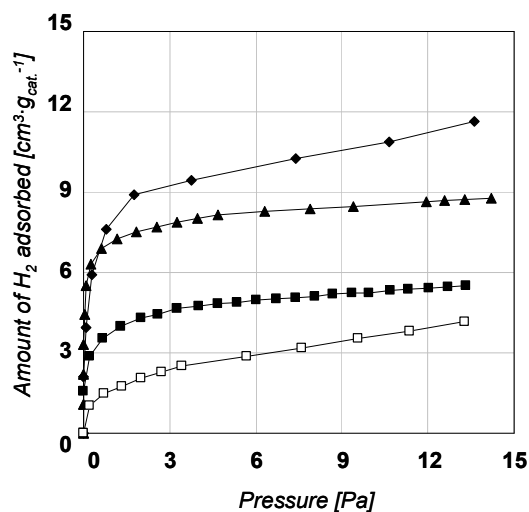


Figure 5.3: Hydrogen adsorption isotherms recorded at 298 K (\blacklozenge Ni-Cr promoted Raney-Co, \blacktriangle Raney-Ni, \blacksquare Raney-Co and \square LiOH modified Raney-Co).

The fraction of surface metal atoms was determined with hydrogen chemisorption (Figure 5.3, Table 5.4). For the four catalysts, the same trend was observed as based on the BET surface area. However, the metal surface area was two to three times lower than the specific surface area. This shows that only a part of the surface was accessible nickel or cobalt. Probably, aluminum, which was not removed during preparation,^[21, 24, 25] Al_2O_3 and other ox-

ides led to a higher specific surface area and covered part of the catalytically active metal surface.

Table 5.4: Number of Ni or Co surface atoms and metal surface area as determined by H₂-chemisorption at 298 K. For comparison, the results from N₂-physisorption are included.

Catalyst	Accessible metal atoms [mmol·g _{cat.} ⁻¹]	Dispersion [%]	Metal surface area* [m ² ·g _{cat.} ⁻¹]	BET surface area [m ² ·g _{cat.} ⁻¹]	Pore volume [cm ³ ·g _{cat.} ⁻¹]
Raney-Ni	0.69	4.06	27.0	55.4	—
Raney-Co	0.40	2.35	15.7	19.2	0.094
Ni-Cr promoted Raney-Co	0.80	4.72	31.3	67.5	—
LiOH modified Raney-Co	0.18	1.06	7.1	14.8	0.095

* Calculated based on a stoichiometry of 1 H atom per metal atom and a transversal section of 6.5 Å² for Ni and Co.

5.3.3. Residual water and hydrogen on the catalyst surface

The concentration of residual molecules, which remained on the catalyst surface after outgassing, was determined by temperature programmed desorption (Figure 5.4 and Figure 5.5^[26]). Raney-Ni exhibited a relatively narrow temperature range for desorption of water and hydrogen (400 – 530 K). The small distribution of desorption states is speculated to be related to a uniform surface structure with low concentration of defects. In this respect, Martin *et al.* demonstrated by measuring the saturation magnetization of Raney-Ni in an electromagnetic field, that the hydrogen evolved during TPD cannot be the result of a reaction between water and metallic aluminum.^[27] Thus, hydrogen evolution can only originate from hydrogen, which remained adsorbed on the material after the preparation procedure. Note that later comprises dissolution of aluminum in aqueous base under evolution of hydrogen.

For the parent and Ni-Cr promoted Raney-Co, the TPD traces of both residual water and hydrogen showed a broad temperature range of desorption (400 – 730 K). In case of hydrogen, the rather difficult deconvolution of the data allowed only a qualitative discussion of the data. Note that metal sintering occurs at higher temperatures, but is a relatively slow process. As the BET area at 633 K is lowered only by about 20% relative to the maximum BET area (Raney-Ni and Raney-Co, see Table 4), we assume that the TPD measurements reflect

the true state of the catalyst. In general, the desorption maxima for water and hydrogen occurred at roughly the same temperature, but the low temperature peaks for water were much more pronounced than for hydrogen.

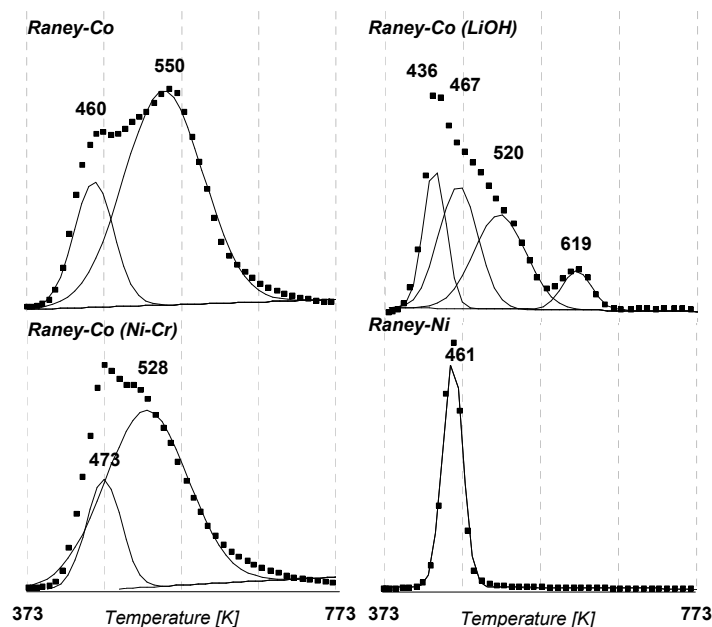


Figure 5.4: TPD traces of residual water (■) for the Raney-catalysts studied and contribution of single sites (solid lines).

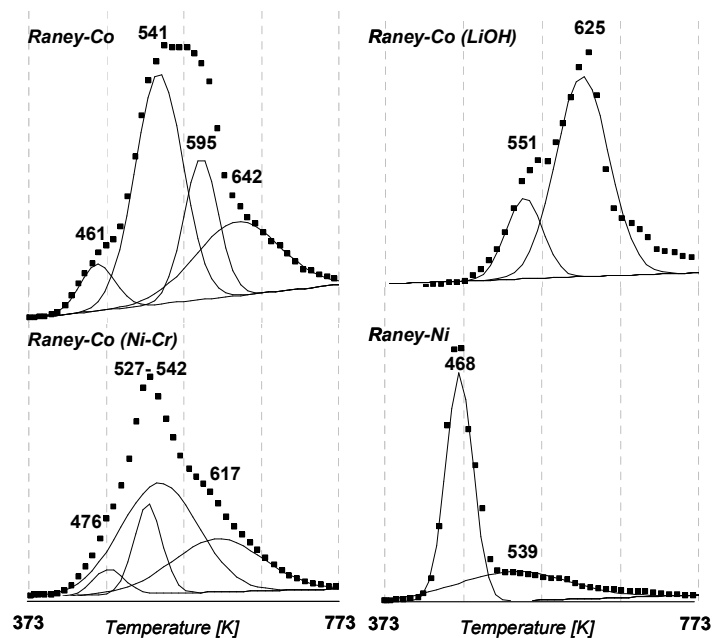
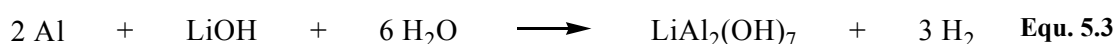
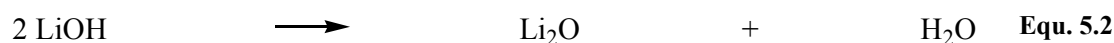


Figure 5.5: TPD traces of residual hydrogen (■) for the Raney-catalysts used in this study and contribution of single sites (solid lines).

For LiOH modified Raney-Co, analysis of the TPD data again did not exhibit a satisfying deconvolution. However, it can be stated that the highest rate of water desorption was found at 436 K and decreased slowly at higher temperatures. In contrast, for the parent Raney-Co the first desorption maximum was observed at 460 K. In this respect, it is known^[28] that lithium hydroxide reacts readily with aluminum hydroxide to $\text{LiAl}_2(\text{OH})_7 \cdot 2\text{H}_2\text{O}$,^[29] which dehydrates at low temperatures (≤ 473 K).



Thus, the desorption maximum at 436 K is probably related to reaction of lithium hydroxide. A second low intensity desorption feature at 619 K is similarly explained by dehydration of LiOH, which occurs in vacuum at 623 K. The desorption peak at 619 K correlates well with a maximum in hydrogen desorption at 625 K. The desorption trace of hydrogen showed two major desorption peaks at 551 and 625 K. The first hydrogen desorption maximum at 551 K is probably due to desorption of residual hydrogen from the metal surface, as for the other two Raney-Co catalysts. The second, more intense peak at 625 K is probably the result of a secondary reaction between aluminum and LiOH (Equ. 5.2 - Equ. 5.4).

5.3.4. Temperature programmed desorption of ammonia

The acid-base properties of Raney-Ni and Raney-Co were explored through TPD of ammonia. Note that acid sites catalyze side reactions during the hydrogenation of nitriles.^[30] The desorption traces of ammonia were generally broad and showed two pronounced maxima (Figure 5.6).

It is particularly noteworthy that for Raney-Ni, a maximum in H_2 -desorption was associated with the low-temperature desorption peak of ammonia at 560 K, whereas a maximum in N_2 desorption was related with the high-temperature peak in NH_3 desorption at 713 K. For Raney-Co, maxima in N_2 and H_2 desorption occurred in parallel with the first desorption peak of NH_3 (595 K), while a second maximum at 709 K was observed only for NH_3 desorption. For Ni-Cr promoted Raney-Co, the desorption maxima were at 559 and 704 K. An additional contribution with very low intensity was detected at 633 K.

The significant differences between cobalt and nickel can be explained by considering the relative stability of cobalt and nickel nitrides.^[31, 32] Baiker *et al.* described that reaction of ammonia with nickel at temperatures above 395 K leads to the formation of nickel nitride Ni_3N and molecular hydrogen.^[33] Nickel nitride is stable up to 683 K, but decomposes to metallic nickel and nitrogen at higher temperatures. When ammonia is adsorbed at 423 K, it partially dissociates on the Ni-surface to surface hydrogen atoms and nitrenes.^[34] The latter species react with nickel to nickel nitride. As the catalyst is heated, surface bound hydrogen and ammonia desorb first. At higher temperatures, Ni_3N decomposes resulting in the maximum rate of nitrogen evolution at 713 K. Part of the nitrogen reacts with residual H_2 and leads to a second maximum in NH_3 desorption.

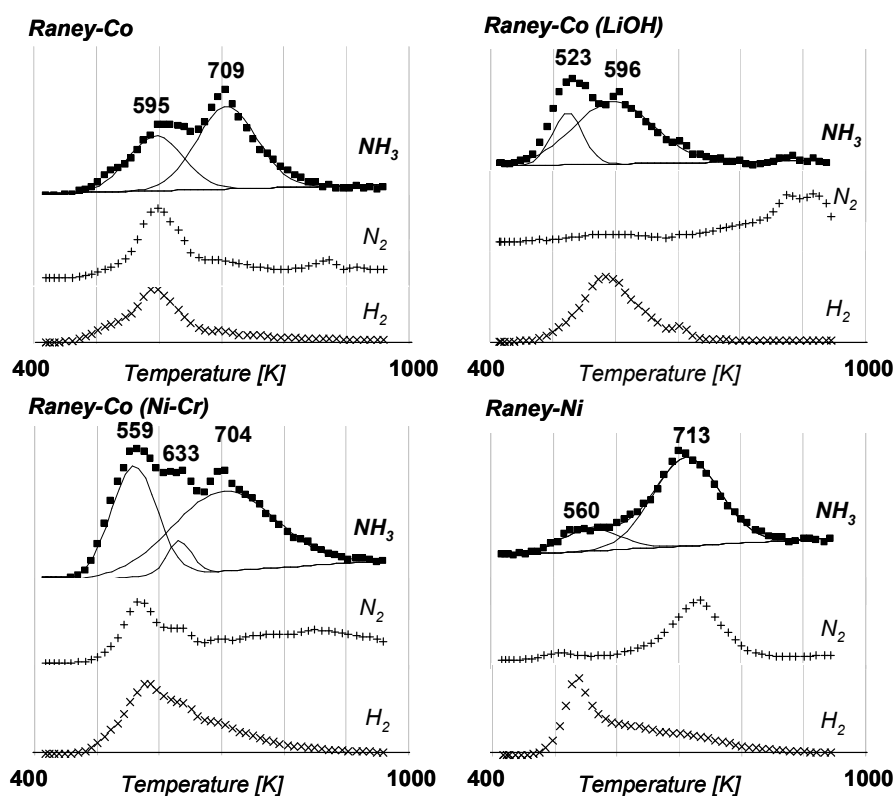


Figure 5.6: TPD traces of NH_3 (■), H_2 (×) and N_2 (+) for Raney-catalysts after adsorption of NH_3 at 423 K.

In contrast, Co_3N is less stable and decomposes, when heated to 549 K.^[32] Consequently, cobalt nitride is hardly formed during the adsorption of ammonia. Upon heating, dissociated surface species recombine to either ammonia or molecular hydrogen and nitrogen. Thus, the second maximum at 709 K, which was observed for Raney-Co, cannot be associated with metallic cobalt. Instead, it is attributed to ammonia molecularly bound to Al^{3+} Lewis acid sites.^[22] Due to the high stability, the Lewis adduct $\text{H}_3\text{N}:\rightarrow\text{Al}^{3+}$ decomposes only at high temperatures.^[35]

In comparison to the parent Raney-Co, the first maximum in the ammonia trace for Ni-Cr promoted Raney-Co was shifted to lower temperatures (559 K) indicating weaker binding of ammonia. It was associated with nitrogen and hydrogen desorption.

For the LiOH modified Raney-Co, the NH₃ desorption trace showed a maximum at 523 K with a broad shoulder centred at 596 K. Similar to the parent Raney-Co the peak at 596 K is tentatively attributed to NH₃ desorption from metallic cobalt. This assignment is supported by the parallel H₂-desorption. It is noteworthy that hardly any nitrogen desorbed from the sample and it is speculated that surface bound nitrenes react with LiOH. The low temperature peak in the NH₃ desorption trace at 523 K is most likely molecular ammonia, which is weakly coordinated to LiOH cluster. The high temperature peak at 709 K (Raney-Co) associated with Lewis acid sites of alumina was not observed, which strongly suggests that LiOH blocks these sites.

5.3.5. Characterization by X-ray photoelectron spectroscopy

The nature of different phases at the catalyst surface was evaluated from XPS (see Figure 5.7). Note that the inelastic mean free path of the electrons (IMPF) for Ni and Co is ~ 1.25 and 1.2 nm, respectively. Thus, the surface is probed to roughly this depth. Peaks, which were not sufficiently separated in deconvolution, are shown in the diagrams but not considered in the further discussion.

For Raney-Ni, three peaks at 857.0, 853.5 and 851.1 eV were observed in the Ni 2p^{3/2} region. The two peaks at 857.0 and 853.5 eV correspond to Ni²⁺ cations, probably NiAl₂O₄ (857.1 eV^[36]) and NiO (853.5 eV^[36]), respectively. In literature, Ni₂O₃,^[37] Ni(OH)₂ and NiAl₂O₄^[21] have also been claimed to be present at the surface of Raney-Ni catalysts. However, the peak at 853.5 eV could also be attributed to Al₃Ni alloy (853.6 eV^[38]). Metallic nickel (Ni⁰) was observed at 851.1 eV, which is lower than the value reported in literature (852.1 eV^[36]).

The XPS spectra of cobalt samples exhibited two maxima at 782.0 and ~779.0 eV in the Co 2p^{3/2} region. The peak at 779.0 is almost completely superposed by other peaks and deconvolution might not exactly afford the real peak position. The spectra of Raney-Co and LiOH modified Raney-Co showed an additional peak between 777.1 and 777.5 eV. The two peaks could not be clearly distinguished in the spectrum of Ni-Cr promoted Raney-Co. Note that after LiOH-treatment of Raney-Co the intensity of the peak at 777.5 eV increased relative to the other peaks in the spectrum. The highest binding energy at 782.0 eV is probably related to oxidized cobalt in a strongly ionic ligand field. Co/Al mixed oxide is speculated to cause

this peak. The photoelectron contribution at 777.1 eV shows that metallic cobalt Co^0 was present at the outermost surface.^[36] The relative contribution of metallic cobalt increased significantly after LiOH modification of the surface. In this respect, it is known that Al_2O_3 can be removed from the surface of Raney-Ni by treatment with bases, such as NaOH.^[21]

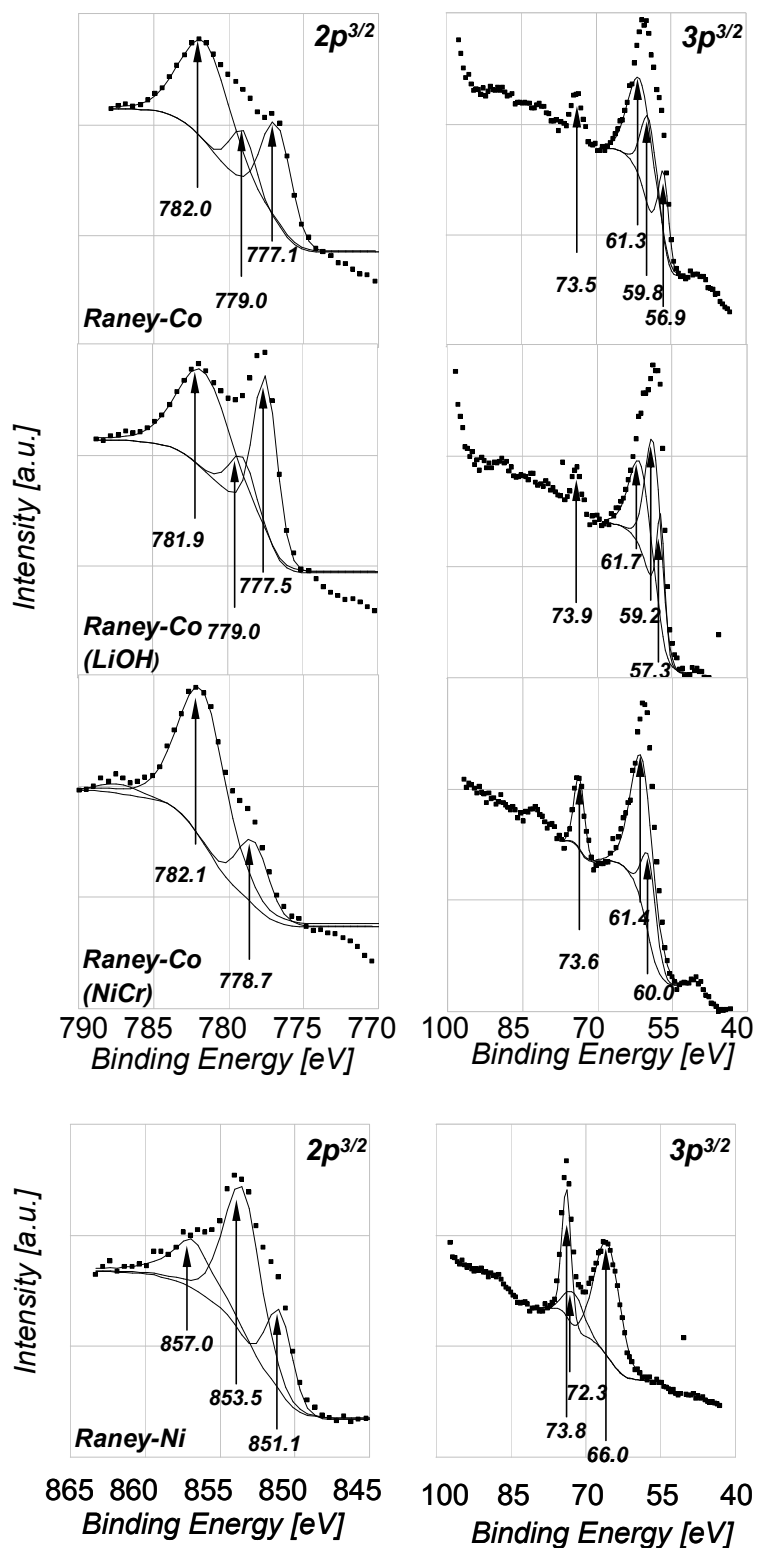


Figure 5.7: XPS spectra for Raney-catalysts and contribution of single states.

The $3p^{3/2}$ region was also analyzed, where the IMPF is $\sim 0.37 - 0.40$ and $0.36 - 0.40$ nm for nickel and cobalt, respectively. Note that, in comparison to the Co and Ni $2p^{3/2}$ region, the XPS spectrum in the $3p^{3/2}$ region bears more information about the catalyst composition on the surface.

The spectrum of Raney-Ni showed a peak at 73.8 eV, an intense peak at 66.0 eV and a small contribution between those two peaks. Spectra of all three cobalt samples featured a peak at 73.5 eV. Additionally, a broad peak between 70 and 55 eV was observed with a maximum at roughly 61 and 60 eV. The XPS spectra of Raney-Co also included a shoulder at approximately 57 eV.

The peak at 73.5-73.9 eV is readily attributed to alumina (Al $2p^{3/2}$ emission line), either α -Al₂O₃ (73.8 eV^[39]), γ -Al₂O₃ (73.5 eV^[36]), or Al(OH)₃ (73.6 eV^[39]). Note that this was the only state of aluminum in the cobalt samples. In contrast, a contribution of metallic aluminum (72.3 eV^[36]) was observed in the XPS spectrum of Raney-Ni at 72.3 eV. In this respect, it has been reported that Raney-Ni contains surface aluminum.^[22] In the Co $3p^{3/2}$ region, both oxidized and metallic cobalt was found (61.3-61.7 and 59.2-60.0 eV, respectively), although the peak positions could not be clearly separated. The contribution of metallic cobalt increased after LiOH modification; Ni-Cr promoted Raney-Co had the least intense metal contribution among the cobalt samples. This is in line with the observations from the Co $2p^{3/2}$ region of the XPS spectra. The peak leading to the shoulder at 57 eV for Raney-Co, indicates the presence of iron on the surface (Fe 3p line, FeOOH 56.3 eV^[40]). As XPS is much more sensitive for iron than for lithium, the Li 1s contribution in the XPS spectrum of the LiOH modified Raney-Co (e.g., Li₂O 55.6 eV^[41]) is difficult to evaluate. In contrast, iron was not observed for Ni-Cr promoted Raney-Co. The XPS spectrum of Raney-Ni in the Ni $3p^{3/2}$ region shows mainly metallic nickel at 66.0 (66.3 eV^[42]).

The elemental surface composition was estimated on basis of the main contributions of the XPS spectra (Table 5.5). Note that XPS mostly probes the outer surface of the catalyst particles, while it is hard to estimate the contribution of X-rays reflected within the pore system. For the further discussion of XPS data, it was assumed that the contribution of inner and outer surface is comparable for the different catalysts. Raney-Co had little aluminum on the surface (4.1 %), although its amount was higher for Ni-Cr promoted Raney-Co and Raney-Ni (5.3 and 13.7 %, respectively). The amount of elemental cobalt or nickel on the surface was in the reverse order (19.0, 17.9 and 11.4 %, respectively). The ratio of elemental cobalt or nickel to aluminum was 4.6, 3.4 and 0.8, respectively. LiOH doping of Raney-Co led to an increase in the elemental ratio of cobalt to aluminum (6.9). As explained in the footnote to Table 5.5 it

was difficult to determine the elemental surface composition of LiOH modified Raney-Co as the contribution of iron and lithium could not be distinguished. Thus, the discussion is restricted to the ratios of the elements oxygen, cobalt and aluminum.

Table 5.5: Estimation of the elemental surface composition of Raney-Ni, Raney-Co, Ni-Cr promoted Raney-Co, and LiOH modified Raney-Co by analysis of the XPS data.

Element	Orbital	Raney-Ni [%]	Raney-Co [%]	Ni-Cr promoted Raney-Co [%]	LiOH modified Raney-Co * [%]
O #	1s	74.9	71.1	76.8	68.1 - 46.6 - 35.5
Co	3p	0	19.0	17.9	21.2 - 14.5 - 11.1
Ni	3p	11.4	—	—	—
Al	2p	13.7	4.1	5.3	3.0 - 2.1 - 1.6
Fe	3p	0	5.7	0	7.7 - 2.6 - 0
Li	1s	0	0	0	0 - 34.1 - 51.9

* Difficulties to separate Fe 3p and Li 1s lines led to ambiguities in the estimation of the iron and lithium content in LiOH modified Raney-Co. The three values shown were calculated assuming (i) 100 % Fe, (ii) equal contribution of Fe and Li and (iii) 100% Li, respectively. For the discussion, the values from assumption (ii) were considered most likely.

The values exceed the real oxygen concentration on the surface as some carbon contamination was unavoidable, which could not be distinguished from the oxygen signal.

5.3.6. Adsorption of butyronitrile and *n*-butylamine from the liquid phase

Adsorption isotherms were recorded to characterize the (competitive) sorption properties of the catalysts. Isotherms derived from breakthrough curves^[43] are shown in Figure 5.8 (adsorption capacity see Table 5.6). The amount of *n*-butylamine, which was adsorbed on the parent Raney-Co catalyst at saturation, was significantly higher than the amount of adsorbed butyronitrile ($7.39 \cdot 10^{-2}$ and $5.37 \cdot 10^{-2}$ mmol·g_{cat.}⁻¹, respectively). After LiOH-modification the amount of *n*-butylamine decreased to $4.25 \cdot 10^{-2}$ mmol·g_{cat.}⁻¹ at saturation. Similarly, the adsorption capacity for butyronitrile was reduced after LiOH doping ($4.06 \cdot 10^{-2}$ mmol·g_{cat.}⁻¹). Note that the intrinsic amount of adsorbents increased considerably upon LiOH doping. Further, the adsorption capacity for butyronitrile increased relative to the adsorption capacity for *n*-butylamine after LiOH modification of the Raney-Co catalyst (ratio 0.72 and 0.96, respectively).

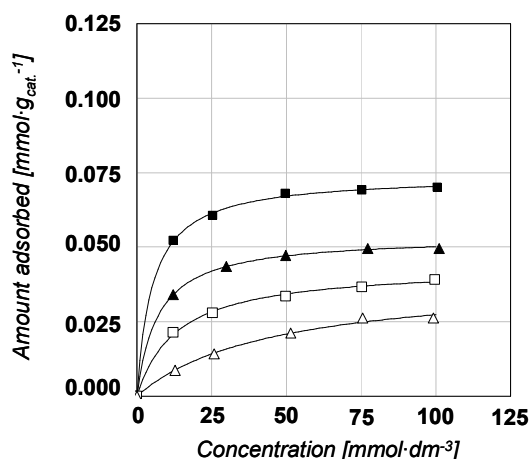


Figure 5.8: Adsorption isotherms for adsorption of *n*-butylamine (■,□) and butyronitrile (▲,△) on parent (filled symbols) and LiOH-doped Raney-Co (open symbols) at 293 K. Solid lines represent a fit of the data according to the Langmuir equation.

Table 5.6: Amount of *n*-butylamine and butyronitrile adsorbed on Raney-Co and adsorption constants derived from break-through curves.

Catalyst	<i>n</i> -Butylamine		Butyronitrile	
	Amount adsorbed		Amount adsorbed	
	[mmol·g _{cat.} ⁻¹]	[mol·mol _{Co,surface} ⁻¹]	[mmol·g _{cat.} ⁻¹]	[mol·mol _{Co,surface} ⁻¹]
Raney-Co	$7.39 \cdot 10^{-2}$	0.185	$5.37 \cdot 10^{-2}$	0.134
LiOH modified Raney-Co	$4.25 \cdot 10^{-2}$	0.236	$4.06 \cdot 10^{-2}$	0.226

To confirm the relative adsorption strength of *n*-butylamine and butyronitrile, competitive adsorption measurements were conducted on parent and LiOH modified Raney-Co (Figure 5.9). After the breakthrough of a non-adsorbing reference, butyronitrile appeared first in the eluent. The concentration of butyronitrile quickly rose above the feed concentration, passed through a maximum and reached steady state at the same time as the breakthrough of *n*-butylamine was observed. This indicates that both molecules adsorb on the same sites and that the steady state surface coverage was higher for *n*-butylamine than for butyronitrile (0.053 and 0.003 mmol·g_{cat.}⁻¹, respectively, at 0.05 mol·l⁻¹ adsorbent concentration). After LiOH doping the molar ratio of *n*-butylamine and butyronitrile adsorbed on the catalyst surface at steady state was decreased significantly (from 17.7 to 3.4).

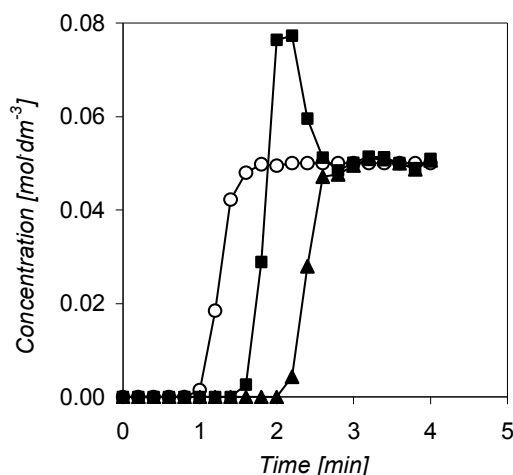


Figure 5.9: Breakthrough curve for the co-adsorption of butyronitrile (■) and *n*-butylamine (▲) on Raney-Co at 293 K. Octane (○) was used as internal reference for determining the residence time distribution in the adsorption column.

5.4. Discussion

5.4.1. Reaction mechanism and role of surface intermediates in the formation of by-product

A general mechanism for the formation of by-products during the hydrogenation of nitriles was first proposed by von Braun in 1923.^[44] According to this model, the hydrogenation of butyronitrile proceeds *via* butan-1-imine, which is further hydrogenated to the primary butylamine. Secondary and tertiary amines are formed by desorption of the imine-intermediate from the catalyst surface, which subsequently reacts in solution with *n*-butylamine or di-*n*-butylamine (Figure 5.10). Elimination of ammonia yields *N*-butylidene-butylamine and *N*-but-1-enyl-dibutylamine as condensation products. Subsequent hydrogenation provides di-*n*-butylamine and tri-*n*-butylamine.

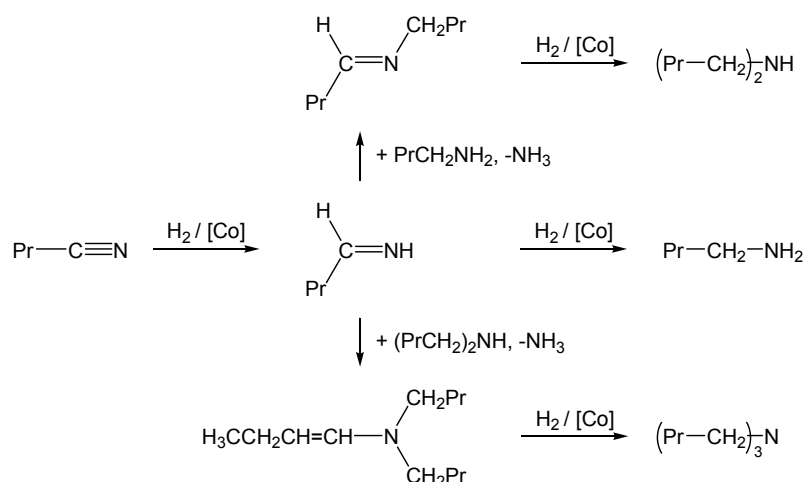


Figure 5.10: Von Braun mechanism explaining the formation of higher amines during the reduction of butyronitrile with molecular hydrogen.

The postulated intermediate butan-1-imine was not found in the reaction mixture. However, the transient concentration of butan-1-imine will be very low, if it is consumed much faster than it is formed. Closer inspection of the time-concentration diagram showed that the formal condensation product of butan-1-imine and *n*-butylamine, *N*-butylidene-butylamine, was a primary kinetic reaction product. This strongly suggests that butan-1-imine or other intermediates taking part in the first step of by-product formation did not desorb into the liquid phase as suggested also in a previous study.^[45] The model also predicts the formation of *N*-but-1-enyl-dibutylamine as the precursor for tri-*n*-butylamine. Huang and Sachtler^[45] detected *N*-but-1-enyl-dibutylamine in the liquid-phase over PdNi/NaY, although in a very low concentration. However in this study, we did not observe *N*-but-1-enyl-dibutylamine and, only in case of the Raney-Ni catalyst, traces of tri-*n*-butylamine.

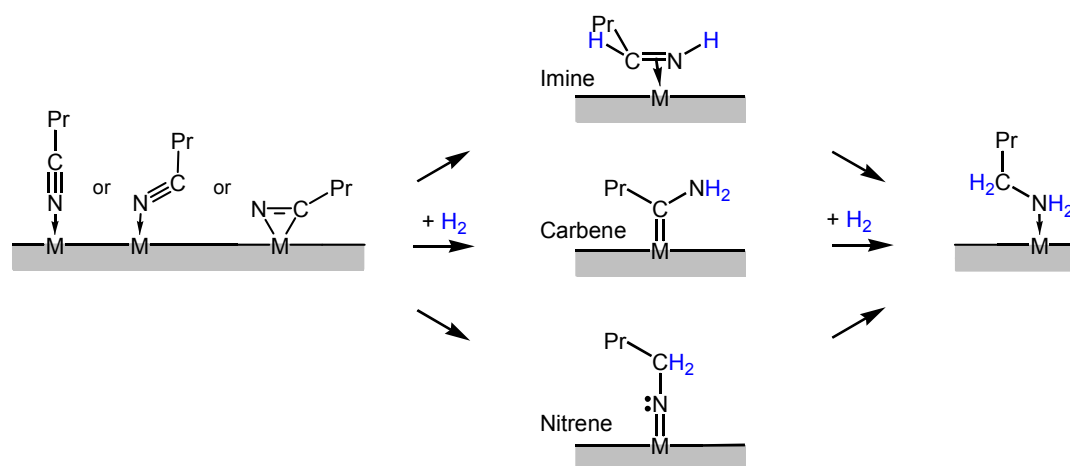


Figure 5.11: Surface reactions suggested for the hydrogenation of butyronitrile.

Thus, the side-product *N*-butylidene-butylamine most likely results from a bimolecular condensation reaction, which takes place on the catalyst surface. Similar to the metal catalyzed disproportionation of amines,^[46] the reaction is speculated to proceed by condensation of unsaturated intermediates.^[47] It was suggested for nickel that carbenes and nitrenes can be formed as surface intermediates (see Figure 5.11) with nitrenes being the preferred species.^[48] In the initial step of the condensation reaction, a nitrogen nucleophile attacks at an unsaturated carbon atom, e.g., the carbon atom of a carbene or a π -coordinated nitrile. This step of the condensation process is probably acid-catalyzed^[30, 49]. Note that nitrenes are much less susceptible to nucleophilic attack, as the carbon atom is fully saturated.^[47] These surface processes will depend on the catalyst properties and, hence, need to be addressed in the discussion on the differences in selectivity and activity, which were observed for the four types of catalysts.

5.4.2. Accessible metal atoms, oxidation state of the surface atoms, and the presence of Lewis acid sites

N_2 -physisorption and H_2 -chemisorption provided similar trends in the four catalysts although different sites were probed. The catalyst with the highest BET surface area (Ni-Cr promoted Raney-Co) had the highest concentration of accessible metal atoms. Thus, with an increasing BET area, it was possible to reach a better dispersion of the catalytically active metal. However, XPS measurements showed that the metal surface was in large parts (> 70 %) covered with multi-oxide deposits, which do not contribute to the number of accessible metal atoms. XPS data also demonstrated that the aluminum content on the surface followed the trend in the bulk.

Accordingly, nickel in Raney-Ni was covered by aluminum oxide to a much larger extent than cobalt in Ni-Cr promoted Raney-Co and Raney-Co. For Raney-Ni, Raney-Co and Ni-Cr promoted Raney-Co, the surface aluminum content was higher than in the bulk, which indicates an enrichment of aluminum in the surface near region. In TPD of NH_3 , a high temperature peak at 704-713 K was observed for those three catalysts and associated with ammonia desorbing from Al^{3+} Lewis acid sites. It appears likely that the Al^{3+} Lewis acid sites are associated with aluminum oxide on the catalyst surface. The nature of this surface oxide is strongly influenced by modification of the catalyst with LiOH. The TPD of NH_3 indicates that LiOH modification led to blocking of the sites associated with strong Lewis acidity and it is speculated that $LiAl_2(OH)_7$ was formed.

Consequently, one possible reason for the enhancement of selectivity after LiOH-addition is, thus, the reduction of the concentration of Lewis acid sites, which are known to catalyze condensation reactions.^[30] A large part of the oxide deposit was removed during LiOH modification and the fraction of the clean metal surface increased as indicated by XPS.

The elemental ratio of the catalytically active metal to alumina and metal oxide was much lower for Raney-Ni, which is a possible explanation for the low selectivity to primary amine. Modification of Raney-Co with LiOH led to a decrease in the number of accessible metal atoms. However, the elemental ratio of cobalt to alumina was increased indicating that, on the one hand, surface alumina was removed or blocked and, on the other hand, LiOH covered part of the previously accessible metal atoms. By taking into account that the pore volume remained constant, whereas the BET area was reduced, it can be concluded that the decrease of accessible metal atoms was due to blocking of micropores, which contribute only little to the pore volume.

5.4.3. *The role of hydrogen in the reaction mechanism*

Assuming a simple Langmuir-Hinshelwood model and surface reaction of the first hydrogen atom with adsorbed nitrile as rate determining step, the rate can be expressed as $r = k \cdot \theta_{\text{H}} \cdot \theta_{\text{butyronitrile}}$. Only little dependence of the reaction rate on nitrile concentration was observed for all catalysts up to about 80% conversion. This observation is in line with previous liquid phase hydrogenation reactions, for which zero order in nitrile was reported.^[50, 51] This suggests that the sites were fully saturated with nitrile during most of the reaction. Under the assumption of a Langmuir-Hinshelwood model, this observation leads to two possible scenarios concerning the co-adsorption of hydrogen and *n*-butyronitrile. The simpler one is that hydrogen and nitrile adsorb on different sites. Alternatively, hydrogen and nitrile might compete for the same sites, but nitrile is adsorbed much more strongly. For nickel, it was shown that more than one metal atom was required for adsorption of one acetonitrile molecule (up to 4).^[48] The resulting space between two nitrile molecules might be available for hydrogen adsorption. Thus, the scenario of different adsorption sites appears more likely. The hydrogen atoms can adsorb in different binding modes (e.g. on top, bridging, in hollow sites), which do not have the same reactivity. In this respect, it has been reported for nickel surfaces that on top bound hydrogen is less strongly adsorbed than hydrogen on bridge and hollow sites and, therefore, is notably more reactive.^[48, 52]

5.4.4. *Influence of the sorption mode on activity and selectivity*

The activation of the C≡N group depends on the sorption mode (see Figure 5.11) and the strength of the interaction between nitrile and metal surface. The nitrile group is able to bind with the C≡N bond normal to the surface plane (preferred mode on cobalt, weak activation) or tilted, with the nitrile σ - and π -orbitals interacting with the surface (preferred mode on nickel, strong activation).^[53, 54] A metallacycle can also be formed, but will not be considered in the further discussion.

In order to understand the influence of Li^+ on the adsorption of butyronitrile and *n*-butylamine better, the adsorption of both molecules from the liquid phase was explored (see Figure 5.8 and Figure 5.9). The experiments were in line with the results from XPS and H_2 -chemisorption measurements. Less butyronitrile and butylamine adsorbed after LiOH doping (with respect to catalyst weight) reflecting that the overall number of accessible cobalt atoms was reduced. It is remarkable that in both cases the coverage was below $0.25 \text{ mol} \cdot \text{mol}_{\text{Co, surface}}^{-1}$. In this respect, theoretical results suggested that acetonitrile adsorbs on nickel preferentially parallel to the surface in 4-fold or even 5-fold mode.^[48, 55] Taking into account that, due to

oxidic species and alumina present on the surface, not all elemental cobalt atoms are in groups of adequate size, the low coverage can be explained. The “steric” constraint around the adsorption sites might be reduced after LiOH doping explaining the higher adsorption capacity. The ratio of adsorbed butyronitrile (*n*-butylamine) to cobalt atoms on the surface decreased from 1:7.5 (1:5.4) to 1:4.4 (1:4.2) after LiOH modification.

The higher surface concentration of reactants is a possible reason for the higher activity observed after LiOH doping. The co-adsorption experiment on Raney-Co (see Figure 5.9) also showed that in part butyronitrile was displaced by *n*-butylamine suggesting that both competed for the same sites. The rate remained constant up to relatively high conversions (80 %). Hence, we tend to attribute the higher activity upon LiOH doping to the lower amount of butylamine, relative to butyronitrile, adsorbing on the catalyst surface leading to a higher surface concentration of butyronitrile for the LiOH modified samples. With respect to selectivity, it should be noted that, due to the lower surface concentration of *n*-butylamine, the integral rate of condensation reactions, which involve amines, is reduced.

5.5. Conclusions

To understand the nature of the critical properties, which influence the selectivity and catalytic activity of Raney-catalysts in the hydrogenation of nitriles, LiOH modified Raney-Co and three commercial Raney-catalysts (Raney-Ni, Raney-Co and Ni-Cr promoted Raney-Co) were tested and thoroughly characterized. Among the commercial catalysts, Ni-Cr promoted Raney-Co showed the highest activity and selectivity to *n*-butylamine.

LiOH-modification of Raney-Co led to enhanced intrinsic activity (second highest) and the highest selectivity of the catalysts tested. This beneficial effect of LiOH was found to be the result of a modified nature of the catalyst surface. Most likely, islands of lithium aluminate and lithium hydroxide are formed on the catalyst surface. This leads to a higher ratio of metallic cobalt to oxidic cobalt and alumina, which results in (i) a reduced number of Al^{3+} Lewis acid sites, which are claimed to catalyze side reactions, (ii) a higher sorption capacity per metal atom for butyronitrile and butylamine and (iii) higher ratio of adsorbed butyronitrile relative to butylamine.

The activity is, thus, increased due to an increased surface concentration of butyronitrile and due to reduced product inhibition by butylamine. In terms of selectivity a lower adsorption constant of butylamine compared to butyronitrile is beneficial, as adsorbed butylamine is necessary for by-product formation.

Acknowledgments

Air Products & Chemicals Inc. is thanked for the generous financial support. Prof. Jenó Bodis is gratefully acknowledged for many stimulating discussions.

References

- [1] M. G. Turcotte, T. A. Johnson, in *Kirk-Othmer Encyclopedia of Chemical Technology*, Vol. 2 (Ed.: J. I. Koschwitz), 4 ed., Wiley, New York, **1992**, pp.396-389.
- [2] M. Serra, P. Salagre, Y. Cesteros, F. Medina, J. E. Sueiras, *J. Catal.* **2002**, *209*, 202.
- [3] S. Alini, A. Bottino, G. Capannelli, R. Carbone, A. Comite, G. Vitulli, *J. Mol. Catal. A-Chem.* **2003**, *206*, 363.
- [4] A. G. M. Barrett, in *Comprehensive Organic Synthesis*, Vol. 8 (Ed.: B. M. Trost), Pergamon, Oxford, **1991**, pp. 251-257.
- [5] J. Barrault, Y. Pouilloux, *Catal. Today* **1997**, *37*, 137.
- [6] P. Baumeister, M. Studer, F. Roessler, in *Handbook of Heterogeneous Catalysis*, Vol. 5 (Eds.: G. Ertl, H. Knözinger, J. Weitkamp), Wiley-VCH, Weinheim, **1997**, pp. 2186-2195.
- [7] F. Medina, P. Salagre, J. E. Sueiras, J. L. G. Fierro, *J. Mol. Catal.* **1993**, *81*, 387.
- [8] P. N. Rylander, *Catalytic Hydrogenation over Platinum Metals*, Academic Press, New York/London, **1967**, pp.203-226.
- [9] P. Scharringer, T. E. Muller, W. Kaltner, J. A. Lercher, *Ind. Eng. Chem. Res.* **2005**, *44*, 9770.
- [10] M. S. Wainwright, in *Preparation of Solid Catalysts* (Eds.: G. Ertl, H. Knözinger, J. Weitkamp), Wiley-VCH, Weinheim, **1999**, pp. 28-43.
- [11] G. Cordier, P. Fouilloux, N. Laurain, J. F. Spindler, US Patent No. 5,777,166, to RhonePoulenc Chimie, **1998**.
- [12] T. A. Johnson, US Patent No. 5,859,653, to Air Products and Chemicals, Inc., **1999**.
- [13] A. F. Elsasser, US Patent No. 5,874,625, to Henkel Corp., **1999**.
- [14] W. Huber, *J. Am. Chem. Soc.* **1944**, *66*, 876.
- [15] P. Tinapp, *Chem. Ber.-Rec.* **1969**, *102*, 2770.
- [16] C. Mathieu, E. Dietrich, H. Delmas, J. Jenck, *Chem. Eng. Sci.* **1992**, *47*, 2289.
- [17] W. Reeve, J. Christian, *J. Am. Chem. Soc.* **1956**, *78*, 860.
- [18] A. J. Chadwell, H. A. Smith, *J. Phys. Chem.* **1956**, *60*, 1339.
- [19] J. P. Orchard, A. D. Tomsett, M. S. Wainwright, D. J. Young, *J. Catal.* **1983**, *84*, 189.
- [20] S. Nishimura, M. Kawashima, S. Inoue, S. Takeoka, M. Shimizu, Y. Takagi, *Appl. Catal.* **1991**, *76*, 19.
- [21] F. Hochardponcet, P. Delichere, B. Moraweck, H. Jobic, A. J. Renouprez, *J. Chem. Soc.-Faraday Trans.* **1995**, *91*, 2891.

- [22] S. N. Thomas-Pryor, T. A. Manz, Z. Liu, T. A. Koch, S. K. Sengupta, W. N. Delgass, in *Chemical Industries Series, Vol. 75* (Ed.: F. E. Herkes), Dekker, New York, **1998**, p. 195.
- [23] G. Moretti, in *Handbook of Heterogeneous Catalysis, Vol. 2* (Eds.: G. Ertl, H. Knözinger, J. Weitkamp), Wiley-VCH, Weinheim, **1997**, pp. 632-641.
- [24] J. R. Anderson, *Structure of Metallic Catalysts*, Academic Press, London, **1975**, p.228.
- [25] A. B. Fasman, in *Chemical Industries Series, Vol. 75* (Ed.: F. E. Herkes), Dekker, New York, **1998**, pp. 151-168.
- [26] J. L. Falconer, J. A. Schwarz, *Catal. Rev.-Sci. Eng.* **1983**, 25, 141.
- [27] G. A. Martin, P. Fouilloux, *J. Catal.* **1975**, 38, 231.
- [28] M. Nayak, T. R. N. Kutty, V. Jayaraman, G. Periaswamy, *J. Mater. Chem.* **1997**, 7, 2131.
- [29] J. P. Thiel, C. K. Chiang, K. R. Poeppelmeier, *Chem. Mater.* **1993**, 5, 297.
- [30] M. Verhaak, A. J. Vandillen, J. W. Geus, *Catal. Lett.* **1994**, 26, 37.
- [31] M. Verhaak, A. J. Vandillen, J. W. Geus, *Appl. Catal. A-Gen.* **1993**, 105, 251.
- [32] *Gmelins Handbuch der Anorganischen Chemie, System-Nr 58: Kobalt, Ergänzungsband, Teil A*, Verlag Chemie, Weinheim, **1961**, p. 511.
- [33] A. Baiker, M. Maciejewski, *J. Chem. Soc.-Faraday Trans. I* **1984**, 80, 2331.
- [34] A. Borgna, R. Frety, M. Primet, M. Guenin, *Appl. Catal.* **1991**, 76, 233.
- [35] Y. Okamoto, *J. Cryst. Growth* **1998**, 191, 405.
- [36] C. D. Wagner, W. M. Riggs, L. E. Davis, J. F. Moulder, in *Handbook of X-Ray Photoelectron Spectroscopy* (Ed.: G. E. Muilenberg), Perkin-Elmer Corporation (Physical Electronics Division), Eden Prairie, MN, **1979**.
- [37] T. Yoshino, T. Abe, S. Abe, I. Nakabayashi, *J. Catal.* **1989**, 118, 436.
- [38] *Practical Surface Analysis, Vol. 1, 2 ed.* (Eds.: D. Briggs, M. P. Seah), Wiley, New York, **1993**.
- [39] T. L. Barr, *J. Vac. Sci. Technol. A* **1991**, 9, 1793.
- [40] D. Brion, *Appl. Surf. Sci.* **1980**, 5, 133.
- [41] J. P. Contour, A. Salesse, M. Froment, M. Garreau, J. Thevenin, D. Warin, *J. Microsc. Spectrosc. Electron.* **1979**, 4, 483.
- [42] N. S. McIntyre, M. G. Cook, *Anal. Chem.* **1975**, 47, 2208.
- [43] A. Dabrowski, M. Jaroniec, *Adv. Colloid Interface Sci.* **1990**, 31, 155.
- [44] J. von Braun, G. Blessing, F. Zobel, *Chem. Ber.* **1923**, 56, 1988.
- [45] Y. Y. Huang, W. M. H. Sachtler, *Appl. Catal. A-Gen.* **1999**, 182, 365.
- [46] A. Ozaki, *Isotopic Studies of heterogeneous Catalysis*, Kodansha Ltd./Academic Press, Tokyo/New York, **1977**, pp. 140-141.
- [47] B. Coq, D. Tichit, S. Ribet, *J. Catal.* **2000**, 189, 117.
- [48] B. Bigot, F. Delbecq, A. Milet, V. H. Peuch, *J. Catal.* **1996**, 159, 383.

-
- [49] P. Sykes, *A Guidebook to Mechanism in Organic Chemistry*, 6 ed., Longman, London/Singapore, **1986**.
- [50] H. X. Li, Y. D. Wu, H. S. Luo, M. G. Wang, Y. P. Xu, *J. Catal.* **2003**, *214*, 15.
- [51] B. W. Hoffer, P. H. J. Schoenmakers, P. R. A. Mooijman, G. M. Hamminga, R. J. Berger, A. D. van Langeveld, J. A. Moulijn, *Chem. Eng. Sci.* **2004**, *59*, 259.
- [52] F. Hochard, H. Jobic, J. Massardier, A. J. Renouprez, *J. Mol. Catal. A-Chem.* **1995**, *95*, 165.
- [53] F. J. G. Alonso, M. G. Sanz, V. Riera, A. A. Abril, A. Tiripicchio, F. Ugozzoli, *Organometallics* **1992**, *11*, 801.
- [54] A. Chojecki, H. Jobic, A. Jentys, T. E. Muller, J. A. Lercher, *Catal. Lett.* **2004**, *97*, 155.
- [55] B. Bigot, F. Delbecq, V. H. Peuch, *Langmuir* **1995**, *11*, 3828.

Chapter 6

***In-situ* measurement of dissolved hydrogen during the liquid-phase hydrogenation of dinitriles – Method and case study**

Abstract

Despite the significance of gas/liquid/solid multiphase systems in the production of chemicals on an industrial scale, measuring the concentration of gases dissolved in the liquid phase – a prerequisite for determining basic reaction data such as rate and adsorption constants – remains challenging. Recently, a new permeation probe became available, which allows *in-situ* measurement of gas concentrations in liquids. To evaluate potential applications, the probe was used to follow the concentration of dissolved hydrogen during the cobalt-catalyzed reduction of an aliphatic dinitrile to the corresponding diamine. The changes in the hydrogen saturation level during the reaction were compared to the gas – liquid (G-L) mass transfer characteristics of the reactor as determined by $k_L a$ measurement. Under the reaction conditions used, G-L mass transfer became the rate-determining step when the stirring speed was decreased. The permeation probe allowed for evaluating the significance of G-L mass transfer in a straightforward manner.

6.1. Introduction

Frequently, a solid catalyst is used to accelerate the reaction between a gaseous reactant and a liquid or dissolved substrate. Examples are manifold and include hydrogenation reactions. Mathematical models of such three-phase gas/liquid/solid systems (G-L-S) are often based on kinetic data obtained in laboratory scale slurry reactors. However, to derive valid data, special attention has to be given to mass transport limitations. During hydrogenation, molecular hydrogen has to diffuse from the gas into the liquid phase, across the stagnant layer and into the catalyst pores before adsorbing at the catalytically active centres (Figure 6.1). If slow relative to the rate of reaction, the transport steps can lead to a significant reduction of the rate of the overall process. Both, the performance of a catalyst and mechanistic details can be evaluated properly, only when the observed rate of reaction is determined by the processes at the active site. Therefore, it is an essential prerequisite for the establishment of an intrinsic kinetic model to verify the absence of transport effects.^[1] However, additional experiments^[2] are necessary to rule out mass transfer limitations. During catalyst screening, e.g., the absence of mass transfer limitations has to be confirmed for every single catalyst when significant activity differences are observed.

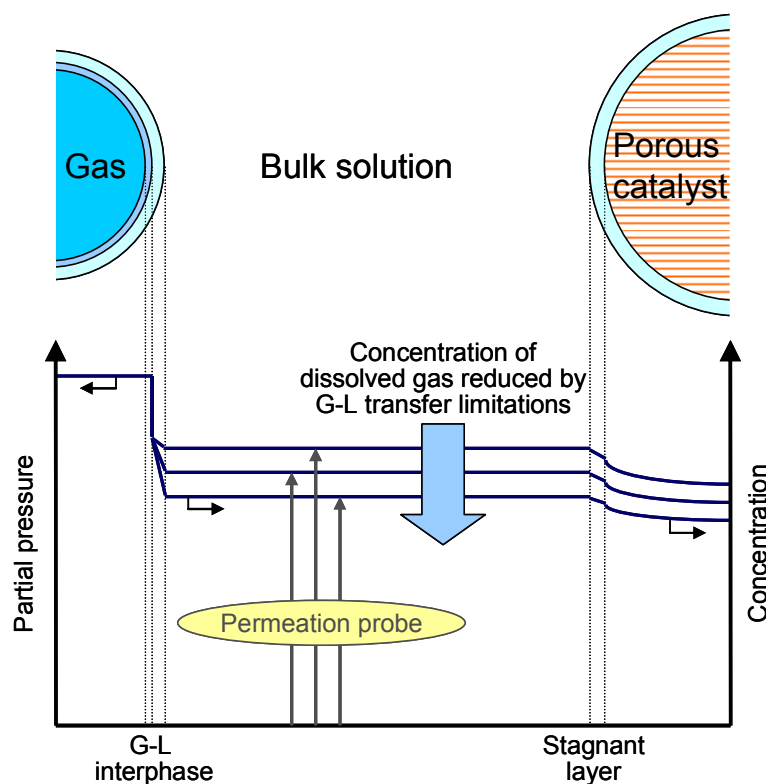


Figure 6.1: Possible concentration profile for gas/liquid/solid multiphase systems in the presence of mass transport limitations illustrating the importance of measuring the gas concentration in bulk solution

Recently, a new permeation probe for *in-situ* measurement of the partial pressure of dissolved gases has become commercially available.^[3] Provided the Henry coefficient has been determined, the concentration of dissolved gases can be measured with this probe, even when the vapour pressures of the single components in the reaction mixture are unknown. Therefore, the probe might provide a useful tool for evaluating the extent of G-L mass transfer limitations in the overall reaction sequence (Figure 6.1). In this study, the permeation probe was used to measure the concentration of dissolved hydrogen during a typical hydrogenation reaction in a laboratory scale slurry reactor. So far, the use of this permeation probe for *in-situ* measurements had not been reported. The results were related to classic methods for the identification of mass transfer limitations to unambiguously establish the working regime.

6.2. Experimental section

6.2.1. Materials

A commercially available silica-supported cobalt catalyst was used as received without further activation. Three different particle sizes (<100, 100-200, 200-300 μm) were available. Liquid ammonia and hydrogen were received from Messer Griesheim with 99.98% and 99.999% purity, respectively.

6.2.2. Catalytic experiments

The hydrogenation of the dinitrile was performed in a tank reactor (160 mL, Parr Instruments) with a hollow shaft stirrer for gas entrainment. The reactor was operated in semi-batch mode at constant pressure. The hydrogen consumption was recorded with a mass flow controller (Bronckhorst). In a typical experiment the autoclave was charged under nitrogen atmosphere with a fresh catalyst sample (4 g with a particle diameter of < 100 μm). After adding liquid ammonia (75 mL), the reactor was pressurized with hydrogen to 2.0 MPa and heated to 363 K. The reactor was charged with dinitrile (37 mL), the hydrogen pressure adjusted to 3.0 MPa, and the stirrer started (start of the reaction). Temperature, hydrogen pressure, hydrogen consumption and hydrogen concentration in the carrier gas of the permeation probe were recorded during each experiment. Samples of the liquid phase were periodically withdrawn and analyzed with a Fisons GC 8160 gas chromatograph equipped with FID detector and 30m Optima 5 column.

6.2.3. Gas-liquid mass transfer coefficient $k_L a$

The gas-liquid volumetric mass transfer coefficient $k_L a$ was determined with the pressure step-method.^[4] After charging the reactor with dinitrile, the system was purged with nitrogen. Ammonia was added and the liquid was stirred at pressure P_0 and temperature T (363 K) until equilibration. The stirrer was stopped and the pressure in the reactor increased rapidly (within 1 s) to P_m . As soon as thermal equilibrium was reached (*ca.* 10 s), the stirrer was started and the pressure drop recorded until the final pressure P_f was reached. Integration of the mass balance between $t = 0$ ($P = P_m$) and t ($P = P(t)$) results in the following equation:

$$\ln\left(\frac{P_m - P_0}{(1 + K)(P - P_0) - K(P_m - P_0)}\right) = \frac{1 + K}{K} k_L a t \quad \text{Equ. 6.1}$$

with

$$K = \frac{P_f - P_0}{P_m - P_f} \quad \text{Equ. 6.2}$$

The $k_L a$ value can be calculated from the slope of a plot of the left side of Equ. 6.1 vs. time.

6.2.4. Measuring the concentration of dissolved hydrogen with the permeation probe

The hydrogen concentration in the liquid phase was determined with a Fugatron ® HYD-200 dissolved hydrogen analyzer. A miniature permeation probe with 7.8 mm outer diameter (MIN-100 Fugatron ® Probe) and a standard permeation probe with 18 mm outer diameter (STD-100 Fugatron ® Probe) were available. Both were mounted in the reactor flange using standard 1/8" tube fittings (Figure 6.2) and immersed into the liquid phase.

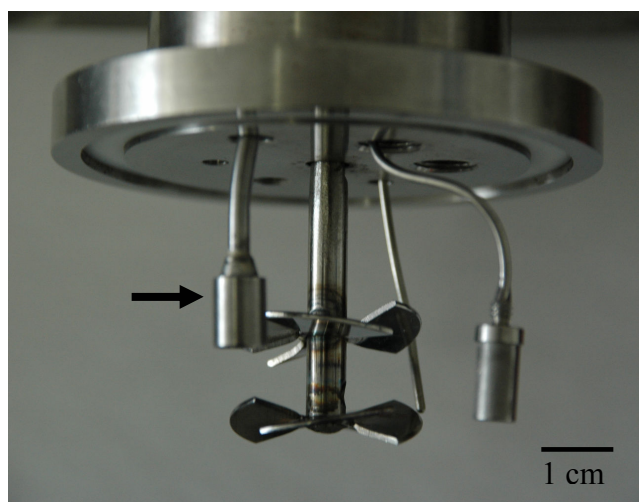


Figure 6.2 Miniature gas permeation probe MIN-100 (outer diameter 7.8 mm) implemented in the laboratory reactor.

The working principle of the instrument is based on the permeation method.^[5] At the tip of the probe the dissolved hydrogen permeates through a dense membrane of a fluorinated polymer with 200 μm thickness and 20 mm^2 and 8 cm^2 area. Internally, the probe is purged by a constant carrier gas stream of 1% O_2 in N_2 (10 $\text{mL}\cdot\text{min}^{-1}$) and the concentration of permeated hydrogen molecules is analyzed. The concentration of hydrogen measured in the carrier gas is directly proportional to the partial pressure of hydrogen outside of the probe tip.

6.3. Results and Discussion

6.3.1. Gas-liquid mass transfer

To determine the mass-transfer characteristics of the autoclave used in this study, the G-L mass transfer coefficient k_{La} was measured for hydrogen at various stirring speeds and two temperatures (353 K and 363 K) (Figure 6.3).

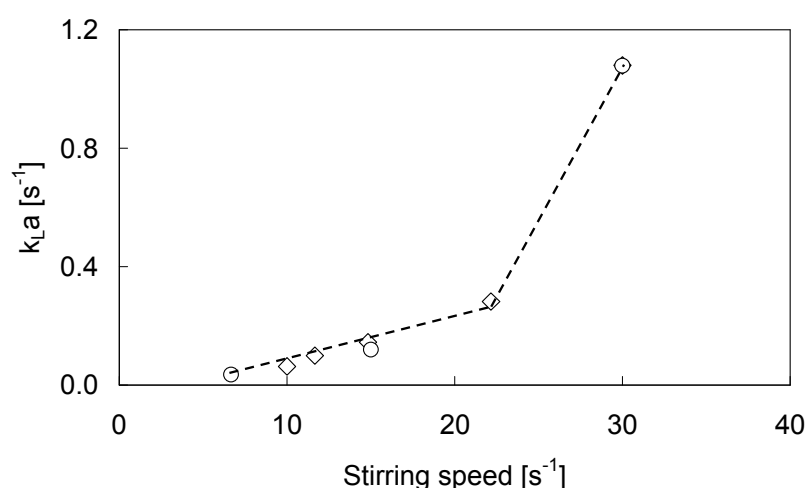


Figure 6.3 Gas-liquid mass transfer coefficient k_{La} in the laboratory reactor as a function of stirring speed. (\diamond) $T = 353$ K; (\circ) $T = 363$ K.

The solvent used in the k_{La} measurements had the same composition as the reaction mixture in the catalytic experiments (75 mL of ammonia; 37 mL of dinitrile). For both temperatures the k_{La} value increased linearly with the stirring speed up to 22 s^{-1} . At a stirring speed of 30 s^{-1} there was a considerably higher k_{La} value than would have been expected with a linear behaviour over the whole range of stirring speeds. This can be attributed to the onset of gas insertion *via* the hollow shaft of the stirrer at a speed of about 24 s^{-1} . In the temperature range investigated no certain trend concerning the temperature dependence of the k_{La} was observed. The k_{La} values obtained are similar to values reported for comparable experimental reactors with gas inducing stirrers.^[6,7] To assess the saturation level of the liquid phase with

hydrogen the permeation probe was used. In preliminary tests,^[8] the cross sensitivity with solvent and reactants as well as the influence of liquid velocity were explored. No signal was observed when the sensor was immersed in ammonia and/or dinitrile without hydrogen being present. This shows that there was no cross sensitivity with the reaction mixture. The velocity of the liquid at the sensor was changed by varying the stirring speed. The signal increased by 6 % in intensity upon raising the stirring speed from 2.5 s^{-1} to 30 s^{-1} (Figure 6.4). At a stirring speed of 6.7 s^{-1} the deviation from the maximum intensity was 2 %. Obviously, a minimum stirring speed is required for constant reading. Probably diffusion limitations across the stagnant liquid-solid interphase at the sensor surface are minimised when the liquid passes the sensor with a sufficiently high speed. Gas bubbles hitting the probe or gas bubbles adhering to the sensor cannot explain this effect as was shown in a parallel study.^[5]

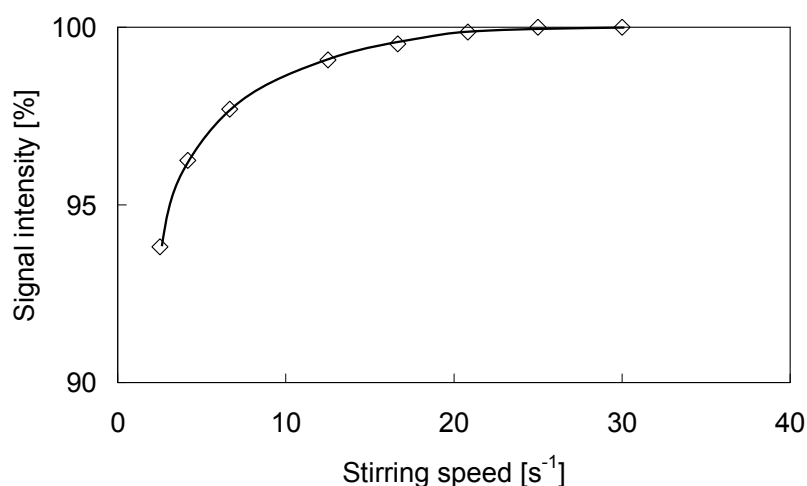


Figure 6.4 Intensity of the sensor signal (MIN-100 probe) as a function of the stirring speed in a mixture of ammonia (75 mL) and dinitrile (37 mL) at $T = 363 \text{ K}$ and a partial pressure of hydrogen of 3.0 MPa .

The response of the signal to a pressure step in hydrogen was recorded for a typical reaction mixture (at different stirring speeds) and for the gas phase. About 15 min were required in all cases until a stable reading for the MIN-100 permeation probe was observed (Figure 6.5). The $t_{10}-t_{90}$ time was about 12 min. The dead time was 0.65 min. On the one hand the response time in the gas phase gives the actual response characteristics of the instrument. On the other hand by comparing the equilibration time in the liquid phase to that in the gas phase one can see that the liquid surrounding the probe has no influence on the response time. Considering the response behaviour of the probe one it has to be stated that its application for transient measurements of the hydrogen concentration will be limited to slow processes. However, qualitative statements concerning the saturation level of hydrogen in the liquid

phase are possible. The second available permeation probe STD-100 showed a shorter $t_{10-t_{90}}$ time ($\sim 3-4$ min) but could not be used during the reaction in the laboratory reactor due to its size. Generally there is a wide field of applications in process control. The probe has high temperature sensitivity with exponential increase of permeability with temperature.^[5]

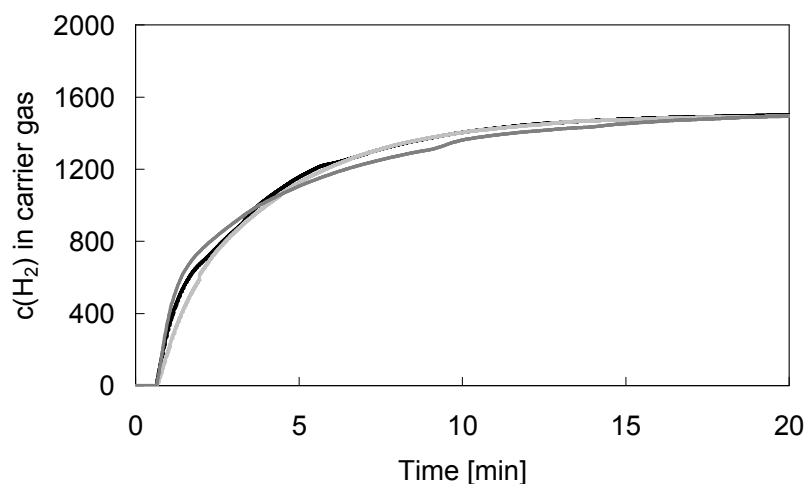


Figure 6.5 Response of the permeation probe to a hydrogen pressure step (from 0 MPa to 3.0 MPa) in gas phase consisting of hydrogen only (dark grey) and in liquid phase consisting of ammonia (75 mL) and dinitrile (37 mL) at a temperature of $T = 363$ K and stirring speeds of 30 s^{-1} (black) and 6.7 s^{-1} (light grey).

6.3.2. Case study: Hydrogenation of dinitriles

6.3.2.1. Reaction without external mass transfer limitation

As case study, the hydrogenation of a dinitrile to diamine over a supported cobalt catalyst was chosen. On industrial scale the reaction is frequently carried out in the liquid phase over unsupported or supported transition metal catalysts.^[9] Undesired by-products (secondary and tertiary amines, cyclization products) are generated by intermolecular or intramolecular condensation reactions.^[10] For nickel and cobalt catalysts the presence of ammonia significantly enhances the selectivity to primary amines.^[11] Liquid ammonia is, therefore, often used as solvent in industrial processes. For high selectivities to the desired primary diamine a high rate of hydrogenation (relative to the rate of condensation reactions) is essential, necessitating sufficient concentrations of hydrogen in the reaction mixture. Further, the overall reaction rate in such three phase systems may be restricted by limited transport of hydrogen across the G-L or the L-S phase boundary.

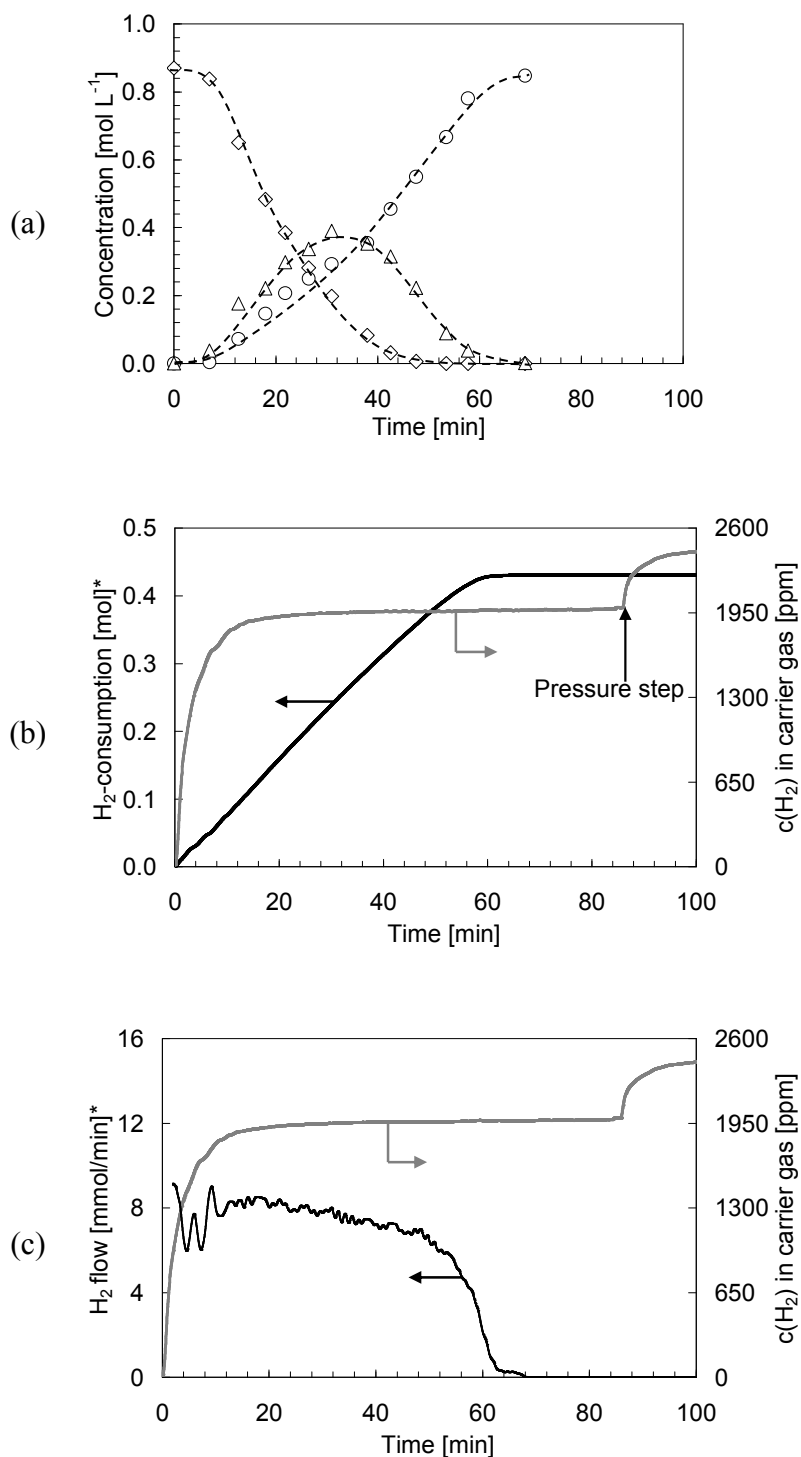
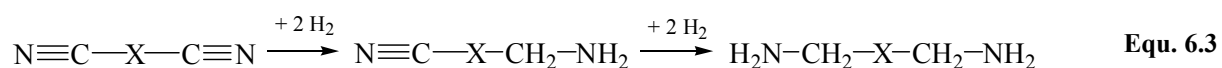


Figure 6.6 (a) Concentration profile of dinitrile hydrogenation at $T = 363\text{ K}$; $P_{\text{H}_2} = 3.0\text{ MPa}$ and stirring speed $N = 30\text{ s}^{-1}$, (◇) dinitrile, (△) aminonitrile, (○) diamine. (b) Hydrogen consumption during the experiment and concentration of hydrogen in the carrier gas of the permeation probe (* for 112 mL solution). The arrow indicates a pressure step from 8.20 MPa to 8.86 MPa (see text). (c) Hydrogen flow profile and concentration of hydrogen in the carrier gas of the permeation probe.

Reaction profile and kinetics

A typical concentration profile for dinitrile hydrogenation in liquid ammonia is shown in Figure 6.6. One of the nitrile groups is hydrogenated first, providing aminonitrile. In a consecutive reaction the aminonitrile is reduced to the diamine (eq. 1, X = alkyl chain). The maximum concentration of the aminonitrile is relatively high (about 45 % of the initial concentration of dinitrile) indicating that the first nitrile group is reduced faster than the second. However, the concentration profile is not consistent with a reaction sequence $A \rightarrow B \rightarrow C$ based on first order reactions. Closer inspection of the time-concentration profile shows that the concentration of the aminonitrile increased until the conversion of the dinitrile reached about 80 % (after 30 min). At longer reaction times, the concentration of the aminonitrile decreased rapidly which is reflected by an increased rate of diamine formation. Such a concentration profile can be explained by a stronger adsorption of the dinitrile on the catalyst surface compared to the aminonitrile.^[12] The reaction was finished after 70 min and almost 100 % selectivity to diamine were obtained.



The concentration profile for the liquid phase is related with the integral hydrogen consumption and the hydrogen flow rate in Figure 6.6. The hydrogen uptake was fastest at the start of the reaction decreasing gradually in the course of the reaction indicating a decrease in the overall rate of reaction.

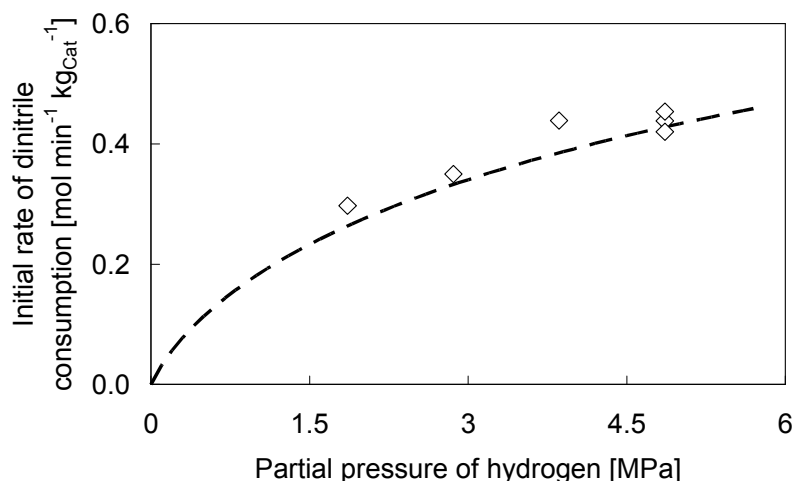


Figure 6.7 Initial rate of dinitrile conversion as a function of hydrogen pressure at $T = 353\text{ K}$. The line represents a Langmuir-Hinshelwood model.

This is consistent with zero order in nitrile at high nitrile concentrations and first order in nitrile at low nitrile concentrations.^[6] In addition, the aminonitrile is reduced more slowly (at reaction times >30 min) than the dinitrile (after a short period (~ 6 min) with a lower rate at the start of the reaction). To determine the reaction order in hydrogen the reaction was repeated at different hydrogen pressures (Figure 6.7). From the initial rate of dinitrile consumption an apparent reaction order of 0.5 in hydrogen was calculated. This is consistent with a Langmuir-Hinshelwood mechanism similar to that suggested by Joly-Vuillemin *et al.* for Raney Nickel catalysts.^[13]

Mass transfer and hydrogen saturation during the reaction

The concentration profile for the hydrogenation of the dinitrile was also related with the sensor signal of the permeation probe (Figure 6.6). The signal intensity increased immediately after the start of the reaction to reach a constant value at 1920 ppm after *ca.* 15-20 min. Comparison with the progression of the signal intensity in the absence of catalyst (see Figure 6.5) shows that the time delay of 15 min can mostly be attributed to the equilibration time of the permeation probe. Hence, the initial saturation of the liquid phase with hydrogen cannot be recorded with the permeation probe. However, it can be concluded that the liquid phase was fully saturated during the final part of the reaction as there was no change of the liquid phase hydrogen concentration after the end of the reaction after 70 min. The significance of mass transfer limitations during the initial phase of the reaction can be judged from the characteristic times of reaction and mass transfer.^[6] The characteristic time for the reaction was calculated from the initial rate of hydrogen uptake ($1.07 \text{ mol m}_{\text{reaction mixture}}^{-3} \text{ s}^{-1}$ at $T = 363 \text{ K}$ and $P_{\text{H}_2} = 3.0 \text{ MPa}$) and the hydrogen concentration in the reaction mixture (93 mol m^{-3}) to $93 / 1.07 = 87 \text{ s}$. For the gas-liquid mass transfer the characteristic time was calculated to 0.9 s as the reciprocal value of k_{La} (1.1 s^{-1} at stirring speed $N = 30 \text{ s}^{-1}$). The long characteristic time for the reaction compared to the gas-liquid mass transfer strongly suggests that transport of hydrogen from the gas to the liquid phase is not rate limiting. This conclusion is supported by the apparent activation energy (74 kJ mol^{-1} in the temperature range 338 K-388 K) which was much higher than that typically observed in the presence of external mass transfer limitations ($5 - 10 \text{ kJ mol}^{-1}$).^[14] The activation energy observed here was similar to that reported previously for the hydrogenation of nitriles over cobalt catalysts.^[11]

Calibration and response behaviour of the permeation probe

A pressure step after the end of the reaction was applied in order to calibrate the sensor on the one hand and to get an insight into the response behaviour of the permeation probe upon a change of the hydrogen saturation level of the liquid. The concentration of hydrogen in the carrier gas of the permeation probe is a linear function of the partial pressure of dissolved hydrogen in the reactor (P_{H_2}).^[5] Here, the concentration of hydrogen in the carrier gas was 1992 ppm prior to the pressure step. A pressure step in hydrogen of 0.63 MPa led to an increase in the sensor signal by 428 ppm. The saturation level of 1992 ppm corresponds according to the linear correlation $P_{H_2} = (0.63 \text{ MPa} \cdot 1992 \text{ ppm}) / 428 \text{ ppm}$ to a partial pressure of hydrogen $P_{H_2} = 2.90 \text{ MPa}$. This value is close to the partial pressure of hydrogen in the gas phase (3.0 MPa) which was calculated from the total pressure in the autoclave and the partial pressures of ammonia (5.12 MPa^[15]) and substrate (<0.1 MPa) assuming that hydrogen behaves as an ideal dilute solution. Note that with the permeation probe the partial pressure of dissolved gases can be derived even when the system does not behave as ideal dilute solution or when the vapour pressure of each single component in the reaction mixture is not available. When the Henry coefficient is known, the partial pressure can be related to the concentration of hydrogen in the liquid phase according to $x_{H_2} = P_{H_2} / K_H$. However, in case of this study only the solubility of hydrogen in pure ammonia was reported ($\alpha = 158 \text{ mol m}^{-3}$ at $T = 373 \text{ K}$).^[16] The Henry coefficient for the reaction mixture was estimated using the initial and final pressure readings during the measurement of the $k_L a$ value for calculating the hydrogen mass balance.^[17] At the conditions of the experiments shown in Figure 6.7 7 the Henry coefficient was calculated to 840 MPa and the concentration of hydrogen in the reaction mixture to 93 mol m^{-3} (at 3.0 MPa).

The sensor shows an increasing signal immediately after the pressure step with a steep ascent in the beginning resulting in a relative signal increase of 50 % of the final reading after 1.2 min. After 7.2 min 90 % are reached. This shows that the hydrogen saturation level of the liquid can be followed at least qualitatively on a relatively short time scale.

6.3.2.2. Reaction with external mass transfer limitation

An experiment at the same conditions as above but a lower stirring speed (6.7 s^{-1}) was conducted in order to show the influence of external mass transfer (G-L or L-S) on the reaction rate and the hydrogen saturation of the liquid phase as measured with the permeation probe (Fig. 8). Comparing the concentration profiles and the course of hydrogen uptake in Fig. 8 to that in Fig. 6 one can see that it takes much longer (210 min) until the end of the re-

action is reached at a reduced stirring speed. The initial rate of dinitrile consumption as calculated from the initial slope of the GC-Data (starting at $t > 6$ min because of the slower rate at the beginning) is strongly reduced by external mass transfer limitations from $1.00 \text{ mol min}^{-1} \text{ kg}_{\text{Cat}}^{-1}$ ($N = 30 \text{ s}^{-1}$) to $0.34 \text{ mol min}^{-1} \text{ kg}_{\text{Cat}}^{-1}$ ($N = 6.7 \text{ s}^{-1}$).

The course of the hydrogen saturation of the liquid phase is related to the hydrogen consumption and to the hydrogen flow in Fig. 8. Due to the above mentioned response time only qualitative statements concerning the hydrogen saturation level of the liquid phase after 15 min reaction time can be made. During the course of the reaction an increase in the signal of the permeation probe can be observed. The increasing hydrogen saturation level nicely corresponds with the decreasing rate of reaction as depicted by the hydrogen consumption profile and more clearly by the hydrogen flow rate. A more detailed comparison of the hydrogen flow and the hydrogen concentration in the carrier gas is given in the enlarged section of Fig. 8 (c) to show the correspondence at the end of the reaction. It can be observed that the hydrogen flow and thus the reaction rate decreases with a steeper slope when getting close to the end of the reaction (starting at about 150 min). In the same manor the hydrogen saturation level increases faster until it reaches a constant value at the end of the reaction corresponding to the saturation of the liquid phase with hydrogen.

By comparing the value of the hydrogen concentration in the carrier gas when reliable reading is reached after 20 min (1830 ppm) and after the reaction (2025 ppm) when the liquid is fully saturated a relative increase in the saturation level of 10 % can be obtained. That means the mass transfer across the gas-liquid interface is too slow to fully replenish the hydrogen consumed during the reaction in the liquid phase. According to Fig. 7 reaction rate depends on the hydrogen pressure that according to Henry's law correlates linearly with the concentration in the liquid phase, with an order of 0.5. However, the reaction rate is decreased by almost a factor of three which would correspond to a concentration lowered by a factor of six during the reaction with external mass transfer limitation compared to the reaction without external mass transfer limitation. Thus the hydrogen saturation level should be much lower during the reaction ($\sim 17 \%$) than observed ($\sim 90 \%$). The explanation for this effect is that by reducing the stirring speed not only the G-L mass transfer rate is lowered but also the L-S mass transfer rate across the stagnant layer surrounding the catalyst particle. At the investigated stirring speed the rate of the two transport steps is in the same order of magnitude with the G-L mass transfer being the slower process. Thus the liquid phase is not fully saturated during the reaction but is on a high saturation level as the rate of the steps is similar.

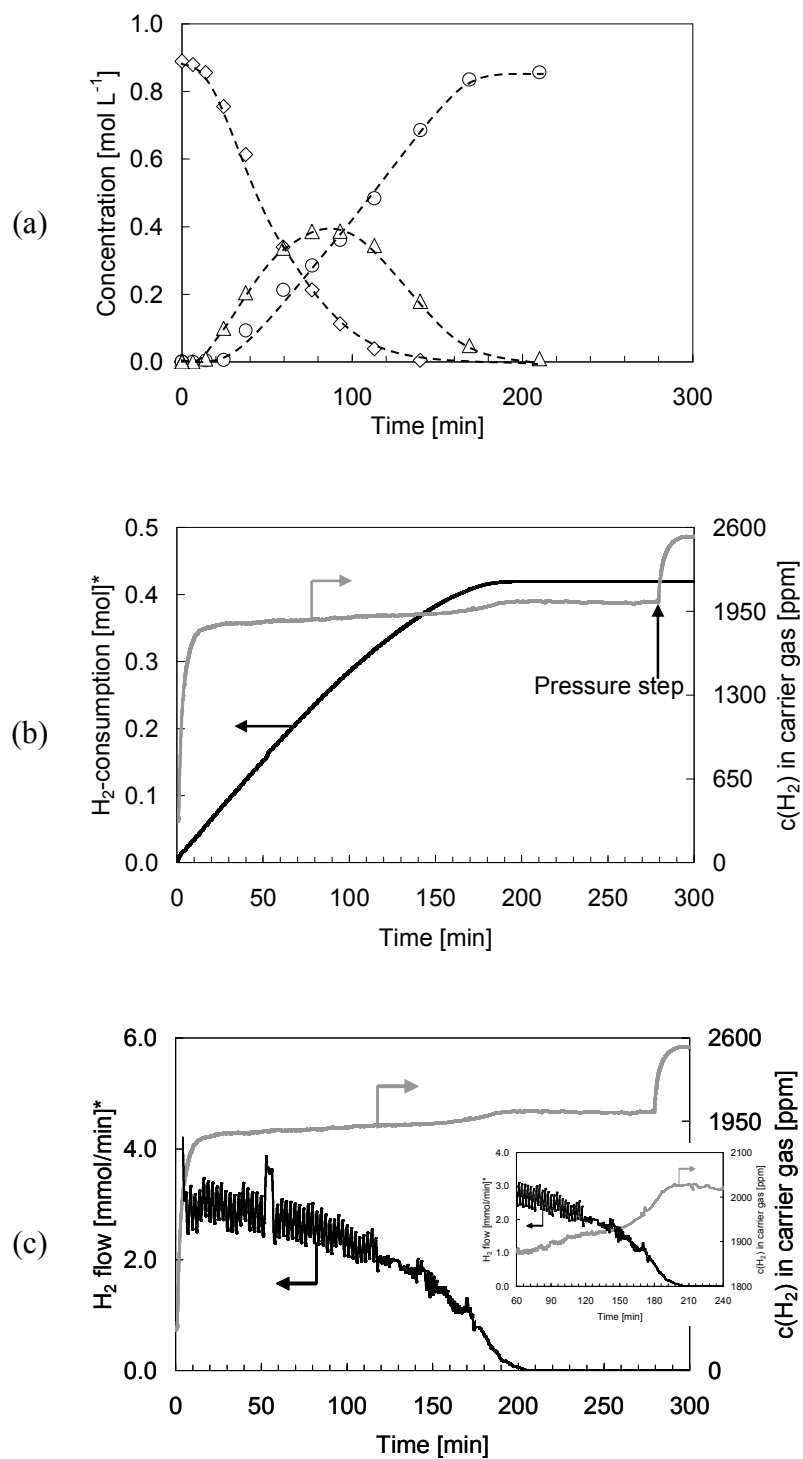


Figure 6.8 (a) Concentration profile of dinitrile hydrogenation at $T = 363\text{ K}$; $P_{\text{H}_2} = 3.0\text{ MPa}$ and stirring speed $N = 6.7\text{ s}^{-1}$, (◇) dinitrile, (△) aminonitrile, (○) diamine. (b) Hydrogen consumption during the experiment and concentration of hydrogen in the carrier gas of the permeation probe (* for 112 mL solution). The arrow indicates a pressure step from 8.26 MPa to 8.98 MPa. (c) Hydrogen flow profile and concentration of hydrogen in the carrier gas of the permeation probe. Enlarged section is shown in the inset.

Again the characteristic times for the reaction and G-L mass transfer are compared. The characteristic time for the reaction without external mass transfer limitation was calculated above to 87 s. The reciprocal of the $k_L a$ value at a stirring speed of $N = 6.7 \text{ s}^{-1}$ (0.038 s^{-1}) is 26 s. It was taken as the characteristic time for the G-L mass transfer. In this case the characteristic time for the two processes is in the same order of magnitude. Considering that the method of characteristic times is an estimation of the presence of G-L mass transfer limitation and that the time of G-L mass transfer is quite close to that of the reaction this method maybe does not allow a concrete statement about the prevailing regime.

6.4. Conclusions

The purpose of this study was to evaluate the potential of a new permeation probe, Fugatron by DMP Ltd., for quantifying the concentration of dissolved gases in typical three phase reaction systems. The model reaction, cobalt-catalyzed hydrogenation of a dinitrile to diamine was performed in a laboratory scale slurry reactor in the presence of liquid ammonia. It is noteworthy that the reaction proceeded stepwise with the two nitrile groups of one molecule hydrogenated in two distinct steps. The observed concentration profile is consistent with stronger adsorption of the dinitrile on the catalyst surface compared to the aminonitrile. In consequence, the rate of aminonitrile hydrogenation increased when the dinitrile had almost depleted.

The concentration of dissolved hydrogen during the reaction was measured with the permeation probe for two regimes: one limited and one not limited by external mass transfer. The response time of the probe (12 min $t_{10}-t_{90}$) was too long to track the hydrogen concentration during the initial phase of the reaction. However, estimation of the characteristic time of the gas-liquid (G-L) mass transfer and the reaction showed that, at a stirring speed of $N = 30 \text{ s}^{-1}$ the reaction is not limited by the G-L transport step. Additionally, the activation energy (74 kJ mol^{-1}) strongly supports the assumption that liquid-solid (L-S) mass transfer limitations were absent. A steady reading of the permeation probe after 15-20 min clearly proved that the reaction mixture was saturated with hydrogen at longer reaction times.

In a second experiment, it was shown that the rate of reaction decreased when lowering the stirring speed ($N = 6.7 \text{ s}^{-1}$). In this case, the signal of the permeation probe provided evidence about the saturation level as the rate of reaction was rather constant throughout the reaction. In consequence, limitations by external mass transfer were not limited to the initial phase of the reaction. The signal of the permeation probe increased during the course of the reaction in parallel with the decreasing hydrogenation rate, which is especially pronounced at

the end of the reaction. Comparing the saturation level with the decrease in the hydrogenation rate upon lowering the stirring speed allowed for differentiation between G-L and L-S mass transfer, proving that G-L mass transfer was the rate-determining step. After internal calibration by a simple pressure step, the permeation probe enabled us to determine the partial pressure of dissolved hydrogen and, after determining the Henry coefficient, the concentration of dissolved hydrogen in the reaction mixture. The latter represents an interesting approach for the development of kinetic models in combination with a description of G-L mass transfer.

Abbreviations

c	concentration	mol L ⁻¹
K _H	Henry coefficient	MPa
k _{La}	volumetric gas-liquid mass transfer coefficient	s ⁻¹
N	stirring speed	s ⁻¹
P	pressure	MPa
P ₀	equilibrium pressure	MPa
P _{H2}	partial pressure of hydrogen	MPa
P _f	pressure after the reaction	MPa
P _m	pressure at t=0	MPa
P _{tot}	total pressure	MPa
r ₀	initial rate of reaction	mol min ⁻¹ kg _{Cat} ⁻¹
T	Temperature	K
t	time	s
x _{H2}	mole fraction of hydrogen in the liquid phase	-

Acknowledgements

Xaver Hecht is thanked for experimental support. Fugatron[®] is a registered trademark of DMP AG. Marko Stapf is thanked for experimental assistance.

References

- [1] R. J. Berger, E. H. Stitt, G. B. Marin, F. Kapteijn, J. A. Moulijn, *Cattech* **2001**, 5, 30.
- [2] F. Kapteijn, J. A. Moulijn, in *Handbook of Heterogeneous Catalysis, Vol. 3* (Eds.: G. Ertl, H. Knözinger, J. Weitkamp), VCH Verlagsgesellschaft mbH, Weinheim, **1997**, p. 1359.
- [3] Fugatron, DMP Ltd., www.Fugatron.com (accessed Sept 2004)

-
- [4] E. Dietrich, C. Mathieu, H. Delmas, J. Jenck, *Chem. Eng. Sci.* **1992**, *47*, 3597.
- [5] M. Meyberg, F. Roessler, *Ind. Eng. Chem. Res.* **2005**, *44*, 9705.
- [6] B. W. Hoffer, P. H. J. Schoenmakers, P. R. A. Mooijman, G. M. Hamminga, R. J. Berger, A. D. van Langeveld, J. A. Moulijn, *Chem. Eng. Sci.* **2004**, *59*, 259.
- [7] A. Lekhal, R. V. Chaudhari, A. M. Wilhelm, H. Delmas, *Chem. Eng. Sci.* **1997**, *52*, 4069.
- [8] *User Manual Fugatron HYD-200*, DMP Ltd., Switzerland, **2004**.
- [9] Y. Y. Huang, V. Adeeva, W. M. H. Sachtler, *App. Catal. A* **2000**, *196*, 73.
- [10] F. Mares, J. E. Galle, S. E. Diamond, F. J. Regina, *J. Catal.* **1988**, *112*, 145.
- [11] J. Volf, J. Pasek, *Stud. Surf. Sci. Catal.* **1986**, *27*, 105.
- [12] For similar conclusions on Raney-Ni catalysts see M. Joucla, P. Marion, P. Grenouillet, J. Jenck, in *Catalysis of organic reactions III* (Eds.: J. R. Kosak, T. A. Johnson), Marcel Dekker, New York, **1994**, p. 127.
- [13] C. Joly-Vuillemin, D. Gavroy, G. Cordier, C. de Bellefon, H. Delmas, *Chem. Eng. Sci.* **1994**, *49*, 4839.
- [14] G. Emig, R. Dittmeyer, in *Handbook of Heterogeneous Catalysis, Vol. 3* (Eds.: G. Ertl, H. Knözinger, J. Weitkamp), VCH Verlagsgesellschaft mbH, Weinheim, **1997**, p. 1359.
- [15] E. W. Lemmon, M. O. McLinden, D. G. Friend, in *NIST Chemistry WebBook*, <http://webbook.nist.gov> (P. J. Lindstrom, W. G. Mallard), National Institute of Standards and Technology, Gaithersburg, MD, **2003**.
- [16] H. Stephen, T. Stephen, *Solubilities of Inorganic and Organic Compounds, Vol. 1*, Pergamon Press, Oxford, **1963**.
- [17] Purwanto, R. M. Deshpande, R. V. Chaudhari, H. Delmas, *J. Chem. Eng. Data* **1996**, *41*, 1414.

Chapter 7

On the activity and selectivity in the hydrogenation of dinitriles with cobalt-based catalysts

Abstract

The gas/liquid/solid three-phase hydrogenation of dinitriles catalyzed by cobalt-based catalysts was investigated in the presence of liquid ammonia and gaseous hydrogen. The reaction kinetics was evaluated in a stirred autoclave and a laboratory-scale trickle-bed reactor allowing to vary the reaction parameters in a wide range. The concentration of ammonia in the liquid phase strongly influenced the selectivity to primary diamines and pore diffusion limited the catalyst utilization with industrially applicable catalyst particle size. By varying the temperature in the trickle-bed reactor it was shown that changes in the phase equilibrium of ammonia markedly influenced the selectivity. Additionally, increasing hydrogen flow led to higher ammonia discharge from the reactor inducing lower selectivity.

7.1. Introduction

A wide range of industrial chemical processes involves gas/liquid/solid multiphase reactions. In such systems, a complex interplay between the flow pattern in the reactor, mass transfer and chemical reaction occurs. The complexity increases when the reaction mixture contains volatile compounds. Although literature on systems with three phases is abundant, the majority of studies consider non-volatile liquid reactants.^[1] However, the phase equilibrium of the reactants or solvents can have a strong effect on activity and selectivity. A particular case is the hydrogenation of dinitriles, such as the reduction of adiponitrile to hexamethylenediamine, which is usually performed in the presence of liquid ammonia in the trickle phase under high pressure conditions.^[2] Ammonia not only acts as diluting agent, but influences directly the selectivity to the desired primary amine. Hence, many patents dealing with the reduction of nitriles over nickel or cobalt-based catalysts state that ammonia has to be added to the reaction mixture to achieve a sufficient selectivity to the primary amine.^[3, 4] Recently, various explanations for this effect were summarized.^[5] A possible thermodynamic effect can be derived from the formal reaction scheme for mononitrile hydrogenation depicted in Figure 7.1. The main product is formed by double hydrogenation of the nitrile group. An imine was suggested as reaction intermediate by von Braun, which can undergo a condensation reaction with an amine group leading to secondary amines accompanied by the formation of ammonia.^[6] By addition of ammonia to the reaction mixture, the thermodynamic equilibrium is shifted to the primary amine.^[7, 8] It was also suggested that ammonia reacts with the imine intermediate giving rise to a diaminoderivative, which can be hydrogenated to the primary amine^[9] or reversibly bind the imine leading to a lower imine concentration.^[3] The latter in turn must result in a decreased rate for the reaction between the imine and primary amine.^[3] A third explanation for the beneficial effect of ammonia is that it adsorbs on the acid sites of the catalyst inhibiting acid catalyzed side reactions.^[10]

The aim of this work was the evaluation of critical parameters influencing the activity and selectivity in the hydrogenation of dinitrile in the presence of ammonia as solvent. Two different experimental setups were used and a wide range of parameters was explored under industrially relevant conditions. A stirred tank reactor was employed to establish the intrinsic kinetics and the role of pore diffusion. Measurements in a laboratory-scale trickle-bed reactor aimed at studying the influence of typical reaction parameters on the selectivity to the desired primary diamine. One advantage of the trickle-bed reactor is its higher degree of freedom in comparison to stirred tank reactors with gas entrainment. In particular, the relative flow rates

of the reactants can be varied. However, in terms of liquid-vapor equilibrium and spatial distribution of reactants in the reactor, the stirred tank reactor yields more precisely defined reaction conditions. Hence, a direct comparison of the two laboratory reactors is expected to help in identifying the most critical parameters.

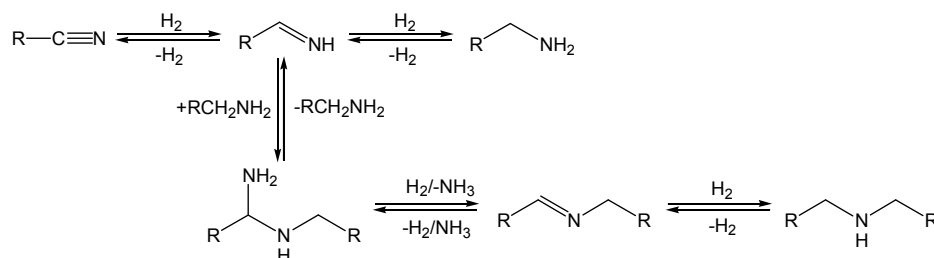


Figure 7.1: Formal reaction mechanism for the hydrogenation of nitriles to primary amines accounting also for the formation of secondary amines.

7.2. Experimental section

7.2.1. Materials

The catalyst was a silica-supported cobalt catalyst composed of Co, Si, Mn, and O. H_2 -chemisorption and BET-measurements were carried out on a ThermoFinnigan Sorptomatic 1990 instrument. The concentration of accessible metal atoms was $257 \mu\text{mol/g}$ and the specific surface area (BET evaluation) was $166 \text{ m}^2/\text{g}$. In its activated form, the catalyst was highly pyrophoric. Thus, after activation the catalyst was handled strictly under oxygen free atmosphere throughout the experiments. Liquid ammonia and hydrogen were received from Messer Griesheim with 99.98% and 99.999% purity, respectively. The feedstock consisted of 95% dinitrile and 5% unspecified impurities. The product diamine used for the calibration of the GC had a purity of approximately 92%. The vapor pressures of dinitrile and diamine were negligible under reaction conditions.

7.2.2. Experiments in the stirred tank reactor

Time-resolved reaction profiles were obtained in a stirred tank reactor ($V_R = 160 \text{ mL}$, Parr Instruments) equipped with a hollow shaft stirrer for gas entrainment. In experiments without ammonia the composition of the reaction mixture was analyzed by *in situ* IR spectroscopy (React-IRTM 1000 spectrophotometer) using a diamond attenuated total reflectance (ATR) crystal inserted at the bottom of the reactor. Experiments at varying stirring speeds showed that gas-liquid and liquid-solid mass transfer limitations were absent at stirring speeds $> 1300 \text{ rpm}$. For the experiments a stirring speed of $1500 \text{ rpm} - 1800 \text{ rpm}$ was used. The hydrogen consumed during the reaction was re-supplied resulting in an almost constant pressure

(within ± 0.1 MPa). In a typical experiment, the autoclave was charged with a fresh catalyst sample (4 g). For the study of intraparticle diffusion effects, catalyst pellets were ground and sieved to obtain fractions with different average diameters. Catalyst particles with diameters ≤ 0.3 mm were used for reactions in the slurry phase. Larger diameter particles ($0.3 \text{ mm} \leq d_p \leq 5.5 \text{ mm}$) were placed in a static catalyst basket. After adding liquid ammonia (0 – 75 mL), the reactor was pressurized with hydrogen to 2.0 MPa and heated to the desired reaction temperature. The reactor was then charged with a known quantity of dinitrile (37 mL – 80 mL). Thereby, the pressure in the autoclave remained nearly equal indicating that the vapor pressure of ammonia remained unchanged. Hydrogen was then quickly admitted to the reactor until the desired partial pressure of hydrogen was obtained (within ~ 2 s). The start of the stirrer was defined as the starting point of the reaction. Temperature, hydrogen pressure and hydrogen consumption rate were recorded during each experiment. Samples of the liquid phase were withdrawn periodically through a dip-tube equipped with a filter for solids.

7.2.3. Experiments in the trickle-bed reactor

The hydrogenation of dinitrile was also carried out in a laboratory-scale trickle-bed reactor (ID = 0.9 cm, length = 15 cm) operated in continuous concurrent down-flow mode. The reactor was filled with a mixture of 1.5 g catalyst (particle diameter < 0.1 mm) and 6 g silicon carbide (SiC, size F 100, 0.106 mm - 0.150 mm). Comparison with well-investigated similar laboratory trickle-bed reactors^[11] and calculations according to generally accepted correlations^[12, 13] suggested that deviations from plug flow were minimal. A fresh catalyst was used for every new set of operating conditions. Glass wool and SiC were placed as layers with a height of at least 2 cm on top of the catalyst bed to avoid entrance effects and to guarantee a well-distributed flow. Prior to the reaction, the lines were flushed with ammonia in order to remove any residual air. Liquid ammonia and dinitrile were dosed by high precision syringe pumps (Teledyne Isco). Hydrogen was fed by a mass flow controller. The feed components were mixed before entering the reactor. Four thermocouples, one in the inert entrance region and three along the catalyst bed, showed that the temperature gradient was ≤ 1 K and, thus, isothermal operation was assumed. A backpressure regulator was used to control the pressure in the reactor. Pressure measurement before and after the reactor allowed the determination of the pressure drop in the reactor, which was < 0.2 MPa. After the reactor, the product mixture was expanded and samples of the liquid phase taken automatically via a 16-port valve. For each data point, at least three samples were taken at intervals of ~ 1 h in order to assure that

steady state was reached and to judge the accuracy of measurement. Catalyst deactivation was not observed during the experiments, which were run for up to 12 h. To evaluate the selectivity at industrially relevant conversion levels, complete conversion ($> 98\%$) was set in all experiments.

The tests for external mass transfer limitations (including diffusion from the gas phase to the liquid phase and through the stagnant layer around the catalyst particle^[14]) at 353 and 373 K showed the rate of reaction increased by a factor of 1.13 (linear velocity tripled) and 1.20 (linear velocity doubled), respectively. Thus, at both temperatures external mass transfer influenced the overall rate of reaction. However, similar flow conditions had to be applied, when almost complete conversion was desired. Consequently, the observed rate of reaction in the laboratory trickle-bed reactor was lower than in the measurements of intrinsic kinetics in the stirred tank reactor. However, in all experiments the selectivity was close to 100%.

7.2.4. *Sample analysis with gas chromatography*

The samples of both reactor systems analyzed with an on-column injection Fisons GC 8160 gas chromatograph equipped with FID (flame ionization detection) detector and 30 m Optima 5 column. As non-volatile compounds, which could not be eluted, were formed during the hydrogenation reaction, it was not possible to quantify all reaction products. Thus, the selectivity to the primary diamine was determined as the ratio of the yield of diamine to the conversion of dinitrile. The accuracy of the selectivity values is $\pm 5\%$.

7.2.5. *Space time yield (SY) in batch wise and continuous operation*

To calculate the space-time yield (SY) in the two reactors, the following equations were used (where m_{DA} , \dot{m}_{DA} and t are the mass and mass flow of diamine and reaction time, respectively):

$$\text{Stirred tank reactor:} \quad SY = \frac{m_{DA}}{t \cdot V_R} \quad \text{Equ. 7.1}$$

$$\text{Trickle-bed reactor:} \quad SY = \frac{\dot{m}_{DA}}{V_R} \quad \text{Equ. 7.2}$$

In the trickle-bed reactor, only experiments with catalyst powder ($d_p < 0.1$ mm) were conducted. In order not to underestimate the SY of the trickle-bed reactor, an experiment was carried out, in which the reaction mixture left the reactor almost exactly at the point, when full conversion was obtained. Assuming that in trickle-bed operation, pore diffusion influences

the overall rate in a similar manner for an estimation of the SY with entire catalyst grains ($d_p = 5 \times 6$ mm), the results from the stirred tank reactor were used. The SY in the trickle-bed reactor was obtained by multiplying the SY observed with catalyst powder with the catalyst effectiveness observed in the stirred tank reactor. About 70% of the volume of the reactor was filled with reaction mixture in agreement with the usual practice.^[15]

For the comparison, the following conditions were chosen:

- *Both reactors:* $T = 353$ °K; $P_{H_2} = 4.86$ MPa; $d_p < 0.1$ mm.
- *Stirred tank:* Catalyst weight: 4.0 g (~ 5 wt-% of the reaction mixture); $V_R = 160$ mL; $V_{DN} = 37$ mL; $V_{NH_3} = 75$ mL; $N = 1800$ rpm
- *Trickle-bed reactor:* Catalyst weight: 1.49 g; $V_R = 3$ mL; $\dot{V}_{DN} = 0.12$ mL \cdot min $^{-1}$; $\dot{V}_{NH_3} = 0.24$ mL \cdot min $^{-1}$.

7.3. Results

7.3.1. Kinetics of hydrogenation in a continuously stirred tank reactor

7.3.1.1. Reaction in presence and absence of ammonia

A typical concentration profile for the hydrogenation of the dinitrile in the absence of ammonia is shown in Figure 7.2, and is related to the integral consumption of hydrogen. After a short induction period (~ 10 min), the main reaction leading to the desired diamine took place according to the reaction scheme in Figure 7.3. One of the two nitrile groups was hydrogenated first to give the aminonitrile. In a consecutive reaction, the aminonitrile was reduced to the diamine. The selectivity to the diamine was approximately 70%. The maximum concentration of aminonitrile was approximately 25% of the starting concentration of dinitrile. A detailed explanation of the reaction profile and the hydrogen consumption profile has been outlined previously.^[16] The mass balance based on the three main components dinitrile, aminonitrile and diamine decreased steadily from the start of the reaction. This shows that the formation of by-products occurred in parallel to the main reaction, which is in accordance with the reaction scheme of Figure 7.1. Among the various by-products identified by GC/MS, the two compounds shown in Figure 7.4 b,c were the most abundant. According to literature,^[3, 17] the formation of both can be explained formally by intra- or intermolecular condensation of an imine group with an amine group resulting in a Schiff base. GC/MS data showed that a cyclic Schiff base was as reaction intermediate formed (Figure 7.4 (a)). Reduction results in formation of the secondary amine b in Figure 7.1. The formation and hydrogenation of the Schiff base intermediates was followed with IR spectroscopy (see Figure 7.5). A strong

band was observed at $1680 - 1650 \text{ cm}^{-1}$ characteristic for the CN double bond as it is found in Schiff bases. The band first increased and then decreased in intensity coinciding with the formation and depletion of the component a in Figure 7.4. After the end of the reaction, the concentration of the diamine was constant under reaction conditions for at least 30 min (after that the experiment was aborted). Hence, no further reaction of diamine to by-products occurred. Heavy compounds, as for example, oligomers could neither be identified with the analysis techniques applied, nor quantified. However, it is assumed that the condensation reaction and the formation of secondary amines are by far the most important routes to by-products.

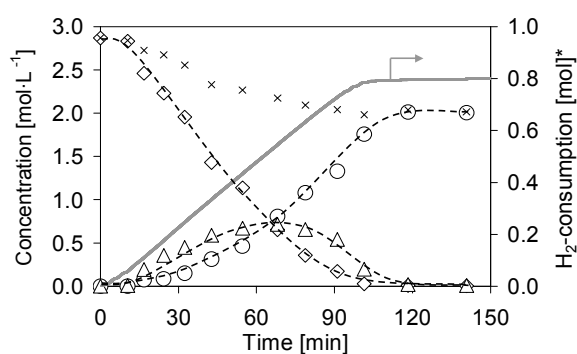


Figure 7.2: Concentration profile and integral hydrogen consumption of dinitrile hydrogenation in substance at $T = 353 \text{ K}$, $P_{\text{H}_2} = 4.86 \text{ MPa}$ and stirring speed $N = 30 \text{ s}^{-1}$: (\diamond) dinitrile, (\triangle) aminonitrile, (\circ) diamine, (\times) mass balance. (*For 72 mL solution).

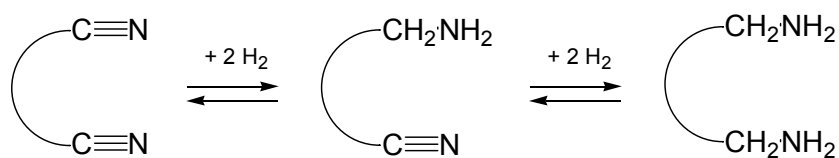


Figure 7.3: Hydrogenation of dinitrile to primary diamine with aminonitrile as isolatable intermediate.

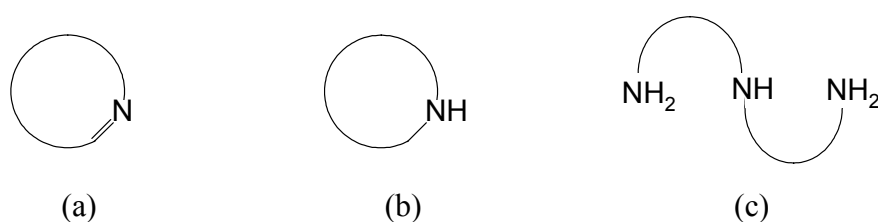


Figure 7.4: Chemical structure of typical side products during the hydrogenation of dinitrile. (a) reaction intermediate (cyclic imine). (b) Intramolecular condensation product (diazocane). (c) Intermolecular condensation product (dimer).

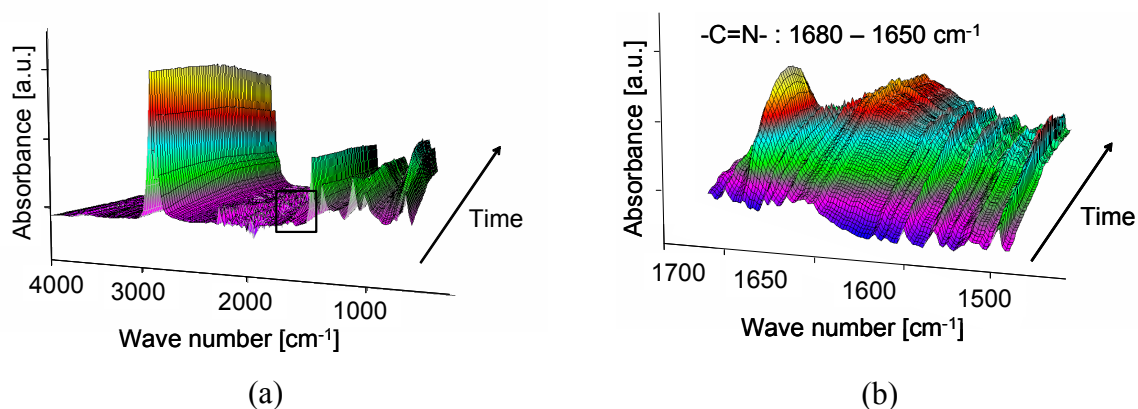


Figure 7.5: (a) Time-resolved IR-spectra dinitrile hydrogenation in substance at $T = 353 \text{ K}$, $P_{\text{H}_2} = 4.86 \text{ MPa}$ and stirring speed $N = 30 \text{ s}^{-1}$. (a) entire spectrum. (b) magnification of region marked in (a).

In order to study the influence of ammonia on the course of the hydrogenation reaction an experiment was conducted with a volume ratio of ammonia/dinitrile of 2 (molar ratio ~ 25 ; also referred to as excess of ammonia) under the same conditions as above. In Figure 7.6, the reaction profile is shown. The main reaction to the desired diamine proceeded according to the sequence in Figure 7.3. The concentration profile is similar to that without ammonia (see Figure 7.2). However, the mass balance of the three compounds dinitrile, aminonitrile and diamine was close to 100% throughout the entire reaction. The formation of by-products was not observed. Accordingly, the selectivity to the primary diamine was $\geq 95\%$. Thus, by adding excess ammonia the selectivity was increased by approximately 30%. Note that the maximum concentration of aminonitrile increased from $\sim 25\%$ to $\sim 45\%$ of the starting concentration of dinitrile, when ammonia was added to the reaction mixture.

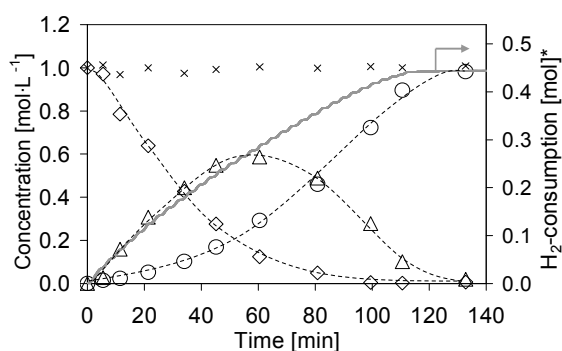


Figure 7.6: Concentration profile and integral hydrogen consumption of dinitrile hydrogenation in excess of ammonia at $T = 353 \text{ K}$, $P_{\text{H}_2} = 4.86 \text{ MPa}$ and stirring speed $N = 30 \text{ s}^{-1}$: (\diamond) dinitrile, (\triangle) aminonitrile, (\circ) diamine, (\times) mass balance in $\text{mol}\cdot\text{L}^{-1}$. * H_2 -consumption for 112 mL solution.

7.3.1.2. Influence of the ammonia concentration on the selectivity

For studying the influence of the ammonia content on the selectivity to primary diamine, experiments with different amounts of ammonia were performed. In Figure 7.7, the

selectivity is shown as a function of the volume ratio ammonia/dinitrile. As expected, the selectivity increased with higher ammonia content in the reactor. In particular, between a volume ratio of ~ 0.05 and ~ 0.2 a significant increase in selectivity from $\sim 70\%$ to $\sim 90\%$ was observed. In this region, the selectivity was apparently very sensitive to the ammonia content. A ratio of 0.5 provided selectivity close to 100%. Lower selectivity was related to an increasing amount of secondary amines formed by intra- or intermolecular condensation reactions. Thus, ammonia was necessary to suppress the side-reactions. A volume ratio ammonia/dinitrile of 2.0 was chosen for the parameter study.

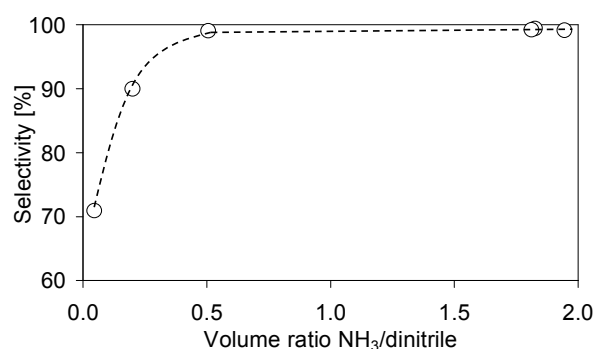


Figure 7.7: Influence of the ammonia content on the selectivity to diamine at $T = 353$ K and $P_{\text{H}_2} = 4.86$ MPa.

7.3.1.3. Influence of the reaction temperature

The temperature dependence of the initial rate of dinitrile hydrogenation (r_0 (Dinitrile)) was investigated to determine the apparent energy of activation of the main reactions. The temperature was varied from 338 K to 388 K, keeping the other conditions (ammonia/dinitrile ratio in the reactor, $P_{\text{H}_2} = 4.86$ MPa) constant. The overall pressure in the reactor changed according to the vapor pressure of ammonia at the respective temperature. In a first set of experiments the catalyst particle size was chosen to $d_p = 0.1 - 0.2$ mm. As shown in Figure 7.8, two distinct regions with different activation energies were found. At $T \leq 353$ K the activation energy was 75 kJ/mol, whereas at $T > 353$ K the activation energy was 45 kJ/mol. This difference in the activation energy is attributed to a change from intrinsic kinetics to pore diffusion control. Note that the ratio in activation energy was 1.7:1, which is close to the value of 2:1 as predicted from the Thiele-modulus. In a second set of experiments, a catalyst particle size of $d_p < 0.1$ mm was applied (see Figure 7.8, dashed line). Here, no change in activation energy was observed in the temperature region investigated (338 K – 388 K). This suggests that pore diffusion limitations did not occur with small particles ($d_p < 0.1$ mm). The same activation energy as in the intrinsic region for larger particles was

found. With an ammonia/dinitrile ratio of 2.0, the influence of temperature on the selectivity to the primary diamine was insignificant. The selectivity was $\geq 95\%$ over the whole temperature range with both catalyst particle sizes applied.

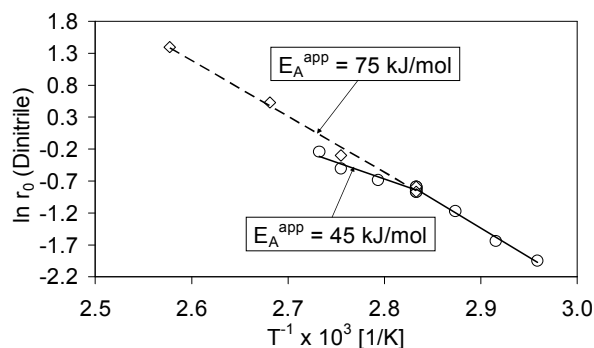


Figure 7.8: Arrhenius-plot for determination of the apparent activation energy at $P_{H_2} = 4.86$ MPa. (○) Catalyst particle size $d_p = 0.1 - 0.2$ mm, (◇) catalyst particle size $d_p < 0.1$ mm.

7.3.1.4. Influence of the hydrogen pressure

The influence of hydrogen concentration on the rate of reaction and the selectivity to the primary diamine was also examined in excess of ammonia. The partial pressure of hydrogen was varied in the range from 1.86 MPa to 9.0 MPa. The rate of reaction increased with increasing hydrogen pressure (Figure 7.9). From the data shown, a reaction order of 0.5 was calculated. This is consistent with a Langmuir-Hinshelwood mechanism with dissociative adsorption of hydrogen^[16]. Such a reaction order in hydrogen has also been suggested for Raney Nickel catalysts.^[18] The selectivity was independent of hydrogen pressure. Even at the lowest hydrogen pressure tested ($P_{H_2} = 1.86$ MPa), the selectivity was high ($\geq 95\%$).

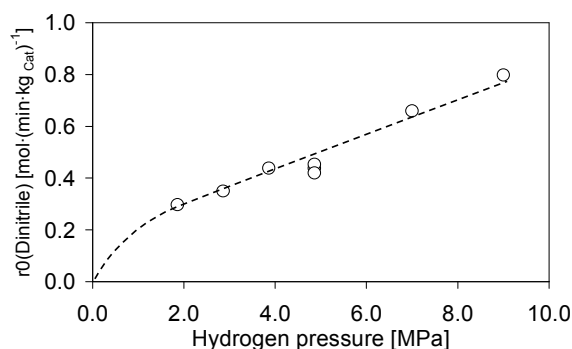


Figure 7.9: Initial rate of dinitrile conversion as a function of hydrogen pressure at $T = 353$ K and $d_p < 0.1$ mm.

7.3.1.5. Potential limitations by pore diffusion

Pore diffusion limitations lead to a lower catalyst effectiveness as only part of the active material is utilized. In the presence of such limitations, reducing the particle diameter

would result in a higher reaction rate per reactor volume. However, at small particle size the pressure drop over a fixed bed increases.^[19] The optimum size and shape of catalyst particles is thus, a compromise between the reaction rate and allowable pressure drop.^[19] In order to explore the impact of diffusion limitations on the product selectivity, the role of pore diffusion was investigated in the present work.

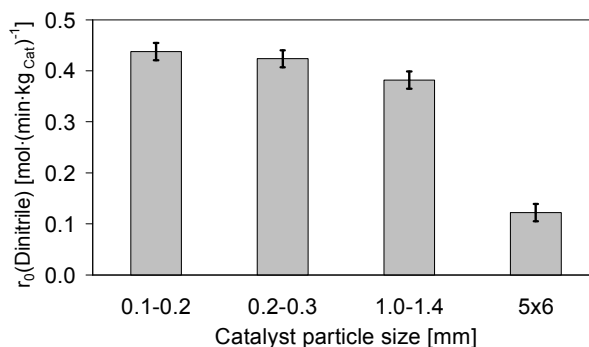


Figure 7.10: Initial rate of reaction as a function of catalyst particle size. The error bars show the standard deviation, which was derived from three independent measurements at $d_p = 0.1 - 0.2$ mm. $T = 353$ K, $P_{\text{H}_2} = 4.86$ MPa.

In Figure 7.10, the initial rate of dinitrile consumption is plotted as a function of catalyst particle size for a temperature of 353 K. Considering the accuracy of measurement (see error bars) changes in the reaction rate were not observed between $d_p = 0.1 - 0.2$ mm and $d_p = 0.2 - 0.3$ mm. Thus, the rate was determined by intrinsic kinetics, when particles with less than 0.3 mm were used. With increase of the catalyst particle size to $d_p = 1.0 - 1.4$ mm, pore diffusion started affecting the reaction rate. With tablets of size $d_p = 5 \times 6$ mm, the overall rate of reaction was reduced considerably. Here, the observed rate was only $\sim 28\%$ of the intrinsic rate. The selectivity was not affected by the increasing particle size and was $\geq 95\%$ with all catalyst fractions.

7.3.2. Continuous hydrogenation in a trickle-bed reactor

7.3.2.1. Influence of ammonia content

The influence of the ammonia content on the selectivity was examined in analogy to the experiments in the stirred tank reactor by varying the volume ratio ammonia/dinitrile at the reactor entrance (see Figure 7.11). For comparison, the selectivity in the batch-wise operated autoclave (see also section 7.3.1.2) is included in Figure 7.11. Up to an ammonia/dinitrile ratio of 1.0, the increasing ammonia concentration led to gradual enhancement in selectivity from 65% to $\geq 95\%$. Compared to the stirred tank reactor, a higher ammonia/dinitrile ratio was necessary to obtain selectivities above 95% (a ratio of at least 0.75 was necessary to

achieve selectivities of approximately 95%). Therefore, this ratio was chosen for examining the sensitivity of the selectivity to operating parameters (temperature, hydrogen pressure, hydrogen flow) in the following parameter study. The results will be compared to measurements in excess of ammonia.

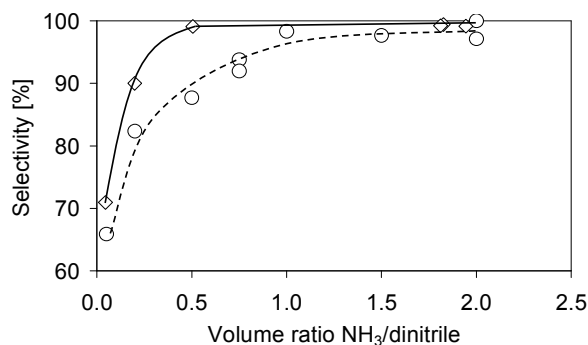


Figure 7.11: Influence of ammonia on the selectivity to diamine. (\diamond) Stirred tank reactor, (\circ) Trickle-bed reactor. $T = 353 \text{ K}$, $P_{\text{H}_2} = 4.86 \text{ MPa}$, $d_p < 0.1 \text{ mm}$, $\dot{V}_{\text{Dinitrile}} = 0.04 - 0.06 \text{ mL}\cdot\text{min}^{-1}$, $\dot{V}_{\text{H}_2} = 50 - 75 \text{ mL}\cdot\text{min}^{-1}$.

7.3.2.2. Dependence on reaction temperature

The influence of temperature on selectivity was investigated between 348 K and 368 K for two different ammonia/dinitrile ratios. The partial pressure of hydrogen was kept constant leading to variations in the overall pressure. The results are depicted in Figure 7.12. Especially in the case of a low ammonia/dinitrile ratio (0.75), the selectivity was strongly dependent on the reaction temperature decreasing from $\sim 95\%$ to $\sim 85\%$ in the temperature range tested. With an ammonia/dinitrile ratio of 2.0, the temperature dependence was less and the selectivity decreased from 98% to 95% when increasing the temperature from 353 K to 368 K.

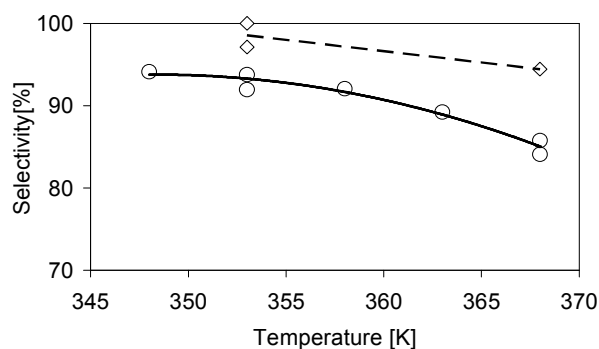


Figure 7.12: Influence of temperature on the selectivity to diamine using the trickle-bed reactor. (\circ) $\dot{V}_{\text{NH}_3}/\dot{V}_{\text{Dinitrile}} = 0.75$, (\diamond) $\dot{V}_{\text{NH}_3}/\dot{V}_{\text{Dinitrile}} = 2.0$. $P_{\text{H}_2} = 4.86 \text{ MPa}$, $\dot{V}_{\text{Dinitrile}} = 0.06 \text{ mL}\cdot\text{min}^{-1}$, $\dot{V}_{\text{NH}_3} = 0.045 \text{ mL}\cdot\text{min}^{-1}$ and $0.120 \text{ mL}\cdot\text{min}^{-1}$, $\dot{V}_{\text{H}_2} = 75 \text{ mL}\cdot\text{min}^{-1}$.

7.3.2.3. Influence of hydrogen pressure

The hydrogen pressure was varied from 2.86 MPa to 10.0 MPa to explore its influence on the selectivity to the primary diamine. As can be seen in Figure 7.13 for an ammonia/dinitrile ratio of 0.75, the selectivity was enhanced significantly by raising the hydrogen pressure in the reactor. A change of hydrogen pressure from 2.86 MPa to 4.86 MPa led to an increase in selectivity of approximately 10%. With further increase of the hydrogen pressure, a selectivity of 96% was obtained. At an ammonia/dinitrile ratio of 2.0, the selectivity was generally higher ($\geq 95\%$). However, when decreasing the hydrogen pressure from 4.86 MPa to 2.86 MPa the selectivity decreased from 98% to 95%.

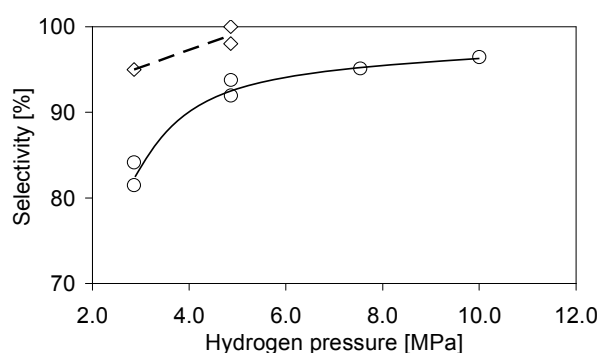


Figure 7.13: Influence of the hydrogen pressure on the selectivity to diamine using the trickle-bed reactor. (\odot) $\dot{V}_{\text{NH}_3}/\dot{V}_{\text{Dinitrile}} = 0.75$, (\diamond) $\dot{V}_{\text{NH}_3}/\dot{V}_{\text{Dinitrile}} = 2.0$. $T = 353 \text{ K}$, $\dot{V}_{\text{Dinitrile}} = 0.06 \text{ mL}\cdot\text{min}^{-1}$, $\dot{V}_{\text{NH}_3} = 0.045 \text{ mL}\cdot\text{min}^{-1}$ and $0.120 \text{ mL}\cdot\text{min}^{-1}$, $\dot{V}_{\text{H}_2} = 75 \text{ mL}\cdot\text{min}^{-1}$.

7.3.2.4. Variation of hydrogen flow

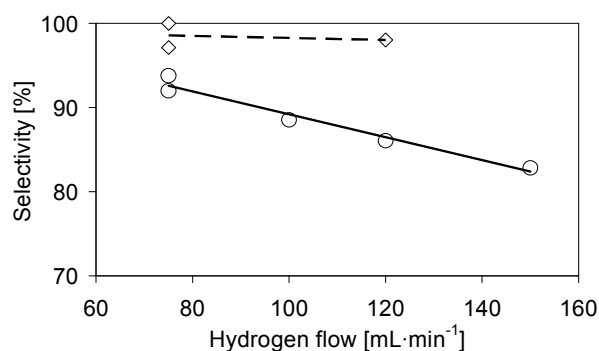


Figure 7.14: Influence of the hydrogen flow (under ambient conditions) on the selectivity to diamine using the trickle-bed reactor. (\odot) $\dot{V}_{\text{NH}_3}/\dot{V}_{\text{Dinitrile}} = 0.75$, (\diamond) $\dot{V}_{\text{NH}_3}/\dot{V}_{\text{Dinitrile}} = 2.0$. $T = 353 \text{ K}$, $P_{\text{H}_2} = 4.86 \text{ MPa}$, $\dot{V}_{\text{Dinitrile}} = 0.06 \text{ mL}\cdot\text{min}^{-1}$, $\dot{V}_{\text{NH}_3} = 0.045 \text{ mL}\cdot\text{min}^{-1}$ and $0.120 \text{ mL}\cdot\text{min}^{-1}$.

Keeping the other conditions (temperature, hydrogen pressure, flow rates of dinitrile and ammonia) constant, the hydrogen flow rate was raised from $75 \text{ mL}\cdot\text{min}^{-1}$ to $150 \text{ mL}\cdot\text{min}^{-1}$ at an ammonia/dinitrile ratio of 0.75. In a further set of experiments, a flow of $75 \text{ mL}\cdot\text{min}^{-1}$

and $120 \text{ mL}\cdot\text{min}^{-1}$ was applied at an ammonia/dinitrile ratio of 2.0. Under these flow conditions, the excess of hydrogen was at least five-fold, as the hydrogen flow necessary for full stoichiometric conversion of the dinitrile was approximately $16 \text{ mL}\cdot\text{min}^{-1}$. At the lower ammonia/dinitrile ratio, the selectivity to the primary diamine decreased linearly with hydrogen flow, whereas no significant influence was observed at a ratio of 2.0.

7.4. Discussion

7.4.1. Influence of ammonia on selectivity

In the hydrogenation of dinitrile, the selectivity to primary diamine was strongly enhanced by addition of ammonia to the reaction mixture. Insight into the way ammonia changes the selectivity was obtained by comparing the reaction under similar conditions but with and without ammonia. The most noticeable effect of adding ammonia was the increase of the relative concentration of the reaction intermediate aminonitrile. This indicates that ammonia changes the adsorption behavior of the molecules on the catalyst surface relative to each other.

Two explanations are possible, which do not exclude each other: In a previous study, it was shown that the relative adsorption constants of amine and nitrile influence the selectivity to primary amine.^[20] If the amine adsorbs less strongly compared to the nitrile the selectivity is increased as the condensation reactions take place in the adsorption layer on the catalyst.^[21] Therefore, depletion of molecules bearing an amine functionality results in a higher selectivity. Either ammonia interacts favorably with aminonitrile (probably *via* hydrogen bonding interactions) leading to a greater percentage of aminonitrile, leaving the catalyst surface or it adsorbs on the catalyst surface displacing aminonitrile. Both scenarios would result in enhanced selectivity. As aminonitrile is found to desorb readily in the presence of ammonia, we conclude that the amino group interacts weaker with the surface than the nitrile group. In consequence, the diamine desorbs even easier than the aminonitrile. If ammonia itself adsorbs on the catalyst surface, the effect will be similar. An additional positive effect arises as ammonia binds preferentially to the Brønsted acid sites of the catalyst, which are responsible for condensation reactions.^[22]

7.4.2. Role of the liquid – vapor equilibrium of ammonia in the formation of by-products

The amount of ammonia in the respective reactor has a strong influence on the selectivity to primary diamine (see Figure 7.7 and Figure 7.11). As the hydrogenation reaction takes place at the interface of liquid and solid, it was speculated that the concentration of am-

monia in the liquid phase governs the selectivity. Therefore, the content of liquid ammonia in the stirred tank reactor was calculated *via* a combined energy and mass balance and related with the selectivity to primary diamine (Figure 7.15). The content of liquid ammonia was varied by filling different amounts of ammonia into the reactor prior to the start of the reaction. During heating, part of ammonia is vaporized. Thus, with low ammonia content in the reactor only a small fraction of ammonia is in the liquid phase. From Figure 7.15 it can be seen that the selectivity correlates well with the molar ammonia fraction in the liquid phase. Up to an ammonia/dinitrile ratio of 0.5, the selectivity increased with the ammonia content, while at higher ratios the selectivity was constant under these conditions. Hence, it is concluded that the content of ammonia in the liquid phase is a crucial factor to obtain high selectivity to primary diamine.

Compared to the stirred tank reactor, a higher ammonia/dinitrile ratio was necessary in the trickle-bed reactor to obtain the same selectivity. As explained above the content of ammonia in the liquid phase is the decisive factor in terms of selectivity. The different hydrodynamics in the two reactor types influences the ammonia liquid-vapor equilibrium in different ways. In the stirred tank reactor, the amount of liquid ammonia is determined exclusively by the phase equilibrium of ammonia. In the trickle-bed mode, hydrogen flows past the liquid film surrounding the catalyst particles. Vaporized ammonia is discharged together with excess hydrogen, which locally disturbs the ammonia liquid-vapor equilibrium. Hence, the equilibrium is re-established leading to a decrease in the amount of liquid ammonia, which in turn results in decreased selectivity.

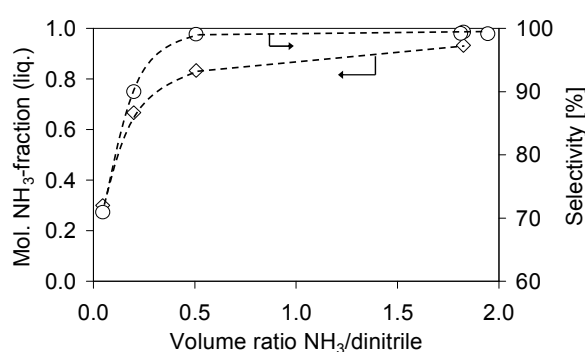


Figure 7.15: Calculated molar ammonia content in the liquid phase of the laboratory stirred tank reactor (◇) and selectivity to primary diamine (○) as a function of the volume ratio ammonia/dinitrile at $T = 353\text{ K}$ and $P_{\text{H}_2} = 4.86\text{ MPa}$.

7.4.3. Influence of temperature on selectivity

Temperature variations in the stirred tank reactor conducted at an ammonia/dinitrile ratio of ~ 2.0 did not influence the selectivity to primary diamine. A high selectivity $\geq 95\%$ was obtained, even when the temperature was varied over a wide range. This shows that in the stirred tank reactor the molar amount of ammonia in the liquid phase was adequate to obtain high selectivity.

In the trickle-bed reactor, two different ammonia/dinitrile ratios (0.75 and 2.0) were tested. At both ratios, the selectivity decreased with increasing temperature. Differences in the performance of the two reactors are the result of the hydrodynamic properties. In trickle-bed operation hydrogen flowing through the reactor leads to depletion of liquid ammonia. This effect is enhanced at higher temperatures as the phase equilibrium of ammonia is shifted towards the vapor phase. Thus, more gas phase ammonia is carried away with the hydrogen flow, the phase equilibrium is adjusted, and the amount of liquid ammonia decreases. The effect of temperature described here is rather indirect, as it influences the selectivity by changing the liquid-vapor distribution of ammonia. However, as the hydrogenation to the primary diamine and the condensation reaction leading to by-products have different temperature dependence, it might also have a direct effect on the selectivity to primary diamine. In this respect, it was reported that the activation energy of the condensation reactions is higher than that of hydrogenation.^[3, 23] In this case, the side reaction would be more favored at higher temperatures.

7.4.4. Influence of hydrogen pressure on selectivity

A positive effect of hydrogen pressure on selectivity was expected because of the different ways hydrogen participates in the main reaction and in the side reactions (Figure 7.1).^[3, 10] A higher hydrogen pressure leads to an increased rate of hydrogenation of dinitrile. In the condensation reaction, hydrogen is not involved in the first step of the by-product formation. Thus, by increasing the partial pressure of hydrogen, the rate of hydrogenation is increased relative to the rate of condensation reactions, which results in enhanced selectivity to the primary diamine. However, hydrogen pressure had no influence on selectivity in the stirred autoclave. It seems that the excess of ammonia was sufficient to suppress side reactions also at low hydrogen pressures.

In the case of trickle-bed operation, ammonia was discharged leading to a strong sensitivity of the selectivity to hydrogen pressure. Increasing hydrogen pressure led to a higher

selectivity, which can be explained by the above-discussed relative increase in the rate of hydrogenation compared to the condensation reaction.

7.4.5. Effect of hydrogen flow in the laboratory trickle-bed reactor

The fact that hydrogen flows through the reactor in the trickle-bed mode led to a remarkably lower selectivity than in the stirred tank reactor (at the same ammonia/dinitrile ratio). In order to support this statement, experiments with different hydrogen flow rates were performed. The decreasing selectivity with increasing hydrogen flow rate is attributed to a stronger discharge of gas phase ammonia, when the flow rate past the liquid film surrounding the catalyst particles is increased. Consequently, the dynamic reestablishment of the ammonia phase equilibrium leads to a lower concentration of ammonia in the liquid phase at higher flow rates^[24].

7.4.6. Space time yield in batch wise and continuous operation

For the conditions applied in this study, the SY are summarized in Table 7.1. The SY, which can be achieved with the trickle-bed reactor, is by a factor 10 – 50 higher, no matter, if the reactor is charged with catalyst powder or catalyst grains. This is due to the well known fact that the catalyst loading in the trickle-bed reactor is a factor of ~ 55 – 65 higher.^[25]

Table 7.1: Space-time yield in the two laboratory reactors.

Diameter of catalyst particles [mm]	Stirred tank reactor [$t_{\text{Product}} \cdot \text{h}^{-1} \cdot \text{m}^{-3}$]	Trickle-bed reactor [$t_{\text{Product}} \cdot \text{h}^{-1} \cdot \text{m}^{-3}$]
0.1	0.087	1.95
5×6	0.023	0.52

7.5. Conclusions

The critical parameters for the hydrogenation of a dinitrile with cobalt-based catalysts have been compared for two reactor types. In the batch wise operated stirred tank reactor, a selectivity of almost 100% was obtained when a sufficient amount of liquid ammonia was used. In excess ammonia, the selectivity was almost insensitive to the other parameters investigated (temperature, hydrogen pressure, diameter of the catalyst particles). By-products formed in the absence of ammonia or at low ammonia concentrations were mainly secondary amines stemming from inter- or intramolecular condensation reactions. When catalyst particle

sizes applicable to industrial fixed bed operations were used, significant pore diffusion limitations were present.

For investigating the influence of the flow regime on the selectivity, a trickle-bed reactor was employed. Here, a lower selectivity was observed, when the same volume ratio ammonia/dinitrile was fed as to a stirred tank reactor. This is mainly affiliated with the strong influence on the concentration of ammonia in the liquid phase. In the stirred tank reactor, gas phase hydrogen is not discharged from the autoclave. In contrast in the trickle bed reactor hydrogen leaves the tubular reactor together with the liquid. Thus, in the first case the concentration of ammonia in the liquid phase is determined by the concentration of ammonia fed and the reaction temperature, while in the latter gaseous ammonia is discharged from the reactor together with excess hydrogen. As the phase equilibrium is dynamically re-established, the average concentration of ammonia in the liquid phase is much lower than in the batch reactor. The higher the hydrogen flow rate was chosen, the lower the concentration of ammonia and, in consequence, the selectivity. This effect was more pronounced at higher temperatures.

In summary, it can be stated that ammonia is the key factor in the selective hydrogenation of the dinitrile investigated. The concentration of liquid ammonia strongly depends on the flow properties in the reactor, which are intrinsically hard to predict. If it is assured that sufficient liquid ammonia is present, the other parameters are adjustable according to the design boundary conditions of industrial processes.

Acknowledgement

Xaver Hecht and Andreas Marx are thanked for experimental support. Experimental assistance of Stefanie Riederer and Niklas Jacobsen is acknowledged.

References

- [1] J. Guo, M. Al-Dahhan, *Ind. Eng. Chem. Res.* **2005**, *44*, 6634.
- [2] K. Weissemel, H. J. Arpe, *Industrial Organic Chemistry*, 3. ed., Wiley-VCH, Weinheim, **1997**.
- [3] J. Volf, J. Pasek, *Stud. Surf. Sci. Catal.* **1986**, *27*, 105.
- [4] L. K. Freidlin, T. A. Sladkova, *Russ. Chem. Rev.* **1964**, *33*, 319.
- [5] R. Novi, Dissertation thesis, ETH Zürich **2004**.
- [6] J. von Braun, G. Blessing, F. Zobel, *Chem. Ber.* **1923**, *56*, 1988.
- [7] F. M. Cabello, D. Tichit, B. Coq, A. Vaccari, N. T. Dung, *J. Catal.* **1997**, *167*, 142.
- [8] W. Pöpel, J. Glaube, *Chem.-Ing.-Tech.* **1988**, *60*, 475.
- [9] E. J. Schwoegler, H. Adkins, *J. Am. Chem. Soc.* **1939**, *61*, 3499.

-
- [10] M. Verhaak, A. J. Vandillen, J. W. Geus, *Catal. Lett.* **1994**, *26*, 37.
- [11] D. van Herk, M. T. Kreutzer, M. Makkee, J. A. Moulijn, *Catal. Today* **2005**, *106*, 227.
- [12] H. Gierman, *Appl. Catal.* **1988**, *43*, 277.
- [13] S. T. Sie, *Rev. Inst. Franc. Pétr.* **1991**, *46*, 501.
- [14] F. Kapteijn, J. A. Moulijn, in *Handbook of Heterogeneous Catalysis, Vol. 3* (Eds.: G. Ertl, H. Knözinger, J. Weitkamp), VCH Verlagsgesellschaft mbH, Weinheim, **1997**, p. 1359.
- [15] M. Baerns, H. Hofmann, A. Renken, *Chemische Reaktionstechnik, Vol. 1*, 3. ed., Wiley-VCH Verlag GmbH, Weinheim, **2002** p.428.
- [16] P. Scharringer, T. E. Muller, W. Kaltner, J. A. Lercher, *Ind. Eng. Chem. Res.* **2005**, *44*, 9770.
- [17] A. Chojecki, Dissertation thesis, TU München **2004**.
- [18] C. Joly-Vuillemin, D. Gavroy, G. Cordier, C. de Bellefon, H. Delmas, *Chem. Eng. Sci.* **1994**, *49*, 4839.
- [19] R. Krishna, S. T. Sie, *Chem. Eng. Sci.* **1994**, *49*, 4029.
- [20] A. Chojecki, M. Veprek-Heijman, T. E. Müller, P. Scharringer, S. Veprek, J. A. Lercher, *J. Catal.* **2007**, *245*, 237.
- [21] Y. Y. Huang, W. M. H. Sachtler, *Appl. Catal. A-Gen.* **1999**, *182*, 365.
- [22] M. J. F. M. Verhaak, Dissertation thesis, Universiteit Utrecht **1994**.
- [23] B. W. Hoffer, P. H. J. Schoenmakers, P. R. A. Mooijman, G. M. Hamminga, R. J. Berger, A. D. van Langeveld, J. A. Moulijn, *Chem. Eng. Sci.* **2004**, *59*, 259.
- [24] V. Lavopa, C. N. Satterfield, *Chem. Eng. Sci.* **1988**, *43*, 2175.
- [25] A. Gianetto, V. Specchia, *Chem. Eng. Sci.* **1992**, *47*, 3197.

Chapter 8

Summary and conclusions

Primary amines are widely used as base chemicals and have manifold applications for further processing. An important method for their preparation on industrial scale is the catalytic hydrogenation of the respective nitriles over heterogeneous transition metal catalysts. However, a mixture of primary, secondary and tertiary amines is generally formed. From an economical as well as environmental point of view, new catalysts and improved processes are required to combine high selectivity to the desired amine with a small reactor size. The optimisation of the catalyst with respect to selectivity and activity requires insight into the elementary reaction steps occurring during the hydrogenation reaction and the influence of the intrinsic properties of the catalysts used. In the present Thesis kinetic and mechanistic investigations on the hydrogenation of nitriles over Raney-Co and supported cobalt catalysts were conducted. One aim was to gain a detailed understanding of the influence of the single mass transfer steps and surface processes (adsorption, surface reaction, desorption) on reaction rate and selectivity to primary amines. With view to industrial applications another objective was to optimize process conditions. Here, special emphasis was placed on the role of ammonia, which is known to increase the selectivity to primary amines when added to the reaction mixture. In detail, the study presented in this Thesis was divided as follows:

The aim of the study presented in Chapter 3 was to obtain insight into the surface structure of partially hydrogenated intermediates occurring during the hydrogenation of nitriles. As it is intrinsically challenging to investigate the surface of metallic catalysts, inelastic neutron scattering (INS) was used as main technique. Experimental and calculated INS spectra were combined with spectroscopic data from literature to examine the co-adsorption of CD_3CN and H_2 on Raney-Co. In TG/DSC measurements two different types of sites for the adsorption of CD_3CN were found. One type showed a particularly strong interaction with CD_3CN . Combination with H_2 chemisorption results showed that roughly one third of the cobalt surface atoms were occupied at the maximum sorption capacity for CD_3CN .

The combination of INS and H_2 chemisorption confirmed that three types of hydrogen adsorption were present (strong chemisorption, chemisorption and physisorption) under the conditions applied. Hydrogen adsorbed on η^3 sites with C_{3v} symmetry was less strongly bound than hydrogen adsorbed on other sites and, thus, most reactive. Comparison of simulated and measured INS results confirmed that the sorbates strongly interacted with the adsorption sites. A band at 1278 cm^{-1} , which was pronounced in the samples with co-adsorbed CD_3CN and H_2 and decreased in intensity with increasing amount of H_2 , was tentatively assigned to the CH_2 twisting mode. The relative decrease of this band compared to the CH_2

wagging mode led to the assumption that a nitrene-like compound was the most abundant intermediate species on the surface.

To get insight into the pathways of alkyl group transfer, the mechanism underlying the formation of secondary amines was investigated in Chapter 4. Two different nitriles, acetonitrile and butyronitrile were co-hydrogenated and hydrogenated in the presence of *n*-butylamine and ethylamine, respectively. In the co-hydrogenation of the two nitriles, acetonitrile was hydrogenated at a significantly higher rate, which in comparison with the hydrogenation of the single nitriles indicates that acetonitrile is more strongly adsorbed on the active sites. The experiments with mixed nitrile reactants suggested that the rate of formation of dialkylimines strongly depended on the type of amine (*n*-butylamine, ethylamine) participating in the condensation reaction. The formation of a partially hydrogenated intermediate, which remained adsorbed on the catalyst surface, was suggested. The reaction of the partly hydrogenated surface intermediate with *n*-butylamine occurred at a higher rate than with ethylamine, which was mainly attributed to the inductive effect of the alkyl group on the N atom and/or to stronger adsorption of *n*-butylamine compared to ethylamine.

The rate of hydrogenation remained approximately the same in the presence of amines and only a slight decrease in selectivity to the primary amine was observed. This led to the conclusion that the condensation to dialkylimine occurred on other sites than the hydrogenation to the corresponding primary amine. It was suggested that alkyl group transfer between monoalkylamines and dialkylimines occurred. The exchange might occur through formation of a surface bound 1-alkyl-aminodialkylamine with subsequent cleavage of the CN bond or a surface bound intermediate formed by 2+2 cycloaddition of two dialkylimines.

To understand the nature of the critical properties, which influence the selectivity and catalytic activity of Raney-catalysts, the hydrogenation of butyronitrile with LiOH modified Raney-Co and three commercial Raney-catalysts (Raney-Ni, Raney-Co and Ni-Cr promoted Raney-Co) was compared in Chapter 5. Thorough characterization of the catalysts allowed to derive structure-activity and structure-selectivity relationships.

LiOH-modification of Raney-Co led to enhanced intrinsic activity (second highest) and the highest selectivity of the catalysts tested. This beneficial effect of LiOH was found to be the result of a modified nature of the catalyst surface. Most likely, islands of lithium aluminate and lithium hydroxide are formed on the catalyst surface. This leads to a higher ratio of metallic cobalt to oxidic cobalt and alumina, which results in (i) a reduced number of Al³⁺ Lewis acid sites, which are claimed to catalyze side reactions, (ii) a higher sorption capacity

per metal atom for butyronitrile and butylamine and (iii) higher ratio of adsorbed butyronitrile relative to butylamine. For a high selectivity a lower adsorption constant of butylamine compared to butyronitrile is beneficial, as adsorbed butylamine is necessary for by-product formation.

The purpose of the study shown in Chapter 6 was to evaluate the role of mass transfer in the hydrogenation of nitriles in three phase reaction systems. For that reason, a permeation probe, which allowed for quantification of the concentration of dissolved gases was applied. The model reaction was the cobalt-catalyzed hydrogenation of a dinitrile to diamine in the presence of liquid ammonia. It is noteworthy that the reaction proceeded stepwise with the two nitrile groups of one molecule hydrogenated in two distinct steps.

The concentration of dissolved hydrogen during the reaction was measured with the permeation probe for the reaction limited and diffusion limited regime. The response time of the probe ($t_{10}-t_{90} = 12$ min) was too long to track the hydrogen concentration during the initial phase of the reaction. However, estimation of the characteristic time of the gas-liquid (G-L) mass transfer and the reaction showed that, at a stirring speed of $N = 30 \text{ s}^{-1}$ the reaction is not limited by the G-L transport step. Additionally, the measured activation energy (74 kJ mol^{-1}) strongly supported the assumption that liquid-solid (L-S) mass transfer limitations were absent.

In a second experiment, it was shown that the rate of reaction decreased, when lowering the stirring speed ($N = 6.7 \text{ s}^{-1}$). The signal of the permeation probe increased during the course of the reaction in parallel with the decreasing hydrogenation rate, which was particularly pronounced at the end of the reaction. Comparing the saturation level with the decrease in the hydrogenation rate upon lowering the stirring speed allowed for differentiation between G-L and L-S mass transfer, proving that G-L mass transfer was the rate-determining step. After internal calibration by a simple pressure step, the permeation probe enabled us to determine the partial pressure of dissolved hydrogen and, after determining the Henry coefficient, the concentration of dissolved hydrogen in the reaction mixture.

The evaluation of the critical parameters in the hydrogenation of a dinitrile under industrially relevant conditions was the aim of the study shown in Chapter 7. Therefore, the hydrogenation of a dinitrile with cobalt-based catalysts was performed in two reactor types. In the batch wise operated stirred tank reactor, a selectivity of almost 100% to primary amines was obtained, when a sufficient amount of liquid ammonia was used. In excess ammonia, the selectivity was almost insensitive to the other parameters investigated (temperature, hydrogen

pressure, diameter of the catalyst particles). By-products formed in the absence of ammonia or at low ammonia concentrations were mainly secondary amines stemming from inter- or intramolecular condensation reactions. When catalyst particle sizes applicable to industrial fixed bed operations were used, significant pore diffusion limitations were present.

For investigating the influence of the flow regime on the selectivity, a trickle-bed reactor was employed. At the same volume ratio of ammonia to dinitrile, a much lower selectivity was observed compared to the stirred tank reactor. This is mainly associated with the strong influence on the ammonia concentration in the liquid phase. In the stirred tank reactor, gas phase hydrogen is not discharged from the autoclave. In contrast, in the trickle bed reactor hydrogen leaves the tubular reactor together with the liquid product mixture. Thus, in the first case, the concentration of ammonia in the liquid phase is determined by the concentration of ammonia fed and the reaction temperature, while in the later case, gaseous ammonia is discharged from the reactor together with excess hydrogen. As the phase equilibrium is dynamically re-established, the average concentration of ammonia in the liquid phase is much lower than in the batch reactor. The higher the hydrogen flow rate was chosen, the lower the concentration of ammonia in the liquid phase and, in consequence, the selectivity. This effect was more pronounced at higher temperatures.

In summary, the mechanistic studies shown in the first part of this Thesis provided a detailed picture about the surface processes occurring on Raney-Co catalysts. It was shown that amines participate in the formation of by-products on the catalyst surface. Thus, the relative adsorption strength of nitriles and amines strongly influences the extent of condensation reactions leading to secondary amines. In this respect, the modification of Raney-Co with LiOH leads to stronger adsorption of amines compared to nitriles, which consequently results in higher selectivity to primary amines. It was suggested that nitrene-like species were the most abundant partially hydrogenated surface intermediates. The main focus of the second part of the Thesis was placed on the optimization of activity and selectivity to primary amines under industrially relevant conditions. It was confirmed that the selectivity is only satisfactory in the presence of ammonia. Thus, the ammonia concentration in the liquid phase is the most important factor in governing the selectivity.